LSU Doctoral Dissertations

Graduate School

2013

Molecular Products from the Thermal Degradation of Selected Tobacco Components: Lignin, Tyrosine, Glutamic Acid, and Modeling of Lignin Pyrolysis using CHEMKIN Combustion Suite

Joshua Kiprotich Kibet
Louisiana State University and Agricultural and Mechanical College, jkibet2@tigers.edu

MOLECULAR PRODUCTS FROM THE THERMAL DEGRADATION OF SELECTED
TOBACCO COMPONENTS: LIGNIN, TYROSINE, GLUTAMIC ACID, AND MODELING
OF LIGNIN PYROLYSIS USING CHEMKIN COMBUSTION SUITE

A Dissertation

Submitted to the Graduate Faculty of the
Louisiana State University and
Agricultural and Mechanical College
In Partial Fulfillment of the
Requirements for the Degree of
Doctor of Philosophy

in

The Department of Chemistry

by
Joshua Kiprotich Kibet
MSc. Moi University, 2007
BEd.Sc. Egerton University, 2004
May 2013

To my sons *Kelvin Kipkoech Rotich* and *Victor Kiptum Rotich*

ACKNOWLEDGEMENTS

TABLE OF CONTENTS

LIST OF TABLES

LIST OF FIGURES

LIST OF SCHEMES

LIST OF ABBREVIATIONS

CHEMKIN	Chemical Kinetics (computer program for Chemical Kinetic studies)
DKP	Diketo Piperazine
DPPH	2,2-diphenyl-1-picrylhydrazyl
EPR	Electron Paramagnetic Resonance
EPFRs	Environmentally Persistent Free Radicals
FID	Flame Ionization Detector
HCN	Hydrogen Cyanide
LT	Landau-Teller Equation
LTMI-EPR	Low Temperature Matrix Isolation- Electron Paramagnetic Resonance
MSD	Mass Selective Detector
NIST	National Institute of Science and Technology
PAHs	Polycyclic Aromatic Hydrocarbons
PTFE	Polytetrafluoroethylene
Py-GC-MS	Pyrolysis-Gas Chromatography-Mass Spectrometry
RT	Retention Time
STDS	System for Thermal Diagnostic Studies
TIC	Total Ion Current
UV	Ultra Violet

ABSTRACT

This study explores the thermal decomposition behavior of selected tobacco components: lignin, tyrosine, and glutamic acid using the system for thermal diagnostic studies (STDS) in an in-line gas chromatography-mass spectrometer analytical technique. The pyrolysis conditions employed in this study were a flowing atmosphere of nitrogen and 4% O_2 in nitrogen at a residence time of 0.2 seconds for a total pyrolysis time of 3 minutes. The results identified common relationships between the two modes of reaction atmospheres, as well as some differences. While some products were favored by an inert regime, some were favored under an oxidative regime. Oxidative pyrolysis of tyrosine for instance yielded compounds of interest, e.g., hydroquinone, *p*-benzoquinone, dibenzofuran, and dibenzo-*p*-dioxin, although no such products were observed under pyrolysis. A comprehensive product distribution at distinct pyrolysis and oxidative pyrolysis temperature of various compounds is presented. The mechanistic channels for the formation of compounds of biological concern such as phenols, and polycyclic aromatic hydrocarbons (PAHs) have also been discussed in detail. Of the classes of compounds analyzed from the thermal degradation of lignin, the phenolic compounds were the most abundant, accounting for over 60% of the total compounds detected. The principal products from pyrolysis of tyrosine were phenol, *p*-cresol, *o*-cresol, and benzaldoxime. For the oxidative pyrolysis, the main products were *p*-tyramine, phenol, *p*-cresol, and benzonitrile. The principal products from pyrolysis of glutamic acid in order of decreasing abundance were succinimide, pyrrole, 2-pyridone, and acetonitrile. On the other hand, succinimide, propiolactone, ethanol, and hydrogen cyanide were the key products under oxidative pyrolysis. CHEMKIN combustion Suite was used to model the pyrolysis of lignin and consequently, a 15 reaction model was developed to determine the kinetics as well as the thermodynamic parameters of reaction products. By use of pseudo first order rate law, the rate coefficients for various products were

evaluated. Arrhenius equation was used to compute the pre-exponential factor A, as well as the activation energy Ea for numerous reaction products including phenol, syringol, 4-vinylguaiacol, furfural, toluene, and benzene. Experimental reaction conditions were used to constrain the model. Simulation data reproduced experimental results with reasonable accuracy.

CHAPTER 1: INTRODUCTION

Studies of potentially toxic by-products from biomass and tobacco at various combustion temperatures have attracted interest because of the health and environmental impacts they cause [1]. Problems such as cardiovascular diseases, emphysema, cancers, oxidative stress, and a variety of reproductive health diseases are to a greater extend a consequence of tobacco use [1, 2]. Accordingly, the toxicology of intermediate radicals and molecular products from the thermal degradation of tobacco and other biomass materials is not only a subject of health concern but also environmental. Molecular products such formaldehyde and acetaldehyde for instance have been classified as carcinogenic, and may be cytotoxic or genetoxic (2, 3). Sugars present in tobacco generate acetaldehyde, which also has addictive properties and acts synergistically with nicotine [1, 3].

Polycyclic aromatic hydrocarbons (PAHs) for instance benzo[a]pyrene are well known environmental carcinogens and have been a subject of intense investigation [4]. Benzene, 1,3-butadiene, and isoprene are some of the major compounds found in tobacco [5-8] believed to be precursors to PAH formation in tobacco smoke. Also, phenoxy and semiquinone radicals produced from biomass and tobacco burning are resonance stabilized environmentally persistent free radicals (EPFRs) with long lifetimes and may cause extensive cellular damage [1, 9].

The primary objective of this study was to gain understanding into the evolution of products at various pyrolysis temperatures and underline the role played by oxygen concentration, residence time, and temperature during tobacco burning. Although many efforts have been engaged towards understanding the pyrolytic charactersitics of tobacco, many complex and uncertain reaction processes are yet to be understood. Clearly, the pyrolysis of tobacco has much in common with the pyrolysis of other forms of biomass [10]. To this end,

biomass pyrolysis remains a critical chemical process in the utilization of renewable energy and feed stocks, in cigarettes, aromatic chemicals, and forest fires [11, 12].

Pyrolysis coupled with gas chromatography and mass spectrometry (Pyr-GC–MS) is known to be a powerful tool in analyzing macromolecular materials and has been widely applied to the study of natural complex organic matter such as biomass and tobacco [13, 14]. This process is defined as the thermal degradation of biomass in the absence of oxygen to yield liquid, solid, and gaseous products [15, 16]. Evidently, the pyrolytic characteristics of individual biomass components are critical in assessing its toxicological nature and unraveling information about its degradation pathways in tobacco burning.

1.1. Pyrolysis of tobacco biomass

The thermolysis of complex plant materials such as tobacco gives rise to a variety of organic substances, most of which are produced by the process of pyrodegradation and pyrosynthesis [17]. Tobacco is a complex plant material consisting of 6-15% cellulose, 10-15% pectin, approximately 2% lignin, and a variety of other components, the exact composition being dependent on the tobacco variety and growing conditions [18]. Tobacco consists of over 2500 chemical constituents, among them biopolymers, non-polymeric and inorganic compounds [19]. Experiments in which individual constituents of the plant such as proteins and amino acids have been pyrolyzed reveal pyrolysis mixtures of similar composition have been produced [17]. Tobacco is of great interest because of its use in the form of cigarettes which generate various smoke compounds during pyrolysis reactions [3, 9, 20, 21].

Cigarette paper as an integral part of the cigarette is believed to contain cellulose [22]. When tobacco is burned, it produces smoke containing thousands of compounds [19].

2

Consequently, several studies have been performed to establish the origin of different chemical species found in tobacco smoke [19, 23, 24].

Tobacco in a smoldering cigarette can reach up to 950 ˚C [25]. It is thought much of the biomass decomposition has occurred by this temperature with the exception of lignin that may decompose above this temperature [26]. The goal of many studies, however; is to establish the relationship between tobacco constituents and smoke products under conditions that simulate actual human smoking although this desire remains a challenge because of the large number of processes occurring inside a burning cigarette (varying temperatures and changes in oxygen
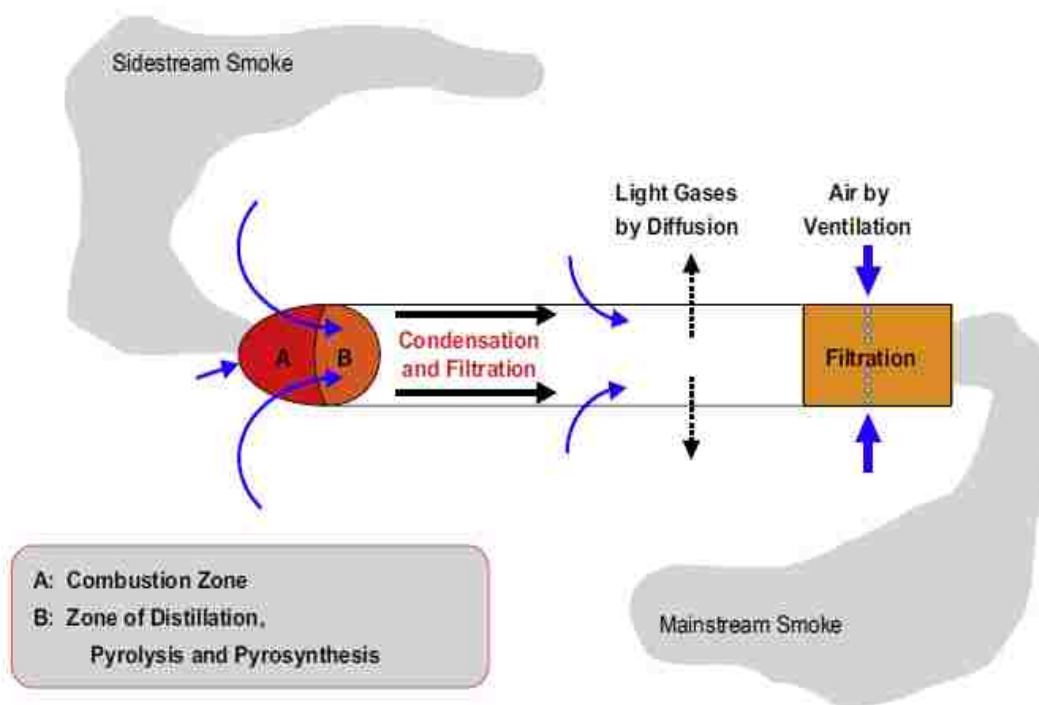
Figure 1.1. The burning cigarette [27].

concentration) [19, 25]. The burning conditions in a cigarette are reflected from the way the cigarette burns from the oxygen rich peripheral surface towards the interior of the cigarette where oxygen is either low or generally absent (cf. Figure 1.1) [27].

3

Tobacco smoke is a highly dynamic and very complex matrix containing over 4800 compounds, therefore, a cigarette can be treated as a chemical reactor where several complex chemical processes take place [19, 28, 29]. About 400 – 500 of these compounds are present in the gas phase, in which about 300 of them can be classified as semi-volatiles [28, 29]. Approximately, 2800 constituents are found in tobacco smoke but not tobacco, indicating the importance of pyrolysis and pyrosynthetic formation mechanism [25]. The tobacco matrix is complex and the range of temperatures and variability of oxidizing and reducing atmospheres within the puffing cigarette is broad and hence it is remarkable that the pyrolysis studies provide analogies to the mainstream smoke precursor-product relationships [30]. The formation of smoke from a burning cigarette depends on a series of mechanisms, including generation of products by pyrolysis and combustion, aerosol formation, and physical mass transfer and filtration processes [3, 31-34].

1.2. Previous research on the pyrolysis of tobacco components

1.2.1. Lignin

The lignin fraction of tobacco is a source of benzene, phenols, dihydroxybenzene and numerous other smoke constituents, including polycyclic aromatic hydrocarbons (PAHs) [35-38]. Lignin is a highly cross-linked polyphenolic polymer without any ordered repeating units and is perhaps one of the most complex organic aromatic polymers in nature [39-42]. However, lignin does not exist in plant tissues as an independent polymer; instead, lignin is bonded with other polymers, cellulose, and hemicellulose forming complexes with them [43]. Lignin is usually interlaced with linear chains of cellulose through chemical bonding and intermolecular forces [44]. Among the major components of biomass, lignin presents the greatest difficulty in understanding the relationship between structure and the devolatilization mechanisms occurring

during typical thermochemical conversion processes [45]. This has been attributed to the complexity of its structure and the difficulty of isolating lignin without altering its structure [45].

1.2.1.1. Structural units of lignin

Together with cellulose and hemicellulose, lignin is one of the three main biopolymers in the cell wall of terrestrial plants (172). The composition of the cell wall changes with the type of tree or plant, but in general 40–45% of wood is cellulose, 25–35% hemicellulose, 15–30% lignin, and up to 10% other compounds [46, 47]. Linkages between the different components consist of hydrogen bonding and covalent ether, ester, and glycoside bonds. The structure is based on three different cinnamyl alcohols as precursors: *p*-coumaryl alcohol, coniferyl alcohol, and sinapyl alcohol compounds (cf. Figure 1.2 A) [46, 47]. The respective aromatic constituents of these alcohols in the polymers are *p*-hydroxyphenyl (H), guaiacyl (2-methoxyphenyl), (G), and
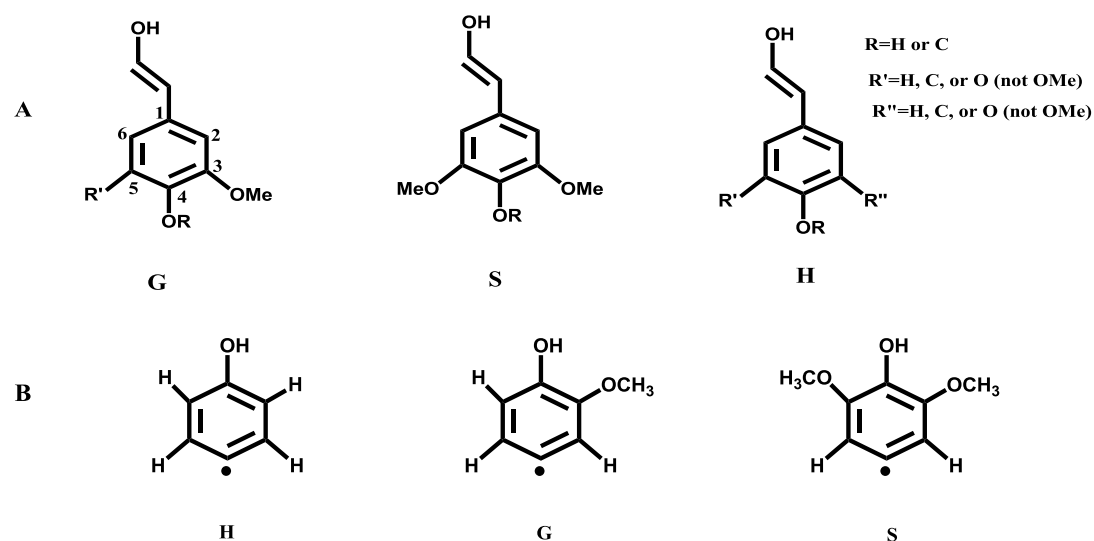
Figure 1.2. The three monolignols (**A**) and H, G, and S derivatives (**B**) [50]

syringyl (2,6-dimethoxyphenyl), (S) units [41, 48] (cf. Figure 1.2 B). The formulation of lignin and the ratio of the three units change with type of cell and plant. In view of this diversity, the exact chemical structure of any lignin cannot be resolved completely [49, 50].

5

The major bonds in the aliphatic linkages of native lignin that significantly affect the type of products observed from the thermal degradation of lignin are $\beta-O-4$, $\alpha-O-4$, $\beta-5$, and *biphenyl* [50] (cf. Figure 1.3). These bonds are considered important because they result in the formation of phenoxy and phenyl radicals [50]. Breaking $\alpha-\beta$ bonds in the $\beta-O-4$ and $\alpha-O-4$ linkages requires approximately 318 kJmol^{-1} and is not influenced by relevant
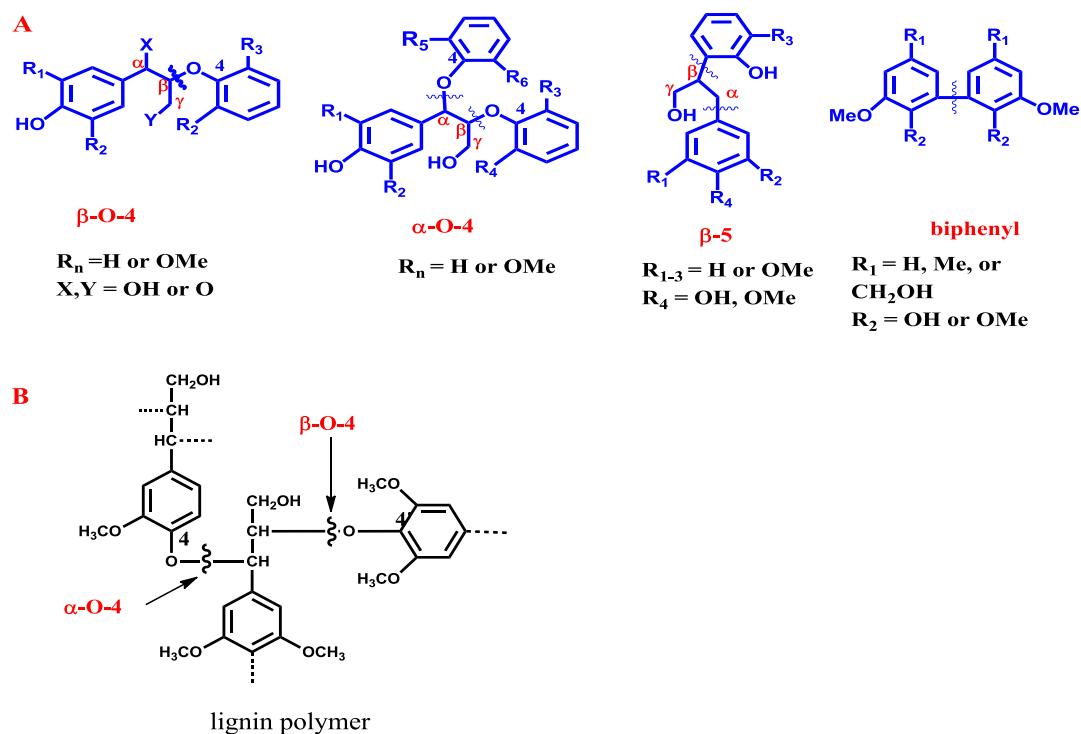
Figure 1.3. The four major Bonds (*β-O-4*, *α-O-4*, and *biphenyl*) in lignin (**A**) and the proposed lignin structure (**B**) [50].

substituents [50-52]. Scission of the $\alpha-\beta$ bond in the $\beta-5$ compounds proceeds with an approximate bond dissociation energy of 265 kJmol^{-1} [50, 52, 53]. Lignin has a tendency to form volatile products in a wide range of temperature between 200 and 500 ˚C [54]. Jakab *et al*. found that the release of molecular products of lignin was independent of the lignin type [55-57]. Thermogravimetric analysis of various lignin samples has indicated that the primary pyrolysis of lignin proceeds mainly in the temperature range between 200 and 400 ˚C [58, 59], and that the

highest degradation rate of lignin was at~ 380 ˚C [60, 61]. Yang et al. suggested that thermal decomposition of lignin occurs at a wide temperature range starting at approximately 150˚ C [56]. The majority of the components were evolved in the temperature region 300-500 ˚C which coincides with the devotilization region of biomass materials. The release of volatile matter begins quickly with increase in temperature and then decrease with increase temperature [57]. This is because at low temperature, the volatile matter slowly evaporates and the carbonization reaction dominates as temperature increase leading to the cracking of unstable components of the volatile matter [57].

During pyrolysis, complex product mixtures are obtained comprising not only numerous substituted 2-methoxy- and 2,6-dimethoxyphenols, but also *o*-cresol and derivatives, which are thought to originate from the degradation of these methoxy phenols [62]. Nevertheless, lignin is believed to thermally decompose via a free radical mechanisms [46, 62]. The thermal degradation of lignin will be discussed in relation to the mechanism of lignin decomposition and the toxicity of its decomposition by-products.

For the first time in this study, low temperature matrix isolation electron paramagnetic resonance was successfully interfaced with the pyrolysis reactor to elucidate the structures of the labile reaction intermediates. The EPR results suggested the presence of methoxyl, phenoxy, and substituted phenoxy radicals as precursors for formation of major pyrolysis products; syringol, guaiacol, phenols, and substituted phenols[1]. Over the years, the study of lignin has lagged behind the pyrolysis of cellulose because of the difficulty in understanding its structure, and the challenges associated with its isolation from other biomass components [45].

---

[1] Reproduced in part with permission from Kibet J. K.; Lavrent K., and Dellinger, B. *Molecular Products and Radicals from the Pyrolysis of Lignin*, Environmental Science & Technology, 2012, **46**, 12994−13001. Copyright American Chemical Society, 2012.

1.2.2. Summary of previous findings from the pyrolysis of lignin

Previously, it was found lignin pyrolysis is a source of benzene, phenols, dihydroxybenzene and numerous other tobacco smoke constituents, including polycyclic hydrocarbons (PAHs) [35]. 2-4 mg sample was heated at rate of 20 ˚C up to 950 ˚C, and concluded the char yield of lignin was inversely proportional to the amount of hydroxyl and methoxy groups [35-36]. This implied that the hydroxyl and methoxy groups are important sources of volatiles [35]. Pyrolysis of lignin investigated using molecular-beam mass spectrometry indicated alkyr-aryl ether linkage was the major bonding in lignin [45]. The scission of the alkyl-aryl ether linkage resulted to preferential formation of precursor monomers; coniferyl and sinapyl alcohols [45]. The decomposition of milled-wood lignin investigated using thermogravimetry/mass-spectrometry produced 26-39% char yield [55]. Volatiles containing methoxy groups, water, methanol, and acetic acid were also identified [35, 55].

1.3. Amino acids

Research on the thermal degradation of tyrosine and glutamic acid is limited despite the fact that pyrolytic processes are commonly used in their manufactures [63]. Pyrolysis studies of amino acids are critical because formation of mutagenic and carcinogenic products in pyrolysates of proteinaceous food products is a health concern in the fields of food processing, preservation, and safety [64]. Also, the investigation of pyrolysis of amino acids can provide helpful information about the type of molecular products observed from decomposition of tobacco and other biomass materials that may contain proteins [65].

The pyrolytic behavior of common amino acids has been investigated in detail but despite this effort, potentially diagnostic fragments bearing polar functional groups, e.g. COOH, NH,

OH frequently escape detection because of thermal instability, low volatility, and high adsorptivity [66]. Our investigations of the thermal degradation of tyrosine avoid many experimental pitfalls by using a continuous flow reactor system, with collection of the reactor effluent with an in-line GC-MS at the head of the GC column at -60˚C.

1.3.1. Tyrosine

Tyrosine is a large amino acid found in substantial quantities in many animal and plant proteins [67] as well in tobacco [68]. The health consequences resulting from consumption of tobacco products has been blamed on the production of toxic molecular products as well as free radicals during tobacco burning. For example, tyrosyl radical has been reported from the fractional pyrolysis of bright tobacco [69]. Tyrosyl radical may originate either from the
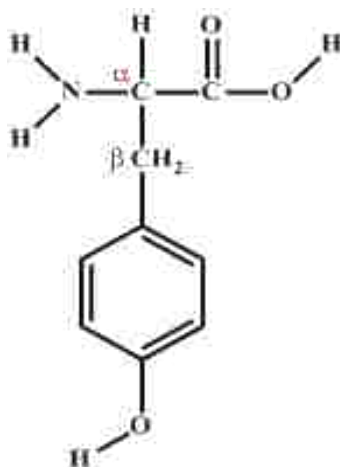
Figure 1.4. The structure of tyrosine

decomposition of protein-containing tyrosine residues or from free tyrosine molecules [69].

The mechanistic pathway for the decomposition of tyrosine was thought to proceed via decarboxylation reactions to form *p*-tyramine and CO_2, although *p*-tyramine has previously never been detected probably because of it low volatility and high thermal stability. Subsequent decomposition of *p*-tyramine was speculated to form 4-methylphenol and ultimately phenol.

Nevertheless, the mechanistic pathways previously proposed by Li et al. [65] is not only controversial but lacks in detail. This study will demonstrate the formation of *p*-tyramine and its subsequent degradation to toxicologically important pollutants, such as phenol, and *p*-cresol. A mechanism of *p*-tyramine formation and degradation from the thermal decomposition of tyrosine is presented for the first time. The high yields of *p*-tyramine observed in oxidative pyrolysis of tyrosine is also decsribed exhasutively.

1.3.1.1. Summary of previous findings from the pyrolysis of tyrosine

Pyrolysis of tyrosine mainly yielded reaction species such as HCN, isocyanic acid (O=C=NH, HNCO), acetonitrile, and other nitrogen containing compounds during biomass/tobacco burning [75]. Also, Pyrolysis of tyrosine in a TGA instrument at a heating rate of 20°C/min yielded phenol, *p*-cresol, acetonitrile and benzonitrile as the major reaction products [70-72]. Pyrolysis Gas-Chromatography was used to study the content of tyrosyl residues in wool [73]. A study of radical products from the fractional pyrolysis of Bright tobacco over the temperature range 200-510 °C revealed the formation of tyrosyl radical and consequently affirming the presence of tyrosine in tobacco biomass [69].

1.3.2. Glutamic acid

Glutamic acid is one of the principal nitrogenous precursors present in Burley tobacco [68, 74]. The thermal behavior of glutamic acid is considered interesting due to its wide spectrum of commercial applications including tobacco products, drugs for the treatment of ulcers, epilepsy, and Parkinson's disease [63, 75-78]. It has also been reported pyrolysates of glutamic acid show more potent mutagenicities in Ames's test [79, 80]. Previously, it was suggested degradation of glutamic acid could proceed via intra-molecular dehydration to form lactam [81]. Glutamic acid in free form has been known to exist in many different foods such as

wheat, soybeans, coffee, cocoa and tobacco, releasing large amounts of 2-pyrrolidone in cooked and roasted foods [82-85]. Nevertheless, there is no data to show 2-pyrrolidone could be genotoxic in cooked food and thus may not be a safety concern [82].

Glutamic acid is also known to be an important precursor for the formation of heterocyclic pyrolysis products such glutarimide and pyroglutamic acid [68]. Whereas succinimide and maleimide has been observed from the pyrolysis of amino acids such as glutamine and aspartic acid, no succinimide or maleimide has been observed from the thermal
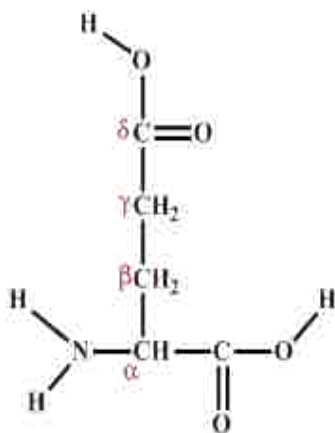
Figure 1.5. The structure of glutamic acid

degradation of glutamic acid. This study however, reveals succinimide and maleimide can actually be formed from thermolysis of glutamic acid. Consequently, a mechanistic treatment on the formation of these products (succinimide and maleimide) from the decomposition of glutamic acid has been described. It was also noted in this study, the yields of succinimide in oxidative pyrolysis were higher than in pyrolysis. This unique phenomenon was attributed to the role an oxidative environment plays during the dehydration of pyroglutamic acid and consequent formation of a tricyclic intermediate (diketo piperazine) that ultimately transforms to succinimide and 2-pyridone. In oxidative pyrolysis, the rate of a reaction is enhanced so that the formation of diketo piperzine is strongly favored.

1.3.2.1. Summary of previous findings from pyrolysis of tyrosine

Pyrolysis of glutamic acid at a heating rate of 5˚C/min in a Pyr-GC-MS system resulted in the formation of 2-pyrrolidone, pyroglutamic acid, and 2-pyrrolidone-5-carboxylic acid [68, 70, 72]. The thermal characteristics of L-glutamic acid was investigated using differential scanning calorimetry, thermogravimetry, powder X-ray diffraction, gel permeation chromatography, and mass spectrometry [74]. The results showed that the major product was pyroglutamic acid. High molecular weight polyglutamic acid was also identified [74].

The pyrolysis of amino acids including glutamic acid at 300 ˚C and 650 ˚C in a tubular flow reactor in a helium atmosphere flowing at 120 cm^3/min. gave rise to gaseous products such as ammonia, HCN, as well as heterocyclic products (2-pyrrolidone, glutarimide, and pyroglutamic acid) [68]. Glutamic acid was heated in air at room temperature to 450 ˚C in a thermogravimetric analyzer at 10 ˚C/min [86]. The weight loss due to evolution of Molecular products was 41% at 390 ˚C [86].

1.3.3. General mechanistic considerations for amino acid pyrolysis

Amino acids in the form of proteins are the main source of nitrogen in wood [87]. Most biomass materials such as tobacco bagasse, straw, and wood contain nitrogen which can be converted to environmentally harmful products [65, 66]. The thermodynamic end products of amino acids are simple inorganic compounds (CO_2, H_2O, NH_3, and CO); however, more complex chemicals are formed as by-products (HCN, amines, nitriles, amides, phenols, and hydrocarbons) [66, 86, 87].

For purposes of this study, a general mechanistic description for the thermal degradation of amino acids is presented in Scheme 1.1, *vide supra* [88]. Scheme 1.1 above summarizes

reactions that are considered fundamental in the formation of observed products in amino acid pyrolysis. Decarboxylation r eactions are certainly the major mechanistic channels, in addition to deamination, dehydration, dehydrogenation, rearrangement, addition, and substitution. Diketo piperazine (DKP) is largely responsible for the formation of various secondary products such as nitriles, HCN, and aromatic hydrocarbons (cf. Scheme 1.1, *vide supra*).

Scheme 1.1. General mechanistic pathways for the thermal degradation of amino acids [88].

13

1.4. Summary of the present study

This study investigates the thermal degradation of selected tobacco components; lignin, tyrosine, and glutamic acid at a residence time of 0.2 s in a tubular flow reactor in flowing N_2 and 4% O_2 in N_2 for a total pyrolysis time of 3 minutes using the System for Thermal Diagnostic Studies (STDS). The fractional pyrolysis technique, in which the same sample was heated continuously at each pyrolysis temperature, was applied. Fractional pyrolysis is defined as a selective *in situ* conversion of biopolymers to desired products [89]. This technique offers some advantages in comparison with conventional pyrolysis. First, only one loading of biomass material is used and can be heated multiple times and cooled down by flushing the system with inert gas (N_2) in addition to exposing the reactor to a cooling fan. Secondly, it provides partial accumulation of any fraction and analysis of products in the gas phase as well as in the residue (charred material). Thirdly, the intermediate neutral, but unstable products may be collected before they disappear in the secondary processes. Table 1.5 summarizes the experimental conditions employed in this study.

Table 1.1. Summary of Experiments

Biomass Component	Experimental Conditions at 1amt. Pressure	Residence Time (s)	Temperature Range (˚C)
Lignin	Fractional Pyrolysis	0.2	200-900
	Conventional pyrolysis	0.2	200-500
	Fractional Oxidative Pyrolysis	0.2	200-500
	Conventional Oxidative Pyrolysis	0.2	200-500
Tyrosine	Fractional Pyrolysis	0.2	300-800
	Fractional Oxidative Pyrolysis	0.2	200-700
Glutamic Acid	Fractional Pyrolysis	0.2	200-600
	Fractional Oxidative Pyrolysis	0.2	200-600
Lignin-tyrosine Mixture	Fractional Pyrolysis	0.2	200-900
	Fractional Oxidative Pyrolysis	0.2	200-500

1.5. References

1. D. Selassie, C., et al., *On the toxicity of phenols to fast growing cells. A QSAR model for a radical-based toxicity.* Journal of the Chemical Society, Perkin Transactions 2, 1999 (12): p. 2729-2733.

2. Lin, H.Q., et al., *Field analysis of acetaldehyde in mainstream tobacco smoke using solid-phase microextraction and a portable gas chromatograph.* Journal of Chromatography A, 2008. **1198**: p. 34-37.

3. Baker, R.R., S. Coburn, and C. Liu, *The pyrolytic formation of formaldehyde from sugars and tobacco.* Journal of Analytical and Applied Pyrolysis, 2006. **77** (1): p. 12-21.

4. Wang, S.F., et al., *Gas chromatographic-mass spectrometric determination of polycyclic aromatic hydrocarbons formed during the pyrolysis of phenylalanine.* Journal of Chromatography A, 2004. **1025** (2): p. 255-261.

5. Laothawornkitkul, J., et al., *Isoprene emissions influence herbivore feeding decisions.* Plant Cell and Environment, 2008. **31** (10): p. 1410-1415.

6. Cook, J.W., et al., *The production of cancer by pure hydrocarbons. Part I.* Proceedings of the Royal Society of London Series B-Containing Papers of a Biological Character, 1932. **111** (773): p. 455-+.

7. Kennaway, E.L., *The formation of a cancer-producing substance from isoprene (2-methylbutadiene).* Journal of Pathology and Bacteriology, 1924. **27**(3): p. 233-238.

8. Kennaway, E.L., *Experiments on cancer-producing substances.* British Medical Journal, 1925. **1925**: p. 1-4.

9. Dellinger, B., et al., *Formation and stabilization of persistent free radicals.* Proceedings of the Combustion Institute, 2007. **31**: p. 521-528.

10. Sharma, R.K., et al., *Characterization of char from the pyrolysis of tobacco.* Journal of Agricultural and Food Chemistry, 2002. **50** (4): p. 771-783.

11. Shin, E.J., M.R. Nimlos, and R.J. Evans, *A study of the mechanisms of vanillin pyrolysis by mass spectrometry and multivariate analysis.* Fuel, 2001. **80** (12): p. 1689-1696.

12. Jiang, G.Z., D.J. Nowakowski, and A.V. Bridgwater, *Effect of the temperature on the composition of lignin pyrolysis products.* Energy & Fuels, 2010. **24**: p. 4470-4475.

13.   Gallois, N., J. Tempher, and S. Derenne, *Pyrolysis-gas chromatography-mass spectrometry of the 20 protein amino acids in the presence of TMAH.* Journal of Analytical and Applied Pyrolysis, 2007. **80** (1): p. 216-230.

14.   Sharma, R.K., G.W. Chan, and M.R. Hajaligol, *Co-pyrolysis of alpha-amino acids with glucose.* Abstracts of Papers of the American Chemical Society, 2003. **226**: p. U534-U535.

15.   Booker, C.J., et al., *Experimental investigations into the insecticidal, fungicidal, and bactericidal properties of pyrolysis bio-oil from tobacco leaves using a fluidized bed pilot plant.* Industrial & Engineering Chemistry Research, 2010. **49** (20): p. 10074-10079.

16.   Demirbas, A., *Mechanisms of liquefaction and pyrolysis reactions of biomass.* Energy Conversion and Management, 2000. **41** (6): p. 633-646.

17.   Patterso.Jm, et al., *Pyrolysis of phenylalanine, 3,6-dibenzyl-2,5-piperazinedione, and phenethylamine.* Journal of Organic Chemistry, 1973. **38** (4): p. 663-666.

18.   Feng, J.W., S.K. Zheng, and G.E. Maciel, *EPR investigations of charring and char/air interaction of cellulose, pectin, and tobacco.* Energy & Fuels, 2004. **18** (2): p. 560-568.

19.   Czegeny, Z., et al., *Formation of selected toxicants from tobacco under different pyrolysis conditions.* Journal of Analytical and Applied Pyrolysis, 2009. **85** (1-2): p. 47-53.

20.   Mitschke, S., et al., *Application of time-of-flight mass spectrometry with laser-based photoionization methods for time-resolved on-line analysis of mainstream cigarette smoke.* Analytical Chemistry, 2005. **77** (8): p. 2288-2296.

21.   Busch, C., et al., *Pyrolysis and combustion of tobacco in a cigarette smoking simulator under air and nitrogen atmosphere.* Analytical and Bioanalytical Chemistry, 2012. **403** (2): p. 419-430.

22.   Zhou, S., et al., *The pyrolysis of cigarette paper under the conditions that simulate cigarette smouldering and puffing.* Journal of Thermal Analysis and Calorimetry, 2011. **104** (3): p. 1097-1106.

23.   Schlotzhauer, W.S., et al., *Pyrolytic studies on the contribution of tobacco leaf constituents to the formation of smoke catechols.* Journal of Agricultural and Food Chemistry, 1982. **30** (2): p. 372-374.

24. Schlotzhauer, W.S., R.F. Arrendale, and O.T. Chortyk, *The rapid pyrolytic characterization of tobacco leaf carbohydrate material.* Beitrage Zur Tabakforschung International, 1985. **13** (2): p. 74-80.

25. Baker, R.R. and L.J. Bishop, *The pyrolysis of tobacco ingredients.* Journal of Analytical and Applied Pyrolysis, 2004. **71** (1): p. 223-311.

26. Orfao, J.J.M., F.J.A. Antunes, and J.L. Figueiredo, *Pyrolysis kinetics of lignocellulosic materials - Three independent reactions model.* Fuel, 1999. **78** (3): p. 349-358.

27. Thielen, A., H. Klus, and L. Muller, *Tobacco smoke: Unraveling a controversial subject.* Experimental and Toxicologic Pathology, 2008. **60** (2-3): p. 141-156.

28. Adam, T., et al., *Simultaneous on-line size and chemical analysis of gas phase and particulate phase of cigarette mainstream smoke.* Analytical and Bioanalytical Chemistry, 2009. **394** (4): p. 1193-1203.

29. Adam, T., et al., *Influence of filter ventilation on the chemical composition of cigarette mainstream smoke.* Analytica Chimica Acta, 2010. **657** (1): p. 36-44.

30. Sanders, E.B., A.I. Goldsmith, and J.I. Seeman, *A model that distinguishes the pyrolysis of D-glucose, D-fructose, and sucrose from that of cellulose. Application to the understanding of cigarette smoke formation.* Journal of Analytical and Applied Pyrolysis, 2003. **66** (1-2): p. 29-50.

31. Baker, R.R., *The generation of formaldehyde in cigarettes - Overview and recent experiments.* Food and Chemical Toxicology, 2006. **44** (11): p. 1799-1822.

32. Uryupin, A.B. and L.M. Fomina, *Analysis of tobacco smoke condensates.* Journal of Analytical Chemistry, 2005. **60** (8): p. 784-787.

33. Gao, L., et al., *Eliminating carcinogenic pollutants in environment: Reducing the tobacco specific nitrosamines level of smoke by zeolite-like calcosilicate.* Journal of Hazardous Materials, 2009. **169** (1-3): p. 1034-1039.

34. Baker, R.R., *Smoke generation inside a burning cigarette: Modifying combustion to develop cigarettes that may be less hazardous to health.* Progress in Energy and Combustion Science, 2006. **32** (4): p. 373-385.

35. Pouwels, A.D., G.B. Eijkel, and J.J. Boon, *Curie-point pyrolysis capillary gas-chromatography high-resolution mass-spectrometry of microcrystalline cellulose.* Journal of Analytical and Applied Pyrolysis, 1989. **14** (4): p. 237-280.

36.   Sharma, R.K. and M.R. Hajaligol, *Polycyclic aromatic hydrocarbon formation in pyrolysis of polyphenolic compounds.* Abstracts of Papers of the American Chemical Society, 2001. **221**: p. U509-U509.

37.   Forehand, J.B., G.L. Dooly, and S.C. Moldoveanu, *Analysis of polycyclic aromatic hydrocarbons, phenols and aromatic amines in particulate phase cigarette smoke using simultaneous distillation and extraction as a sole sample clean-up step.* Journal of Chromatography A, 2000. **898** (1): p. 111-124.

38.   Boon, J.J., et al., *Structural studies on cellulose pyrolysis and cellulose chars by pyms, pygcms, ftir, nmr and by wet chemical techniques.* Biomass & Bioenergy, 1994. **7** (1-6): p. 25-32.

39.   Sharma, R.K., et al., *Characterization of chars from pyrolysis of lignin.* Fuel, 2004. **83** (11-12): p. 1469-1482.

40.   Wan, J.K.S. and M.C. Depew, *Applications of ESR and CIDEP to mechanistic studies of lignin chemistry.* Research on Chemical Intermediates, 1998. **24** (8): p. 831-847.

41.   Lewis, N.G. and E. Yamamoto, *Lignin - Occurrence, biogenesis and biodegradation.* Annual Review of Plant Physiology and Plant Molecular Biology, 1990. **41**: p. 455-496.

42.   Kuzina, S.I., et al., *Free radicals in the photolysis and radiolysis of polymers: IV. Radicals in gamma- and UV-irradiated wood and lignin.* High Energy Chemistry, 2004. **38** (5): p. 298-305.

43.   Buranov, A.U. and G. Mazza, *Lignin in straw of herbaceous crops.* Industrial Crops and Products, 2008. **28** (3): p. 237-259.

44.   Kuzina, S.I., I.A. Shilova, and A.I. Mikhailov, *Chemical and radiation-chemical radical reactions in lignocellulose materials.* Radiation Physics and Chemistry, 2011. **80** (9): p. 937-946.

45.   Evans, R.J., T.A. Milne, and M.N. Soltys, *Direct mass-spectrometric studies of the pyrolysis of carbonaceous fuels .3. Primary pyrolysis of lignin.* Journal of Analytical and Applied Pyrolysis, 1986. **9** (3): p. 207-236.

46.   Dorrestijn, E., et al., *The occurrence and reactivity of phenoxyl linkages in lignin and low rank coal.* Journal of Analytical and Applied Pyrolysis, 2000. **54** (1-2): p. 153-192.

47.   Baliga, V., et al., *Physical characterization of pyrolyzed tobacco and tobacco components.* Journal of Analytical and Applied Pyrolysis, 2003. **66** (1-2): p. 191-215.

48.   Freudenb.K, *Lignin - its constitution and formation from p-hydroxycinnamyl alcohols.* Science, 1965. **148** (3670): p. 595-&.

49.   Yuan, T.Q., et al., *Structural characterization of lignin from triploid of populus tomentosa carr.* Journal of Agricultural and Food Chemistry, 2011. **59** (12): p. 6605-6615.

50.   Kim, S., et al., *Computational study of bond dissociation enthalpies for a large range of native and modified lignins.* Journal of Physical Chemistry Letters, 2011. **2** (22): p. 2846-2852.

51.   Jarvis, M.W., et al., *Direct detection of products from the pyrolysis of 2-phenethyl phenyl ether.* Journal of Physical Chemistry A, 2011. **115** (4): p. 428-438.

52.   Beste, A. and A.C. Buchanan, *Kinetic analysis of the phenyl-shift reaction in beta-o-4 lignin model compounds: A computational study.* Journal of Organic Chemistry, 2011. **76** (7): p. 2195-2203.

53.   Ellison, G.B., et al., *Thermochemistry of the benzyl and allyl radicals and ions.* International Journal of Mass Spectrometry and Ion Processes, 1996. **156** (1-2): p. 109-131.

54.   Ramiah, M.V., *Thermogravimetric and differential thermal analysis of cellulose, hemicellulose, and lignin.* Journal of Applied Polymer Science, 1970. **14** (5): p. 1323-&.

55.   Jakab, E., O. Faix, and F. Till, *Thermal decomposition of milled wood lignins studied by thermogravimetry mass spectrometry.* Journal of Analytical and Applied Pyrolysis, 1997. **40-1**: p. 171-186.

56.   Yang, Q., et al., *Analysis of wheat straw lignin by thermogravimetry and pyrolysis-gas chromatography/mass spectrometry (vol 87, pg 65, 2009).* Journal of Analytical and Applied Pyrolysis, 2010. **87** (2): p. 291-291.

57.   Qu, T.T., et al., *Experimental study of biomass pyrolysis based on three major components: hemicellulose, cellulose, and lignin.* Industrial & Engineering Chemistry Research, 2011. **50** (18): p. 10424-10433.

58.   Kawamoto, H., M. Ryoritani, and S. Saka, *Different pyrolytic cleavage mechanisms of beta-ether bond depending on the side-chain structure of lignin dimers.* Journal of Analytical and Applied Pyrolysis, 2008. **81** (1): p. 88-94.

59.   Nakamura, T., H. Kawamoto, and S. Saka, *Pyrolysis behavior of Japanese cedar wood lignin studied with various model dimers.* Journal of Analytical and Applied Pyrolysis, 2008. **81** (2): p. 173-182.

60.   Jiang, G.Z., D.J. Nowakowski, and A.V. Bridgwater, *A systematic study of the kinetics of lignin pyrolysis.* Thermochimica Acta, 2010. **498** (1-2): p. 61-66.

61.   Ben, H.X. and A.J. Ragauskas, *NMR Characterization of Pyrolysis Oils from Kraft Lignin.* Energy & Fuels, 2011. **25** (5): p. 2322-2332.

62.   Dorrestijn, E. and P. Mulder, *The radical-induced decomposition of 2-methoxyphenol.* Journal of the Chemical Society-Perkin Transactions 2, 1999 (4): p. 777-780.

63.   Chiavari, G. and G.C. Galletti, *Pyrolysis-gas chromatography mass-spectrometry of amino-acids.* Journal of Analytical and Applied Pyrolysis, 1992. **24** (2): p. 123-137.

64.   Djilas, S.M., B.L. Milić, and J.M. Čanadanović-Brunet, *ESR spectral study of free radical formation during the pyrolysis of hydroxyamino acids.* Journal of Analytical and Applied Pyrolysis, 1994. **28**(1): p. 157-161.

65.   Li, J., et al., *The investigation of thermal decomposition pathways of phenylalanine and tyrosine by TG-FTIR.* Thermochimica Acta, 2008. **467** (1-2): p. 20-29.

66.   Chiavari, G., D. Fabbri, and S. Prati, *Gas chromatographic-mass spectrometric analysis of products arising from pyrolysis of amino acids in the presence of hexamethyldisilazane.* Journal of Chromatography A, 2001. **922** (1-2): p. 235-241.

67.   Mahoney, C.R., et al., *Tyrosine supplementation mitigates working memory decrements during cold exposure.* Physiology & Behavior, 2007. **92** (4): p. 575-582.

68.   Sharma, R.K., W.G. Chan, and M.R. Hajaligol, *Product compositions from pyrolysis of some aliphatic alpha-amino acids.* Journal of Analytical and Applied Pyrolysis, 2006. **75** (2): p. 69-81.

69.   Maskos, Z., L. Khachatryan, and B. Dellinger, *Formation of the persistent primary radicals from the pyrolysis of tobacco.* Energy & Fuels, 2008. **22** (2): p. 1027-1033.

70.   Sharma, R.K., W.G. Chan, and M.R. Hajaligol, *Effect of reaction conditions on product distribution from the co-pyrolysis of alpha-amino acids with glucose.* Journal of Analytical and Applied Pyrolysis, 2009. **86** (1): p. 122-134.

71.	K. Abdul-Sada, A.a., et al., *Isolation and characterisation of fluorinated derivatives of [76]- and [78]fullerenes.* Journal of the Chemical Society, Perkin Transactions 2, 1999 (12): p. 2659-2666.

72.	Sharma, R.K., et al., *On the role of peptides in the pyrolysis of amino acids.* Journal of Analytical and Applied Pyrolysis, 2004. **72** (1): p. 153-163.

73.	Marmer, W.N. and P. Magidman, *Pyrolysis-gas chromatography of wool .3. Detection and quantitation of tyrosine.* Textile Research Journal, 1990. **60** (7): p. 417-420.

74.	Stedman, R.L., *Chemical composition of tobacco and tobacco smoke.* Chemical Reviews, 1968. **68** (2): p. 153-&.

75.	Wu, H., et al., *Phase Transformations of glutamic acid and its decomposition products.* Crystal Growth & Design, 2010. **10** (2): p. 988-994.

76.	Lloyd, K.G. and Hornykie.O, *L-glutamic acid decarboxylase in parkinsons-disease - Effect of l-dopa therapy.* Nature, 1973. **243**(5409): p. 521-523.

77.	Lloyd, K.G., et al., *Biochemical-evidence of dysfunction of brain neurotransmitters in the lesch-nyhan syndrome.* New England Journal of Medicine, 1981. **305** (19): p. 1106-1111.

78.	Lloyd, K.G., et al., *Neurochemical alterations in the basal ganglia in the lesch-nyhan syndrome.* Canadian Journal of Neurological Sciences, 1982. **9** (2): p. 278-279.

79.	Ames, B.N., J. McCann, and E. Yamasaki, *Carcinogens are mutagens - Simple test system.* Mutation Research, 1975. **33**: p. 27-28.

80.	Ames, B.N., J. McCann, and E. Yamasaki, *Methods for detecting carcinogens and mutagens with salmonella-mammalian-microsome mutagenicity test.* Mutation Research, 1975. **31** (6): p. 347-363.

81.	Povoledo, D. and J.R. Vallentyne, *Thermal reaction kinetics of the glutamic acid-pyroglutamic acid system in water.* Geochimica Et Cosmochimica Acta, 1964. **28** (May): p. 731-734.

82.	Stadler, R.H., et al., *Formation of vinylogous compounds in model Maillard reaction systems.* Chemical Research in Toxicology, 2003. **16** (10): p. 1242-1250.

83.	Wolf, W.J., *Gel-electrophoresis and amino-acid-analysis of the nonprotein nitrogen fractions of defatted soybean and almond meals.* Cereal Chemistry, 1995. **72** (1): p. 115-121.

84. Hurst, W.J. and R.A. Martin, *Use of ortho-phthaldehyde derivatives and high-pressure liquid-chromatography in determining the free amino-acids in cocoa beans.* Journal of Agricultural and Food Chemistry, 1980. **28** (5): p. 1039-1039.

85. Arnold, U. and E. Ludwig, *Analysis of free amino acids in green coffee beans .2. Changes of the amino acid content in arabica coffees in connection with post-harvest model treatment.* Zeitschrift Fur Lebensmittel-Untersuchung Und-Forschung, 1996. **203** (4): p. 379-384.

86. Baczkowicz, M., et al., *Reaction of some polysaccharides with biogenic alpha-amino-acids.* Starch-Starke, 1991. **43** (8): p. 294-299.

87. Hansson, K.M., et al., *Formation of HNCO, HCN, and NH3 from the pyrolysis of bark and nitrogen-containing model compounds.* Combustion and Flame, 2004. **137** (3): p. 265-277.

88. Ratcliff, M.A., E.E. Medley, and P.G. Simmonds, *Pyrolysis of amino-acids - Mechanistic considerations.* Journal of Organic Chemistry, 1974. **39** (11): p. 1481-1490. 2003. **82**(6): p. 653-660.

89. Agblevor, F.A., et al., *Fractional catalytic pyrolysis of hybrid poplar wood.* Industrial & Engineering Chemistry Research, 2010. **49** (8): p. 3533-3538.

CHAPTER 2: EXPERIMENTAL SECTION

2.1. The system for thermal diagnostic studies

The system for thermal diagnostic studies (STDS) was developed to study the thermal characteristics of a broad range of organic compounds under various conditions [1-3]. This system permits the testing of pure organic compounds and mixtures consisting of gaseous, liquids, solids, and polymeric, composites as well as multiphase components [1, 3]. The STDS contains various units each of which is critical towards the analysis of organic materials: the reactor compartment, the temperature control console, the sample injection port, a cryogenic trap, and a detection system that consists of a GC (Flame ionization detector, FID) and a mass spectrometer detector (MSD).

The STDS was designed as an in line system to allow the quantitative transport of samples from the reactor via a transfer line to a GC injection port where they are trapped at -60˚C before being desorbed to a downstream GC column for detection. The dwell time of the pyrolysate in the transfer line was very short (~ 1-2 ms) because of the high gas flow rates. Consequently, no degradation was expected to occur along the transfer line.

Many parameters influence the gas-phase thermal degradation of organic materials [3]. Contact temperature, residence time, and composition of gas-phase environment are three critical variables [3]. The objective of thermal degradation investigation of organic materials is to measure and experimentally characterize samples' thermal decomposition behavior and their effluent products, and also identify those physiochemical variables and operational parameters influencing degradation [4]. A typical residence time of 0.2 seconds was maintained for each

run. The pyrolysis gas was varied in such a way that the residence time was held constant for every temperature change. This is in accordance with the ideal gas law (equation 2.1) [3].

$$\frac{V_0 P_0}{T_0} = \frac{V_1 P_1}{T_1}$$ *Equation 2.1*

where is V volume, P is pressure and T is temperature. The subscript 0 and 1 denote the ambient and reactor conditions respectively. By substituting V_1 with the volume of the reactor $\pi r^2 l$ and taking the flow through the reactor to be equal to $V_0 = F_0 t_0$ [3], where F_o and t_o represent the flow rate and residence time respectively, the following relationship (equation 2) [3] is established.

$$\frac{\pi r^2 L P_1}{T_1} = \frac{F_0 t_0}{T_0}$$ *Equation 2.2*

The differential pressure P_d can be described as $P_1 - P_0$ if the resistance to the gas flow of the quartz tube reactor is much less than the sum of the downstream resistance to the gas flow (the transfer lines and the cryogenic trap). Consequently, the average residence time admitted to a high temperature tubular-flow reactor is described by equation 3 [3].

$$t_o = \left(\frac{\pi r^2 L}{F_0} \right) \left(\frac{T_1}{T_0} \right) \left[1 + \frac{P_d}{P_0} \right]$$ *Equation 2.3*

Equation 3 was used to determine the flow needed for each temperature in order to maintain a constant residence time of 0.2 seconds. The residence time of 0.2 seconds was chosen in order to simulate real human cigarette smoking conditions. Table 2.1 shows the flow rates for each temperature run based on equation 2.3.

Table 2.1. Gas Flow Rates for Each Experimental Temperature for Degradation of Biopolymers

Temp. (˚C)	200	250	300	350	400	450	500	550	600	650	700	750	800	850	900
Flow rates (mL/min.)	272	246	224	206	191	178	166	156	147	139	132	127	120	114	110

2.2. Reactor for bio-polymeric materials[2]

A straight quartz tubular reactor of dimensions, 0.3 cm i.d. x 17.7 cm was used for the pyrolysis of Bio-polymeric components (cf. Figure 2.1). 30±0.2 mg of sample was placed inside the quartz tube and held in place by quartz wool. The volume of the reactor was 1.25 mL. A residence time of 0.2 seconds was chosen for all temperature runs. Equation 3 above was used to calculate the flow rates of the pyrolysis gas through the reactor based on a residence time, t = 0.2 seconds. Table 2.0 gives the flow rates for each temperature run derived from equation 3. The
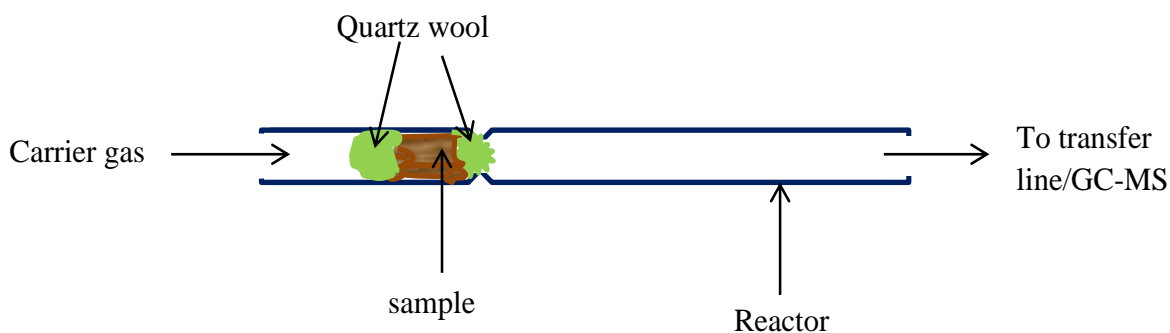
Figure 2.1. Straight-tubular flow reactor for biopolymer pyrolysis

quartz tubular flow reactor shown in Figure 2.1 was designed and constructed by a quartz blower assigned by the chemistry department to fabricating glass/quartz materials. Tubular reactors have been in use for many years and are generally acceptable because in addition to withstanding high temperatures (about 1400 K), they have very small coefficient of thermal expansion [3, 5].

---

[2] Reproduced in part with permission from Kibet J. K.; Lavrent K., and Dellinger, B. *Molecular Products and Radicals from the Pyrolysis of Lignin*, Environmental Science & Technology, 2012, **46**, 12994−13001. Copyright American Chemical Society, 2012

All the connections to the quartz tubular flow reactor are made of silica to maintain an inert atmosphere [5]. Nitrogen was the carrier gas for the pyrolytic condition while 4% O_2 in N_2 was the carrier gas for the reactive (oxidative) condition. The flow of the carrier gas was controlled by a digital mass flow controller (Siera, Model 810-DR-2) which has the capacity to deliver up to 700 mL/min of gas into the reactor system.

The flow-reactor effluent is transported through a transfer line heated at 275 ˚C to prevent condensation along the transfer line. The transfer line is coated with deactivated silica lined with steel tube. In addition, there is a splitter in the transfer line to deliver only a small amount of sample to the GC-MS system without damage to the detector. The splitter also helps to maintain a constant pressure of 1 atm. in the reactor. This splitter is controlled by a pressure gauge where the excess effluent flows through a charcoal trap and out to a fume hood.

2.3. Sample preparation

The compounds used in this study were lignin (hydrolytic lignin extracted using sulphuric acid), L-tyrosine and L-glutamic acid. The samples were obtained from Sigma Aldrich, USA, (percent purity, ≥ 99%) and were used without further treatment. 30±0.2 mg of sample was weighed and packed in a straight tube reactor and held in place by quartz wool. Thermolysis of sample was conducted at typical increments of 50 ˚C starting at 200 ˚C until no more products were detected. The residence time was kept constant at 0.2 seconds within a total pyrolysis time of 3 minutes. The pyrolysis gas for pyrolysis under inert conditions was N_2 while for oxidative, the pyrolysis gas was 4% O_2 in N_2. These conditions were chosen to mimic the burning conditions in a cigarette.

2.4. Detailed operation of the Pyr-GC-MS system[3]

In order to obtain results that are not only consistent but reproducible, the System for Thermal Diagnostic Studies (STDS) must be cleaned and baked out daily. To do this, all the portions of the system must be baked out at appropriate temperatures in a flow of air. The GC housing the reactor and the gas lines, and the transfer line were baked at a temperature of 400 ˚C under an air flow of 50 mL/min. The injection port was baked at 300 ˚C. At the end of each day, the transfer line was removed and cleaned using isopropyl alcohol before baking it out overnight. This procedure usually cleaned out the entire system except the GC/MS. The GC oven was set at 250 ˚C for Gas-Pro column or 300 ˚C for the DB5-MS column and held for 30 minutes before setting it at 120 ˚C for the entire night. Each day before the start of any experiment the mass spectrometer was tuned to check for any leakages, and water levels in the instrument. This procedure was very critical in order to prevent contamination and prolong the life of the EI filament.

Quantitative transport was initiated before any experiment was conducted to ensure that there were no leaks in the system and guarantee the pyrolysis system was clean. This test was carried out under conditions that the sample did not degrade. The flow rate in the transfer line was monitored to make sure that it was constant and did not fluctuate. If the flow rate was not consistent, and the pressure was not stable when the transfer line was connected to the GC/MS then leaks could be present in the system. This was corrected before any experiment could begin. To correct for any leaks in the system, a gas leak detector was used to check for leaks. Whenever leaks were found along the gas lines, transfer lines, or reactor-injection port interface, the

---

[3] Reproduced in part with permission from Kibet J. K.; Lavrent K., and Dellinger, B. *Molecular Products and Radicals from the Pyrolysis of Lignin*, Environmental Science & Technology, 2012, **46**, 12994−13001. Copyright American Chemical Society, 2012

connections were tightened and quantitative transport experiment repeated to make sure no leaks were in the system.

A step by step procedure for conducting a single experiment is described in detail as follows.

1. Set the GC injection port at a temperature that will vaporize the sample into the gas phase

2. The GC oven was set at 200 ˚C in order to maintain the sample in the gas phase throughout the system

3. The transfer line was set at 275˚C to ensure the pyrolysate transported was in the gas phase and no condensation occurred along the transfer line

4. The temperature in the reactor and the pyrolysis gas flow rate was set as desired

5. Connect the transfer line to the GC/MS system where the pyrolysate are condensed at the head of the column under liquid nitrogen at -60˚C before being desorbed down the GC column after a pyrolysis time of 3 minutes

6. Steps 1-5 are repeated for subsequent runs

2.5. Fractional pyrolysis and fractional oxidative pyrolysis[4]

The thermal degradation of biopolymer/biopolymer mixture was investigated in a tubular flow reactor over the temperature range of 200-900 ˚C at atmospheric pressure, typically in 50 ˚C increments under two reaction regimes (pyrolysis in N_2 and oxidative pyrolysis in 4% O_2 in N_2) using the System for Thermal Diagnostic Studies (STDS) [1, 3]. The gas flow rate was designed to maintain a constant residence time of 0.2 s. 30±0.2 mg of sample were loaded into the tubular

---

[4] Reproduced in part with permission from Kibet J. K.; Lavrent K., and Dellinger, B. *Molecular Products and Radicals from the Pyrolysis of Lignin*, Environmental Science & Technology, 2012, **46**, 12994−13001. Copyright American Chemical Society, 2012

quartz reactor (0.3 cm i.d. x 17.7 cm, volume 1.25 mL) and held in place by quartz wool to avoid being swept by carrier gas flowing through the reactor. The reactor containing the sample was then placed inside an electrically heated furnace at a heating rate of 10°C/sec for 3 minutes. The furnace was then turned off and the sample cooled with flowing N_2 while exposing the reactor to a cooling fan. This method of thermolysis of sample closely resembles the TGA technique wherein a sample boat is used to hold the sample in the reactor. The benefits of this technique are two-fold: 1) the sample is held intact in the reactor, and 2) the carrier gas flows uniformly through the sample during the entire analysis, resulting in highly reproducible analyses. Besides, due to high flow rates, the contact time with charred material is short enough (0.2 seconds) to minimize secondary reactions. For longer residence times in the region of several seconds to minutes, secondary reactions dominate.

2.6. GC – MS characterization of molecular products [5]

The gas chromatography–mass spectroscopy (GC/MS) analysis of the pyrolysate was conducted with an Agilent 6890N gas chromatography equipped with a 5973N mass selective
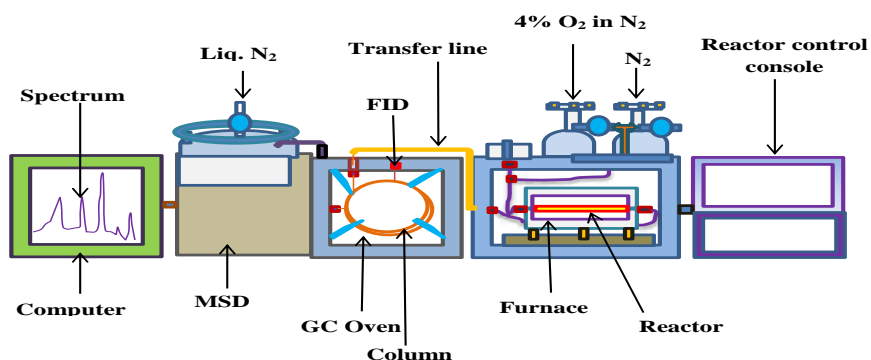
Figure 2.2. Instrumentation assembly (system for thermal diagnostic studies, STDS)

[5] Reproduced in part with permission from Kibet J. K.; Lavrent K., and Dellinger, B. *Molecular Products and Radicals from the Pyrolysis of Lignin*, Environmental Science & Technology, 2012, **46**, 12994−13001. Copyright American Chemical Society, 2012

detector (MSD) with an ion source of electron impact (EI) at 70 eV. Two GC columns, a Gas-pro column (60 m x 0.32 mm i.d x 0.25 μm) for analysis of low molecular weight products and a DB5-MS column (30 m x 0.25 mm x 0.25 μm) for the determination of high molecular weight products were used. A 'Y' connector was introduced to the Gas-Pro column to connect it to a Flame Ionization Detector (FID) for analysis of small hydrocarbons that could not be condensed at -60 ˚C (cf. Figure 2.2). To analyze small hydrocarbons, a gas sampling valve was used in place of a cold finger. The temperature programming was typically: -60 ˚C initial temperature; holding for 3 min to heating rate of 15 ˚C/min to 130 ˚C intermediate temperature; holding for 1 min to heating rate of 25 ˚C/min to 300 ˚C for the DB5-MS column and 260 ˚C for the Gas-Pro column (final temperature; holding for 5 min). The injector, FID detector, and MSD detector temperatures were 250, 275, and 280 ˚C, respectively. Ultra high purity (UHP, 99.999%) helium was used as the carrier gas at constant flow of 3.3 mL/min. The MS was operated on Total Ion Current Mode (TIC) on a mass scan range of 15 - 600 amu. The compounds were identified using a NIST software package and confirmed by enhanced data software package. Standards were used in identification of compounds i n conjunction with NIST data base, enhanced data software package developed by Agilent technologies and thorough literature searches, resulting to sufficiently high confidence in the pyrolysis products presented in this work. Accordingly, critical emphasis has been given to those products which can easily be correlated with the structure of the starting material.

2.7. Calibration of molecular products

Standards for most reaction products were purchased from Sigma Aldrich Inc. (USA). Standards of percent purity $\geq$ 99% were used for calibration of pyrolysis products. For those pyrolysis products where standards were not available, the peak area count obtained from

integration of respective TIC chromatograms were plotted as a function of temperature in order to determine their yield distribution over the entire pyrolysis temperature range.

The percent yield of each calibrated product was evaluated using equation 2.7.

$$Y = \left(\frac{weight\ of\ product, w}{weight\ of\ sample, W} \right) x\,100 \qquad\qquad Equation\ 2.7$$

where Y is the yield of the pyrolysis product in Wt %.

After the compounds were calibrated, product distribution curves displaying the yield of various products with pyrolysis temperature were generated. A list of the products and their respective Wt % yields at various temperatures was also presented.

2.8. Electron paramagnetic resonance (EPR) analysis

The term electron paramagnetic resonance refers to the resonant absorption of the electromagnetic radiation by electronic systems which possess permanent magnetic moments due
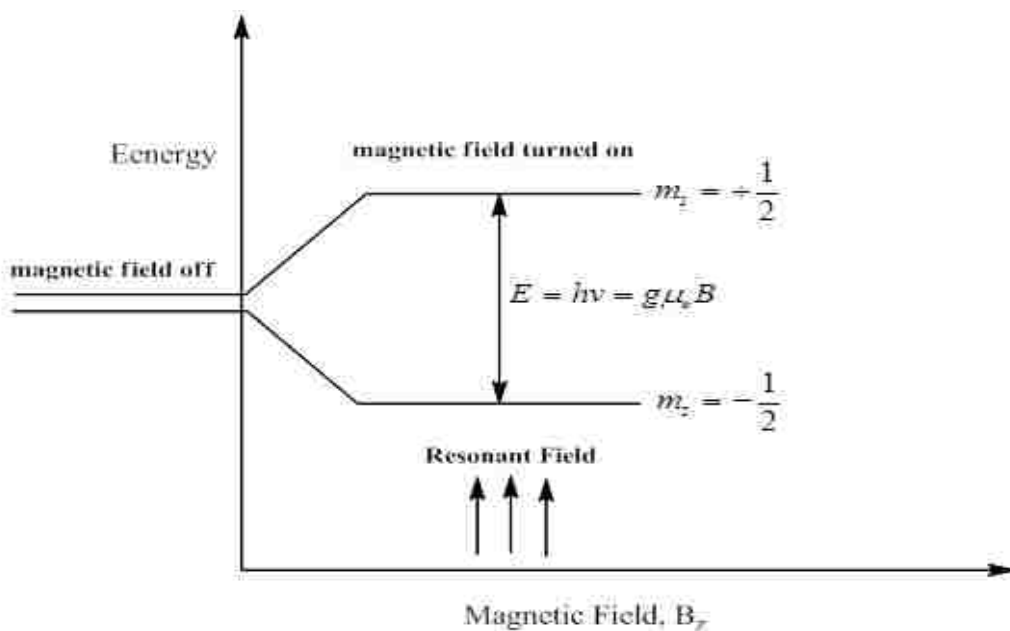
Figure 2.3. The effect of magnetic field on unpaired electron

to the orbital as well as spin angular momentum of electrons which are therefore paramagnetic [6]. According to Lancaster [6], for a free electron having a total angular momentum J situated in a magnetic field B, the energy levels are $W_{MJ} = g\beta BM_J$ *Equation 2.4*

where β is the Bohr magneton, M_j the projection of *J* in the direction of the magnetic field *B,* and ranges from $-J$ to $+J$ in integral steps. The g-factor (spectroscopic splitting factor) is given by

Landěs formula: $g = 1 + \left(\dfrac{J(J+1) + S(S+1) - L(L+L)}{2J(J+1)} \right)$ *Equation 2.5*

where J and L are the orbital and the spin angular momenta respectively [6].

Accordingly, EPR is a spectroscopic technique used to detect species having one or unpaired electrons. When an external magnetic field is applied, the paramagnetic electrons can either orient in a direction parallel or anti-parallel to the path of the magnetic field. This phenomenon creates two different energy levels for the unpaired electrons and making it possible for absorption of electro-magnetic radiation to occur when electrons are focused between the two energy levels. The condition where the magnetic field and the microwave frequency produce absorption is known as the resonance condition. The g-factor is characteristic of EPR analysis. It is a dimensionless quantity proportional to the frequency and the magnetic field at resonance condition.

$$hv = g\mu_o B$$ *Equation 2.6*

where h is planks constant (6.63 x 10^{-34} Js), ν is frequency (Hz), μ_o is the Bohr magneton (9.27 x 10^{-24} J T^{-1}), B is magnetic field (Teslas).

2.9. EPR analysis of radicals[6]

To determine the existence of gas-phase radicals in the thermal degradation of lignin, pyrolysis was investigated in an isothermal flow reactor in conjunction with a cold finger-EPR assembly depicted in Figure 2.4, *vide infra*. A straight tube isothermal quartz flow reactor (10 mm x 50 mm) was used for pyrolysis of lignin at a fixed temperature 450 ^{o}C. 10-15 mg of lignin was loaded into the inlet of the reactor at ~ 200 ^{o}C and held in place by quartz wool. Elimination of low molecular products of lignin pyrolysis initiated between 50 and 150 $^{\circ}$C [7, 8]. The flow of N_2/CO_2 gas at less than 0.3 torr pressure swept the evaporated volatile components into the reactor. The pyrolyzed products exiting the reactor were pumped directly onto a cold finger.
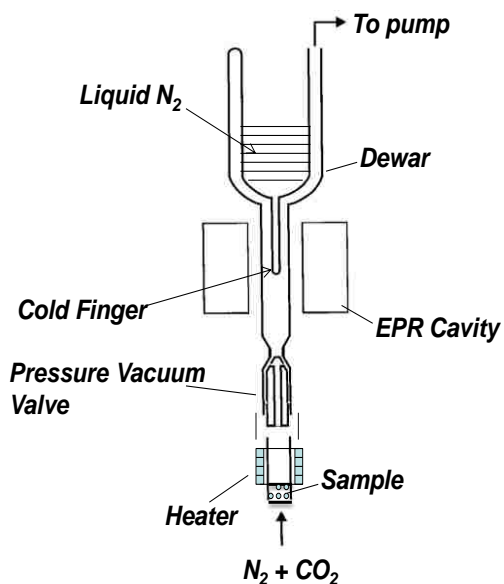
Figure 2.4. Cold finger assembly for LTMI-EPR.

The CO_2 carrier easily freezes at liquid nitrogen temperature, creating an ideal matrix for condensation of radicals [9]. To avoid product condensation on the walls, all transfer lines from

---

[6] Reproduced in part with permission from Kibet J. K.; Lavrent K., and Dellinger, B. *Molecular Products and Radicals from the Pyrolysis of Lignin*, Environmental Science & Technology, 2012, **46**, 12994−13001. Copyright American Chemical Society, 2012

the reactor to the EPR cavity were maintained at 100 ^{o}C regardless of the pyrolysis reactor temperature. The Dewar was also equipped with a special PTFE pressure – vacuum valve (PV-ANV, Wilmad) which allowed the Dewar (maintained at liquid N_2 temperature) to be separated from the reactor and evacuated to 10^{-4} torr for EPR analysis.

To generate reference phenoxy-type radicals, the frozen aquatic solutions of different phenols in 4 mm EPR tubes were subjected to UV photolysis in a Dewar with liquid nitrogen at 253.7 nm. The 253.7 nm light was generated using a conventional, mercury vapor, ozone-free pencil lamp from Jelight, Inc. This double bore lamp, with a 9 mm O.D, produced a 4 inch light at a power of ~9 mW/cm^2 at 254 nm measured at a distance of 15 mm from the lamp. The phenoxy, *o*-hydroxy phenoxy, and *p*-hydroxyphenoxy radicals were also produced from gas-phase photolysis of phenol, catechol and hydroquinone, respectively, at room temperature and very low pressure (≤ 0.1 torr).

All EPR spectra were recorded on a Bruker EMX-20/2.7 EPR spectrometer (X-band) with dual cavities, modulation and microwave frequencies of 100 kHz and 9.516 GHz, respectively. The typical parameters were: sweep width of 200 G, EPR microwave power of 1 - 20 mW, and modulation amplitude of ≤ 4 G. Time constant and sweep time were varied. Values of g-factors were calculated using Bruker's WINEPR program, which is a comprehensive line of software, allowing control of the Bruker EPR spectrometer, data-acquisition, automation routines, tuning, and calibration programs on a windows-based PC [10]. The exact g-values for key spectra were determined by comparison with a 2,2-diphenyl-1-picrylhydrazyl (DPPH) standard. In some experiments, gradual warming of the Dewar was employed to allow annealing of the matrix and annihilation of mobile or very reactive radicals. This resulted in production of cleaner, sharper spectra of single radicals under environmentally isolated conditions.

2.10. Modeling of lignin pyrolysis using CHEMKIN

Simulations of lignin pyrolysis using CHEMKIN was conducted for comparison with experimental data obtained from Pyr-GC-MS analysis. Modeling makes predictions for conditions where experimental results cannot be accessed, such as at high heating rates and shorter residence times. Modeling is also important when testing the validity of experimental results. Nevertheless, the robustness of the model must be verified by running sensitivity analysis tests. The first step in setting up the lignin model was to use experimental data to constraint the model. Kinetic models using mechanisms for fundamental thermodynamic and kinetic principles are necessary in describing reaction systems in combustion. A major condition for these simulations is accurate thermodynamic property data (estimated or experimental) for all molecular or radical species considered in the mechanism [11].

2.10.1. The principles of CHEMKIN combustion suite

- To model experimental data with the objective of testing mechanistic hypothesis

- To predict the time dependence of reaction species concentration in complex chemical mechanisms

- To optimize the reaction conditions of chemical processes in the gas-phase, in atmospheric and bio-organic chemistry etc.

- Supports large chemical kinetic mechanisms, hundreds of species and thousands of reactions

- Provides accurate information about a reacting system: complex dependency between major and minor species, dominant reaction paths, sensitivity of results to reaction parameters etc.

2.10.2. Gas-phase rate expressions for CHEMKIN

CHEMKIN provides the user with a variety of options for expressing gas-phase chemical reactions where reaction rates can depend on species composition, temperature, and pressure [12, 13]. While elementary reactions that obey the law of mass action are the default formulations, the user has available a variety of optimal formulations for specifying global or lumped expressions. To formulate reduced mechanism for thermal degradation of lignin, reactions that bear resemblance to the key elementary reactions and bear reference to combustion behavior of lignin were lumped together [11]. Often in gas-phase kinetics, it is useful to use reduced chemistry with options that allow the user to define arbitrary reaction order for a species in place of the coefficients used [12].

2.10.3. The Landau-Teller formulation of the rate expression

The basic Landau-Teller expression is given by equation 2.8.

$$k_{f\ i} = A_i \exp\left(\frac{B_i}{T^{\frac{1}{3}}} + \frac{C_i}{T^{\frac{2}{3}}}\right) \qquad \qquad Equation\ 2.8$$

In the gas-phase kinetics, there is the possibility of unifying the Arrhenius equation and the Landau-Teller equation to give equation 2.9.

$$k_{f\ i} = A_i T^{\beta i} \exp\left(-\frac{E_i}{RT} + \frac{B_i}{T^{\frac{1}{3}}} + \frac{C_i}{T^{\frac{2}{3}}}\right) \qquad \qquad Equation\ 2.9$$

where B and C are the Landau-Teller Constants, E is the activation energy, β is a fitting parameter, and A is a pre-exponential factor representing the collision frequency between reacting species. By setting β_i and C_i to zero, the Arrhenius equation is regenerated while setting

β_i and E_i to zero, the standard Landau-Teller expression is recovered [12, 13]. The temperature-dependent portion of the rate equation contains and expression which is computationally, expensive to calculate [12, 13]. Nonetheless, CHEMKIN provides additional sub-routines for the temperature-dependent rate coefficients. The sub-routine for evaluation of the temperature-dependent rate coefficient for each reaction is called CKKFRT, while the sub-routine that takes in the rate constant as input and returns the species net rates of production is called CKWYPK [12, 13].

The symbols representing the compounds to be modeled in lignin pyrolysis are shown in Table 2.2 whereas the input file (gas-phase scheme) developed to be able to run CHEMKIN is presented in table 2.3. In this input, the thermodynamic functions; entropy (S), heat capacity (Cp), enthalpy (H) were taken as 0. This is because, reversible reactions were assumed not to occur and consequently the principle of detailed balancing does not apply. The input parameters (pre-exponential factor, A, the activation energies, Ea, and the rate constants were determined from experimental results.

Table 2.2. Symbols used to represent intermediates in CHEMKIN simulation

Symbol		Compound
1.	B(L)	lignin
2.	B(furf)	furfural
3.	B	benzene
4.	B(S)	syringol
5.	B(Ph)	phenol
6.	B(tol)	toluene
7.	B(v)	4-vinylguaiacol
8.	B(G)	gases
9.	B(C)	char

Table 2.3. Reactions considered for lignin pyrolysis

```
REACTIONS CONSIDERED                   (k = A T**b exp(-E/RT))
                                       A            b            E
        B(L)=>B(S)                     3.47E+02     0.0          6000.0
        B(L)=>B(ph)                    3.55E+03     0.0          10000.0
        B(L)=>B(furf)                  5.75E+01     0.0          5600.0
        B(L)=>B(tol)                   8.32E+05     0.0          17000.0
        B(L)=>B                        6.31E+06     0.0          22400.0
        B(L)=>B(V)                     4.90E+01     0.0          4200.0
        B(S)=>B(Ps)                    1.98E+05     0.0          19000.0
        B(ph)=>B(Pph)                  4.00E+02     0.0          6300.0
        B(furf)=>B(Pfurf)              5.60E+03     0.0          9000.0
        B(tol)=>B(Ptol)                7.20E+02     0.0          7500.0
        B=>B(P)                        4.10E+02     0.0          7000.0
        B(V)=>B(Pv)                    2.10E+02     0.0          5000.0
        B(L)=>B(G1)                    1.10E+02     0.0          4600.0

UNITS for the preceding reactions (unless otherwise noted): A units mole-cm-sec-K, E units cal/mole

NOTE (for information purposes only), the following species do not participate in any reaction: B(C1) B(G2)
B(C2)
```

2.11. References

1. Rubey, W.A. and R.A. Grant, *Design aspects of a modular instrumentation system for thermal diagnostic studies.* Review of Scientific Instruments, 1988. **59** (2): p. 265-269.

2. Striebich, R.C. and W.A. Rubey, *A System for thermal diagnostic studies.* American Laboratory, 1990. **22** (1): p. 64-&.

3. Rubey, W.A. and R.A. Carnes, *Design of a tubular reactor instrumentation assembly for conducting thermal-decomposition studies.* Review of Scientific Instruments, 1985. **56** (9): p. 1795-1798.

4. Dellinger, B., et al., *Incinerability of hazardous wastes.* Hazardous Waste & Hazardous Materials, 1986. **3**(2): p. 139-150.

5. Hair, M.L., *Hydroxyl-Groups on silica surface.* Journal of Non-Crystalline Solids, 1975. **19** (Dec): p. 299-309.

6. Lancaster, G., *Electron paramagnetic resonance (A Review).* Journal of Materials Science, 1967. **2** (5): p. 489-495.

7. Shafizadeh, F., *Introduction to pyrolysis of biomass.* Journal of Analytical and Applied Pyrolysis, 1982. **3** (4): p. 283-305.

8.   Serio, M.A., et al., *Measurement and modeling of lignin pyrolysis.* Biomass & Bioenergy, 1994. **7** (1-6): p. 107-124.

9.   Khachatryan, L., et al., *Formation of cyclopentadienyl radical from the gas-phase pyrolysis of hydroquinone, catechol, and phenol.* Environmental Science & Technology, 2006. **40** (16): p. 5071-5076.

10.   Eaton, G.R., et al., *Quantitative EPR.* 2010. **Springer Wien NewYork** (Germany): p. 185

11.   Ritter, E.R. and J.W. Bozzelli, *Therm - Thermodynamic property estimation for gas-phase radicals and molecules.* International Journal of Chemical Kinetics, 1991. **23** (9): p. 767-778.

12.   ChemKin 15101, *Reaction design*: San Diego, 2010

13.   ChemKin 10101, *Reaction design*: San Diego, 2010

CHAPTER 3: RESULTS[7]

      The System for Thermal Diagnostic Studies (STDS), Gas-Chromatography (GC-MS), Low Temperature Isolation Matrix Electron Paramagnetic Resonance (LTIM-EPR), and CHEMKIN combustion suite were used to obtain the data presented in this study. The details of the above techniques were discussed in chapter 2. The STDS system consists of the reactor where pyrolysis of sample (lignin, tyrosine, and glutamic acid) occurs before pyrolysis gas (N_2 or 4% O_2 in N_2) sweeps the pyrolysate through a transfer line. The pyrolysate was trapped at the head of the GC column at -60 ˚C (using liquid nitrogen) for three minutes before desorbing down the column for analysis using a mass selective detector (MSD). The residence time inside the reactor was kept constant at 0.2 seconds for each pyrolysis temperature. LTIM-EPR was used to investigate the presence of intermediate phenoxy radicals from the pyrolysis of lignin. CHEMKIN combustion code was used to model (simulate) the pyrolysis of lignin. Experimental data was used to determine the kinetic and thermodynamic parameters such as the rate constant, k, the Arrhenius factor A, and the activation energy, Ea.

3.1. Molecular products and radicals from pyrolysis of lignin

3.1.1. Fractional pyrolysis

      The primary compounds detected and their relative distributions for fractional pyrolysis of lignin are presented in Figure 3.1. Syringol, 4-propenyl syringol, guaiacol (and its derivatives) were the most abundant products of lignin pyrolysis (cf. Figure 3.1 A). The second most abundant products were catechol, phenol, and their derivatives (cf. Figure 3.1 B). These data are consistent with work performed by other researchers, indicating the three marker compounds of

---

[7] Reproduced in part with permission from Kibet J. K.; Lavrent K., and Dellinger, B. *Molecular Products and Radicals from the Pyrolysis of Lignin*, Environmental Science & Technology, 2012, **46**, 12994−13001. Copyright American Chemical Society, 2012

lignin (syringyl, guaiacyl, and hydroxyphenyl units) should be the major products. Of the classes of compounds analyzed, phenols (phenol, *p*-cresol, and catechol), syringol, 4-propenyl syringol, and guaiacols (guaiacol, eugenol, 4-ethylguaiacol, and 5-methylguaiacol etc.) were the most abundant products contributing over 40% of the total compounds analyzed.

Furfuryl alcohol achieved a maxima at ~300 ˚C while methanol, furan, 2-methyl furan, and 2,5-dimethylfuran maxima were at ~450 ˚C (cf. Figure 3.1 C). The low molecular weight, oxygenated products peaked between 250 and 400 ˚C, while the majority of the phenolic
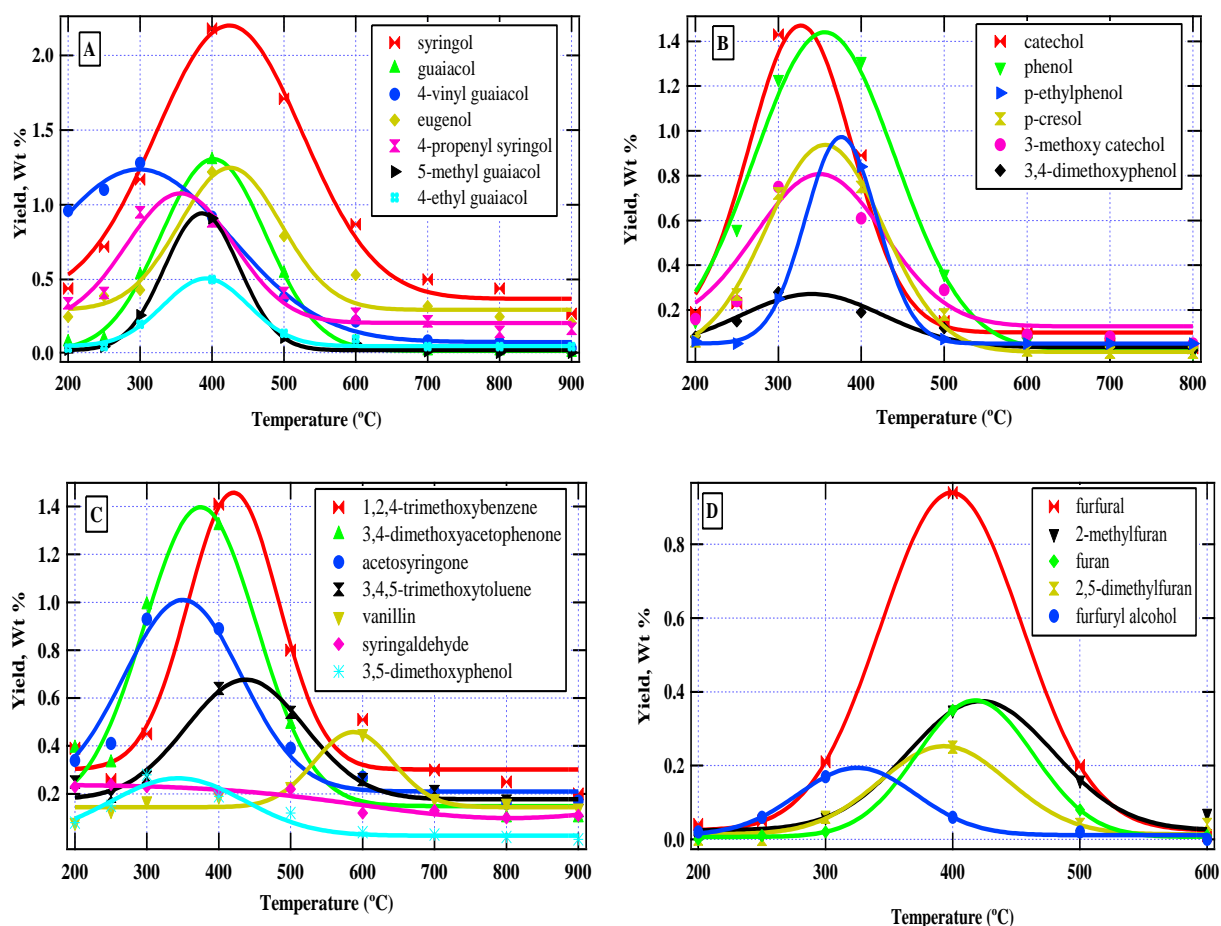
Figure 3.1. Wt % yields of major oxygenated products (A-D) from fractional pyrolysis of lignin in N_2 at 1 atm.

compounds exhibited maxima between 350 and 500 ˚C. The aromatic hydrocarbons (benzene, toluene, and styrene) exhibited maxima between 500 and 700 ˚C (cf. Figure 3.2 D). The benzene concentration peaked at ~ 650 ˚C, while that of toluene peaked at~500 ˚C.

Common PAHs, e.g. anthracene, phenanthrene, and fluorene, in contrast to other reports, were not detected [1]. This may be due to the low reactivity of lignin and longer residence time of 1.4 s [1], instead of the 0.2 s in this work. However, trace quantities of some large PAHs, i.e.
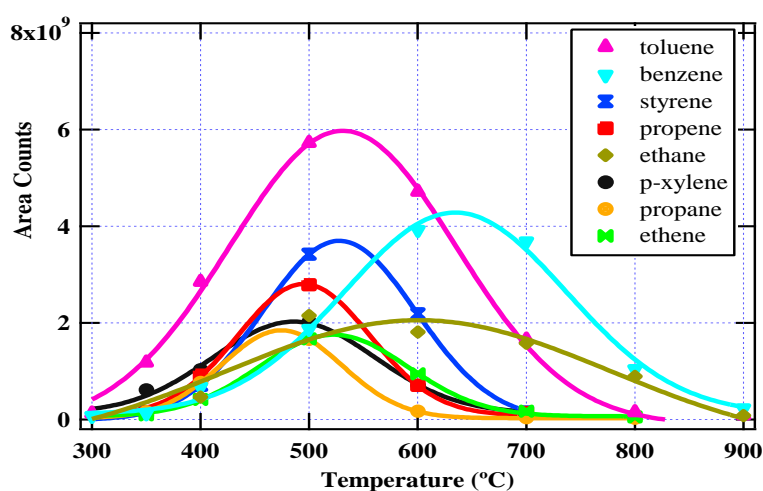
Figure 3.2. Yields (based on GC area counts) of the major hydrocarbon products from fractional pyrolysis of lignin in N_2 at 1 atm.

2,4,5,7-tetramethylphenanthrene, dibenzo(fg,op)naphthacene, benzo(a)pentacene, and dibenzo(b,k)chrysene were observed between 400 and 900 ˚C. Small hydrocarbons such as ethene, propene, propane, and olefins (1-butene and 2-butene) were also formed. In this category, propene was the major product. Ethene, which is a major precursor for PAH formation was present in low amounts and this may explain why many PAHs have not been detected in pyrolysis studies of lignin. The general mechanism for PAH formation under the severe temperature conditions encountered during biomass pyrolysis is that PAH are formed from the pyrosynthesis of smaller unstable fragments produced by biomass pyrolysis [2]. The structures

for large molecular compounds detected are presented for purposes of enhancing our comprehension on the pyrolysis character of lignin (cf. Schemes 3.1). The quantified weight % yields for the major products determined from fractional pyrolysis of lignin are presented in Table 3.1.

Table 3.1. Quantified yields of fractional pyrolysis of lignin at different temperatures (Wt % yields) in N_2 at 1 atm.

Quantified Compounds	Pyrolysis Temperature (˚C)								
	200	250	300	400	500	600	700	800	900
phenol	0.00	0.15	0.56	1.23	1.31	0.36	0.06	0.03	0.01
p-cresol	0.00	0.06	0.27	0.72	0.75	0.18	0.02	0.01	0.01
catechol	0.00	0.19	0.23	1.43	0.89	0.15	0.10	0.05	0.03
4-ethyl phenol	0.06	0.05	0.25	0.84	0.07	0.05	0.050	0.50	0.00
guaiacol	0.08	0.10	0.53	1.30	0.54	0.08	0.02	0.02	0.01
syringol	0.44	0.72	1.11	2.18	1.71	0.87	0.50	0.44	0.27
4-vinyl guaiacol	0.96	1.10	1.28	0.92	0.38	0.22	0.09	0.08	0.04
vanillin	0.08	0.13	0.17	0.19	0.23	0.45	0.18	0.16	0.14
syringaldehyde	0.23	0.24	0.23	0.21	0.22	0.12	0.13	0.10	0.11
acetosyringone	0.34	0.41	0.93	0.89	0.39	0.27	0.21	0.16	0.12
eugenol	0.25	0.39	0.43	1.22	0.79	0.53	0.32	0.25	0.21
4-propenyl syringol	0.41	0.34	0.95	0.89	0.27	0.41	0.22	0.15	0.17
5-methyl guaiacol	0.03	0.05	0.26	0.91	0.11	0.07	0.02	0.01	0.01
4-ethyl guaiacol	0.04	0.05	0.20	0.50	0.14	0.10	0.05	0.05	0.05
3,5-dimethoxy phenol	0.08	0.15	0.28	0.19	0.12	0.04	0.03	0.02	0.00
3-methoxy catechol	0.16	0.24	0.75	0.61	0.29	0.09	0.08	0.05	0.00
1,2,4-trimethoxybenzene	0.39	0.26	0.45	1.45	0.80	0.51	0.30	0.25	0.20
3,4-dimethoxyacetophenone	0.39	0.33	0.99	1.32	0.49	0.27	0.13	0.10	0.10
furan	0.00	0.01	0.06	0.35	0.16	0.07	0.00	0.00	0.00
2-methyl furan	0.00	0.01	0.06	0.35	0.16	0.07	0.00	0.00	0.00
2,5-dimethy furan	0.00	0.01	0.02	0.25	0.08	0.01	0.00	0.00	0.00
furfural	0.04	0.05	0.21	0.94	0.20	0.01	0.00	0.00	0.00
Furfuryl alcohol	0.02	0.06	0.17	0.06	0.02	0.00	0.00	0.00	0.00
benzene	0.00	0.00	0.01	0.11	0.31	0.66	0.62	0.18	0.04
toluene	0.00	0.00	0.02	0.47	0.95	0.78	0.27	0.02	0.02
p-xylene	0.00	0.00	0.00	0.17	0.34	0.12	0.02	0.00	0.00
styrene	0.00	0.00	0.00	0.12	0.57	0.37	0.03	0.00	0.00
Wt % Total	**4.00**	**5.10**	**10.42**	**19.82**	**12.29**	**6.86**	**3.53**	**2.63**	**1.54**

The release of volatile matter begins quickly with increase in temperature and then decreases with increasing temperature [3]. This is because at low temperature, the volatile matter

slowly evaporates and the carbonization reactions dominate as temperature increases leading to the cracking of unstable components of the volatile matter [3]. Similar trends were observed for the oxidative pyrolysis of lignin except that in this case the pyrolysis product yields were lower owing to oxidation effects.

3.1.2. Conventional pyrolysis

Under conventional pyrolysis, new sample was loaded into the reactor for every pyrolysis
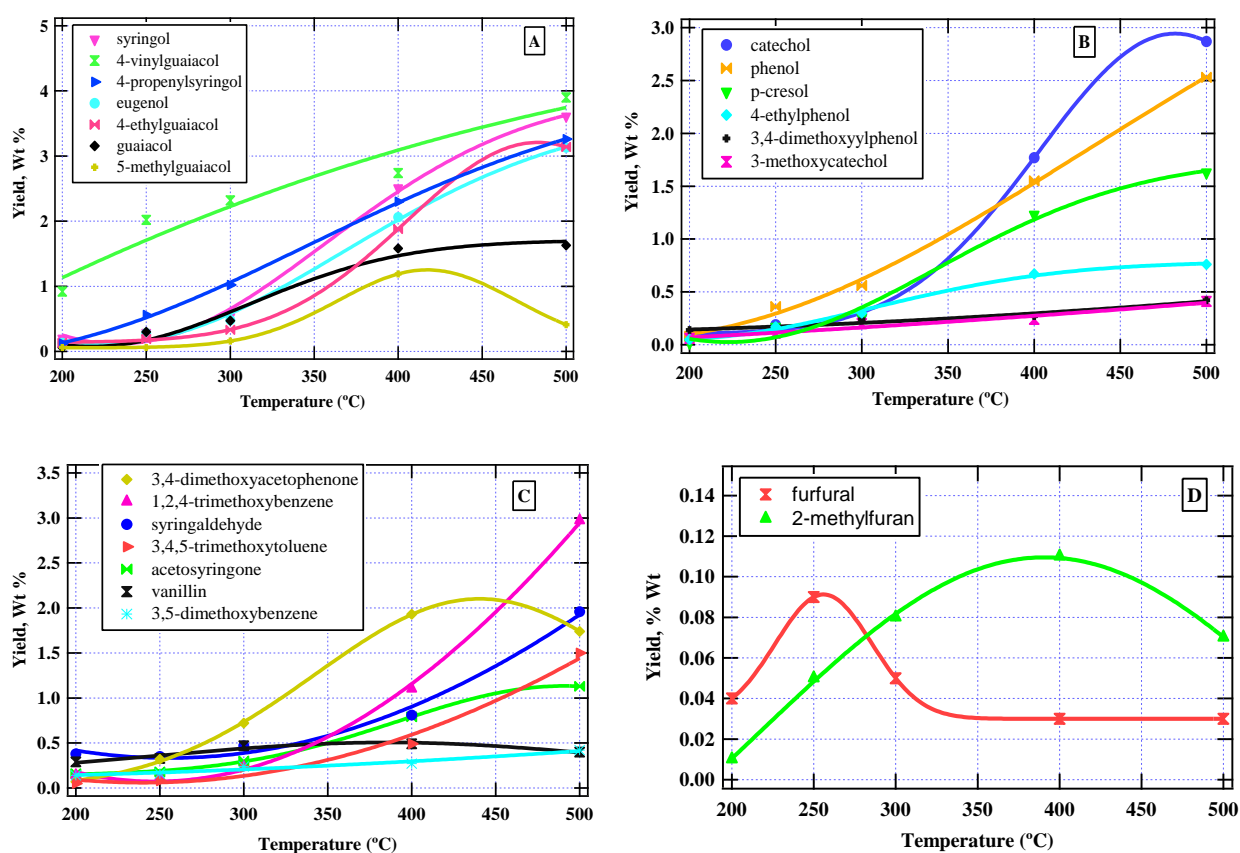
Figure 3.3. Wt % yields of major oxygenated products (A-D) from conventional pyrolysis of lignin in N_2 at 1 atm.

temperature. For this reason, the growth of molecular products from pyrolysis was expected to increase with increasing temperature as opposed to those observed from fractional pyrolysis. Product distributions for pyrolysis of fresh lignin samples at every temperature were very similar

to results from fractional pyrolysis of lignin; however, the concentration maxima were > 400 ˚C (cf. Figure 3.3). Syringol and 4-vinylguaiacol were the primary products (cf. Figure 3.3 A) while catechol and phenol were the main products from the simple phenol family (cf. Figure 3.3 B). Some compounds, such as 3-methoxycatechol and 3,4-dimethyl phenol did not increase significantly with increased temperature, (cf. Figure 3.3 B). It is clear from Figure 3.3 A, syringol and 4-vinylguaiacol are exclusively the major products from the conventional pyrolysis of lignin.

Whereas the concentration of 3,4-dimethoxyacetophenone increased linearly with temperature before decreasing at about 450 ˚C, that of 1,2,4-trimethoxybenzene, 3,4,5-trimethoxybenzene, syringaldehyde, and acetosyringone increased linearly with temperature for the entire temperature range (cf. Figure 3.3 C). The concentration of vanillin remained virtually constant and did not appear to change with increase in temperature. Generally, the molecular products from conventional pyrolysis of lignin increased with increase in temperature as shown in Figures 3.3 A, 3.3 B, and 3.3 C. Nevertheless, the concentrations of low molecular weight products, furfural, and 2-methyl furan first increased and then dropped as the pyrolysis temperature was increased, Figure 3.3 D.

It is clear from Tables 3.1, and 3.2 *vide infra* that there are distinct similarities as well as differences between Conventional and Fractional pyrolysis with respect to the type of products evolved and the yields of those reaction products. While the reaction products evolved are similar in both cases, their respective product yields are characteristically different. The reaction products from conventional pyrolysis achieve high yields with increased temperature while the yields of products from fractional pyrolysis decrease with increasing temperature. This is not surprising because while products are continually generated from the same sample in the case

fractional pyrolysis, products are generated from a new sample in the case of conventional pyrolysis. A list of quantified compounds from thermolysis of lignin is presented in Table 3.2.

Table 3.2. Quantified yields of conventional pyrolysis of lignin at different temperatures (Wt % yields) in N_2 at 1 atm.

Quantified Compounds	Pyrolysis Temperature (˚C)				
	200	250	300	400	500
phenol	0.08	0.36	0.56	1.55	2.53
p-cresol	0.02	0.17	0.26	1.23	1.63
catechol	0.07	0.19	0.29	1.77	2.87
4-ethyl phenol	0.05	0.17	0.30	0.67	0.76
guaiacol	0.06	0.30	0.47	1.58	1.63
syringol	0.20	0.29	0.53	2.51	3.61
4-vinyl guaiacol	0.92	2.02	2.32	2.74	3.90
vanilin	0.29	0.33	0.47	0.49	0.40
syringaldehyde	0.38	0.35	0.47	0.81	1.96
acetosyringone	0.16	0.18	0.30	0.79	1.13
eugenol	0.13	0.28	0.48	2.06	3.13
4-propenyl syringol	0.12	0.56	1.02	2.30	3.26
5-methyl guaiacol	0.06	0.06	0.16	1.19	0.41
4-ethyl guaiacol	0.13	0.19	0.33	1.88	3.14
3,5-dimethoxyphenol	0.14	0.16	0.24	0.27	0.42
3-methoxy catechol	0.06	0.11	0.20	0.24	0.41
1,2,4-trimethoxybenzene	0.14	0.12	0.23	1.10	2.97
3,4-dimethoxyacetophenone	0.07	0.32	0.72	1.93	1.74
3,4,5-trimethoxy toluene	0.05	0.08	0.23	0.49	1.50
2-methyl furan	0.01	0.05	0.08	0.11	0.07
furfural	0.04	0.09	0.05	0.03	0.03
Wt % Total	**3.18**	**6.38**	**9.71**	**25.74**	**37.50**

3.1.3. Fractional oxidative pyrolysis

The maximum product distributions were between 200 and 400˚C. (cf. Figure 3.4). The major products were syringol, guaiacol and phenol, (cf. Figure 3.4 A). The syringol maximum was at ~ 350 ˚C, while guaiacol and phenol maxima were at ~ 330 ˚C. While formaldehyde and acetone were formed in significant quantities under oxidative pyrolysis, they were only formed in trace quantities under pyrolysis. Formaldehyde achieved a maximum concentration at ~250

˚C while acetone achieved a maxi mum concentration at ~350 ˚C (cf. Figure 3.4 A). Most of the phenol compounds, i.e. catechol, and 3-methoxyphenol were formed in low yields, compared to pyrolysis. This is because and oxidizing atmosphere decreases the concentration of certain
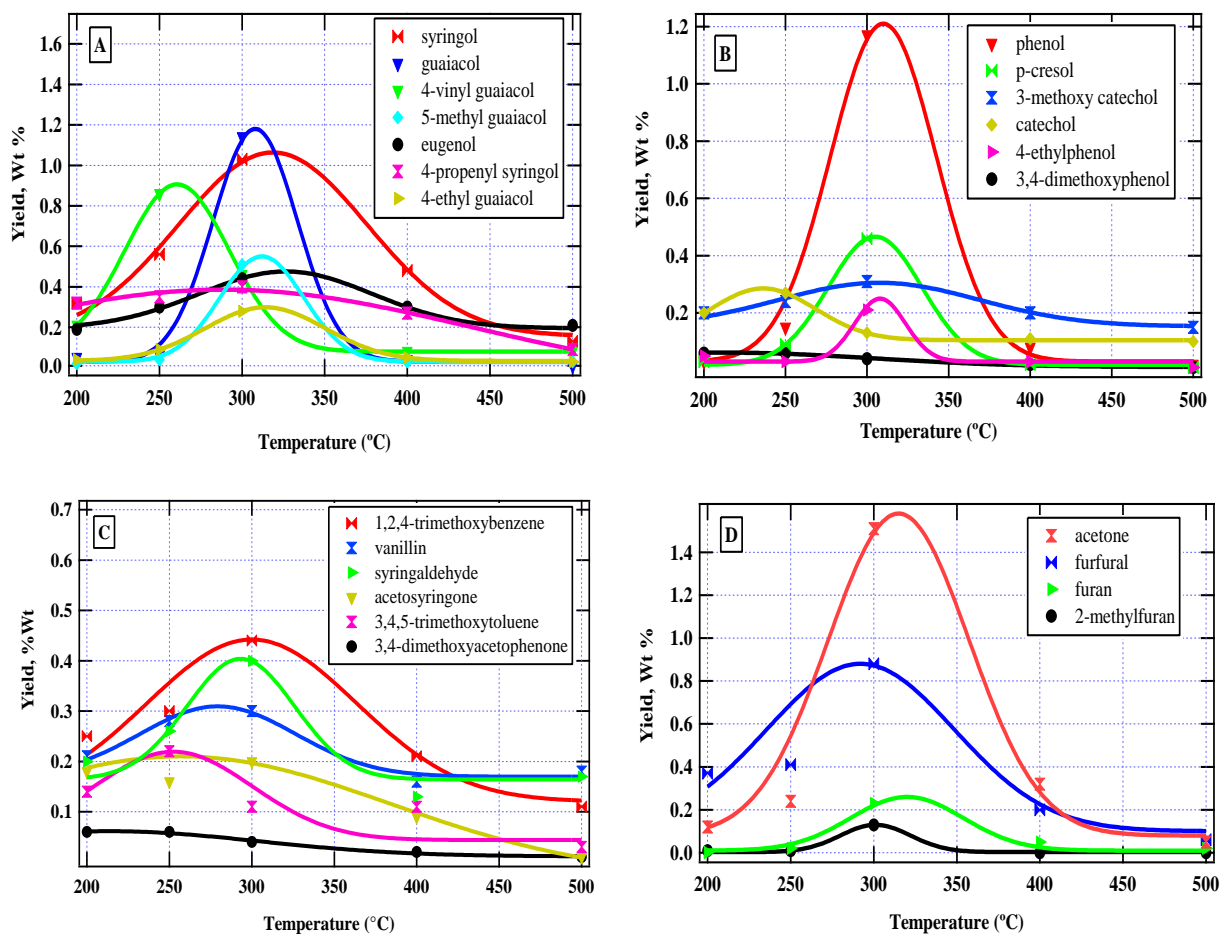
Figure 3.4. Wt % yields of major oxygenated products (A) and hydrocarbons (B) from fractional oxidative pyrolysis of lignin in 4% O_2 in N_2 at 1 atm.

reaction products by converting them to CO, CO_2 or H_2O. An oxidizing phenomenon becomes more pronounced with increase in temperature. PAHs were not observed, probably due to oxidation of precursors [1]. The already partially oxidized lignin components, i.e. syringol, guaiacol and phenol did not exhibit a significant decrease in yield. Another group of compounds which comprised 1,2,4-trimethoxybenzene, syringaldehyde, 3,4-dimethoxy benzene, vanillin,

acetosyringone, and 3,4,5-trimethoxy toluene (cf. Figure 3.4 C) peaked at about 300 ˚C. Interestingly, this group of compounds appears to have a similar release temperature range. Their yields growth rapidly between 200 and 300 ˚C before decreasing rapidly between 350 and 400 ˚C, and generally level off between 400 and 500 ˚C. Although PAHs were not formed from this experiment, a number of hydrocarbon products were determined. These included, in order of decreasing abundance toluene, benzene, propene and propane.

Hydrocarbon products are normally formed at high temperatures because they are the result of thermal cracking reactions but under an oxidizing atmosphere, the rate of formation of reaction products is increased because a reactive atmosphere (oxidation) enhances the formation of reaction products although an oxidizing atmosphere can oxidize the products and hence reduce their concentrations. Table 3.3 above summarizes the major reaction products quantified under oxidative Fractional pyrolysis. Majority of the products pass through a maximum between 250 and 300 ˚C.
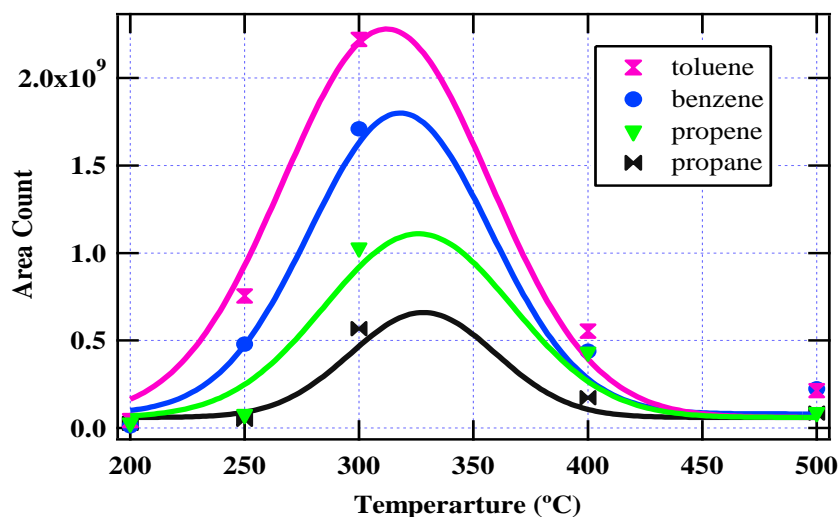
Figure 3.5. Yields (based on GC area counts) of the major hydrocarbon products from oxidative fractional pyrolysis of lignin 4% O_2 in N_2 at 1 atm.

Table 3.3. Quantified yields of oxidative fractional pyrolysis of lignin at different temperatures (Wt % yields) in 4% O_2 in N_2 at 1 atm.

Quantified Compounds	Pyrolysis Temperature (˚C)				
	200	250	300	400	500
phenol	0.03	0.15	1.17	0.08	0.02
p-cresol	0.03	0.09	0.46	0.02	0.01
catechol	0.20	0.27	0.13	0.11	0.10
4-ethyl phenol	0.05	0.03	0.21	0.03	0.01
guaiacol	0.05	0.06	1.14	0.04	0.01
syringol	0.32	0.36	1.03	0.48	0.13
4-vinyl guaiacol	0.21	0.86	0.46	0.08	0.08
vanilin	0.21	0.28	0.30	0.16	0.18
syringaldehyde	0.20	0.26	0.40	0.13	0.17
acetosyringone	0.18	0.16	0.20	0.09	0.01
eugenol	0.19	0.30	0.44	0.30	0.21
4-propenyl syringol	0.32	0.35	0.40	0.27	0.09
5-methyl guaiacol	0.02	0.04	0.51	0.03	0.03
4-ethyl guaiacol	0.04	0.09	0.28	0.05	0.03
3,5-dimethoxy phenol	0.06	0.06	0.04	0.02	0.01
3-methoxy catechol	0.20	0.24	0.31	0.21	0.15
1,2,4-trimethoxybenzene	0.25	0.30	0.44	0.21	0.11
3,4-dimethoxyacetophenone	0.06	0.06	0.04	0.02	0.02
3,4,5-trimethoxy toluene	0.14	0.22	0.11	0.11	0.03
furan	0.00	0.02	0.23	0.05	0.02
2-methyl furan	0.01	0.01	0.13	0.00	0.00
acetone	0.12	0.24	1.51	0.32	0.05
furfural	0.07	0.12	0.17	0.26	0.06
furfuryl alcohol	0.37	0.41	0.88	0.20	0.06
benzene	0.00	0.01	0.29	0.07	0.04
toluene	0.01	0.13	0.37	0.09	0.09
Wt % Total	**3.34**	**5.12**	**11.5**	**3.43**	**1.72**

3.1.4. Conventional oxidative pyrolysis

The maximum yields for most compounds were at slightly lower temperature, 400 – 450 ˚C, with syringol, guaiacol, catechol, and phenol being the dominant products (cf. Figures 3.6). While the concentration of majority of reaction products increased with increase in temperature, the concentration of some reaction products including 4-ethyl guaiacol, 3,5-dimethoxyphenol, 3-methoxy catechol, and acetone did not appear to increase with increase in temperature. Only a

few hydrocarbon products were detected, including benzene, toluene, and *p*-xylene. We believe

an oxidizing atmosphere inhibits the formation of hydrocarbon products since their precusrsors

are oxidized to smaller molceules such as H_2O, CO and CO_2. This observation has been
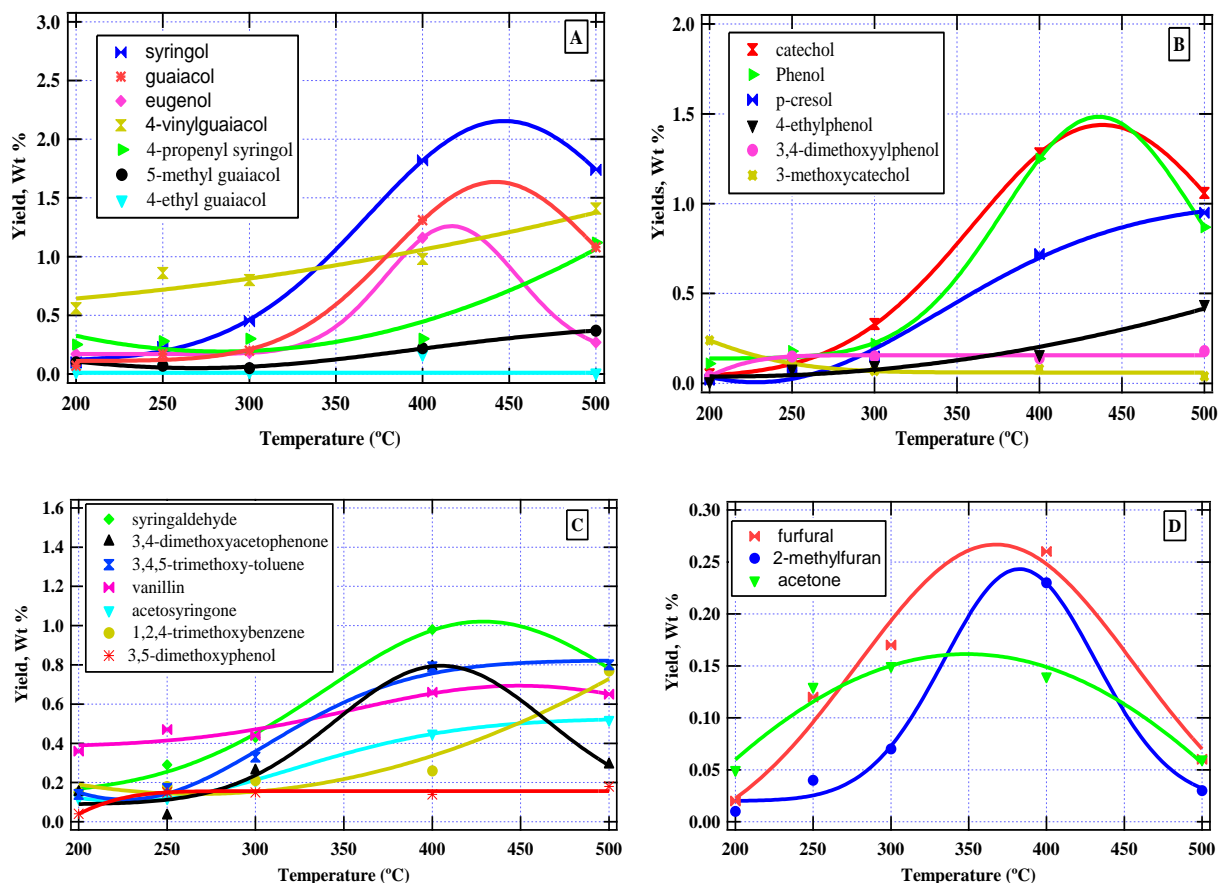
Figure 3.6. Wt % yields of major oxygenated products (A-D) from conventional oxidative pyrolysis of lignin in 4% O_2 in N_2 at 1 atm.

supported previously by Sharma *et al*. that an oxidizing atmosphere may enhance the yields of

reaction products but may also oxidize some of the reactive species or their precursors before

they are formed [1]. A list of the major products and their Wt % yields are presented in Table 3.4

below. From the table, it is notable that the concentrations of most products pass through a

maximum at 400 ˚C before decreasing significantly at 500 ˚C.

Table 3.4. Quantified yields of conventional oxidative pyrolysis of lignin at different temperatures (Wt % yields) in 4% O_2 in N_2 at 1 atm.

Quantified Compounds	Pyrolysis Temperature (˚C)				
	200	250	300	400	500
phenol	0.11	0.18	0.22	1.25	0.87
p-cresol	0.02	0.07	0.15	0.72	0.95
catechol	0.05	0.10	0.33	1.28	1.06
4-ethyl phenol	0.01	0.08	0.10	0.16	0.44
guaiacol	0.07	0.17	0.20	1.31	1.08
syringol	0.10	0.23	0.45	1.82	1.74
4-vinyl guaiacol	0.56	0.86	0.80	0.98	1.41
vanilin	0.36	0.47	0.44	0.66	0.65
syringaldehyde	0.15	0.29	0.43	0.98	0.78
acetosyringone	0.12	0.12	0.21	0.45	0.52
eugenol	0.17	0.17	0.18	1.16	0.27
4-propenyl syringol	0.25	0.28	0.30	0.30	1.12
5-methyl guaiacol	0.10	0.07	0.05	0.22	0.37
4-ethyl guaiacol	0.02	0.06	0.02	0.17	0.01
3,5-dimethoxyphenol	0.04	0.15	0.15	0.14	0.18
3-methoxy catechol	0.24	0.11	0.07	0.08	0.04
1,2,4-trimethoxybenzene	0.15	0.18	0.21	0.26	0.77
3,4-dimethoxyacetophenone	0.15	0.03	0.26	0.79	0.29
3,4,5-trimethoxy toluene	0.14	0.17	0.33	0.79	0.80
2-methyl furan	0.01	0.04	0.07	0.23	0.03
furfural	0.02	0.12	0.17	0.26	0.06
acetone	0.05	0.13	0.15	0.14	0.06
Wt % Total	**2.89**	**4.08**	**5.29**	**14.15**	**13.5**

3.1.5. Decomposition profile for lignin

The thermal degradation profile of lignin under a wide range of pyrolysis conditions is presented in Figure 3.7. At 200 ˚C, the weight loss of lignin under pyrolytic conditions (partial and conventional pyrolysis) was small, however; a rapid weight loss of ~20% was recorded between 300 and 400 ˚C. For partial oxidative pyrolysis, the weight loss was more rapid over the same temperature range, viz. ~40%. A percent weight loss of~30% was observed for conventional oxidative pyrolysis. Consequently, the partial oxidative pyrolysis curve exhibited a

faster decomposition rate than that of conventional oxidative pyrolysis. Both partial and conventional oxidative pyrolysis curves approached zero mass at 500°C (cf. Figure 3.7).

At about 400 °C the change in the percent mass loss is at its maximum for both pyrolysis and oxidative pyrolysis. This is the region where the release of volatile products is the highest and the char yield is the lowest [4]. Two fundamental temperature zones were observed in the
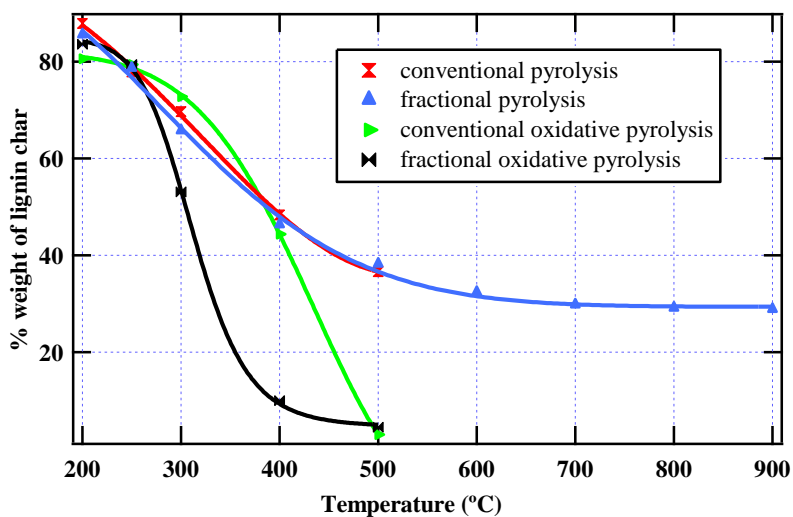
Figure 3.7: % Char yields from pyrolysis and oxidative pyrolysis of lignin in N_2 and 4% O_2 in N_2 at 1 atm.

decomposition profile of lignin. The first zone, with high weight loss (200-500 °C), yielded the majority of the volatile components (cf. Figures 3.1-3.5). The second stage of weight loss (500-900 °C), the decomposition of lignin was nearly constant for pyrolysis experiments, and the lignin char was largely aromatic. This resulted in the formation of hydrocarbon products such as, propene, propane, benzene, toluene, and styrene, etc., (cf. Figure 3.2). Table 3.5 gives the Wt % char yields from the thermal degradation of lignin under different reaction conditions. Temperature, oxygen concentration, and pyrolysis technique were the major variables in lignin pyrolysis.

Table 3.5. Wt % Yields of char from the thermal degradation of lignin at 1 atm.

Temp. (°C)	200	250	300	400	500	600	700	800	900
Fractional Pyrolysis	85.57	78.64	65.74	46.30	38.19	32.36	29.77	29.12	28.83
Oxidative Fractional Pyrolysis	83.62	79.40	53.16	10.12	4.53	-	-	-	-
Conventional Pyrolysis	87.91	77.93	69.70	48.34	36.67	-	-	-	-
Conventional Oxidative Pyrolysis	80.64	79.44	72.83	44.40	3.12	-	-	-	-

3.1.6. Radicals from conventional pyrolysis of lignin

Radical intermediates from lignin pyrolysis at 450 °C were collected and analyzed using the LTMI-EPR technique.   A representative spectrum of trapped radicals at 77 K is depicted in Figure 3.8, spectrum 1. The spectrum is an unstructured singlet (with some anisotropy) with g =
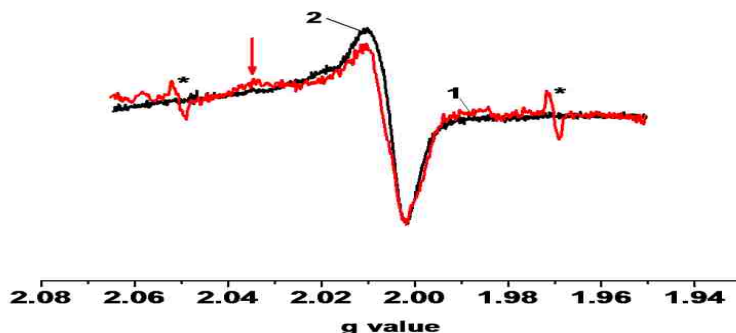
Figure 3.8. The EPR Spectra of Radicals Accumulated on Cold Finger from Lignin Pyrolysis at 450 °C (spectrum 1, g = 2.0071, ΔHp-p = 13.5G) and from Burley Tobacco Pyrolysis at 450 °C (spectrum 2, g = 2.0056, ΔHp-p = 13G).

2.0072 and ΔHp-p = 14.0G. The small peaks on both sides of the main spectrum (marked with an asterisk in Figure 3.8) indicate the presence of trace quantities of oxygen as E-lines (K=1, J=2, M=1→2) [5]. These are readily removed by annealing [6].   The E-lines are absorption bands observed when excited oxygen species absorb electromagnetic radiations.

Because the pyrolysis of tobacco has much in common with the pyrolysis of lignin [7, 8], an EPR spectrum from Burley tobacco pyrolysis at 450 ^{o}C in the presence of less than 1 torr of air was overlaid with the spectrum of lignin (cf. Figure 3.8, spectrum 2). The tobacco spectral parameters were g = 2.0056 and ΔHp-p = 13G. Both spectra were similar and exhibited similar anisotropy, which is believed to be due $RO_2^{\bullet}$ easily formed in the pyrolysis of tobacco, catechol,
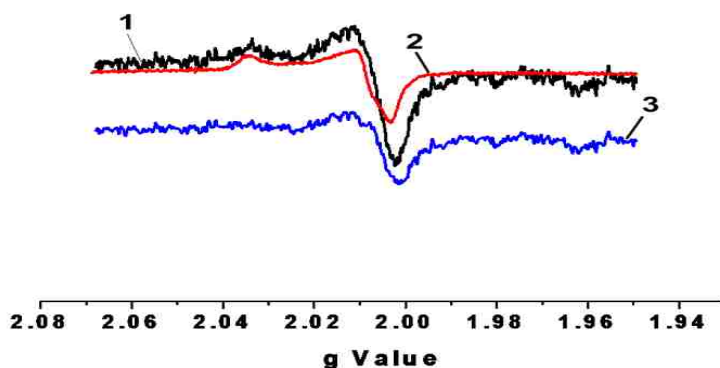
Figure 3.9. The EPR Spectra of Radicals Accumulated on Cold Finger from Lignin Pyrolysis at 450 ^{o}C and 0.1 torr air (black line, g = 2.0073, ΔHp-p = 15.0 G) and Overlaid Red reference EPR Spectrum of $RO_2^{\bullet}$ (g = 2.0089) Produced from Heating of Tobacco to 450 ^{o}C in Vacuum. The Blue Spectrum (g = 2.0064, ΔHp-p = 18G) is the Subtraction Spectrum of the Lignin and $RO_2^{\bullet}$.

hydroquinone, and other organics in presence of small quantities of oxygen [6, 9-13]. When the expected spectrum of $RO_2^{\bullet}$ (cf. Figure 3.9, spectrum 2) was subtracted from the spectrum of EPR radicals from lignin pyrolysis (cf. Figure 3.9, spectrum 1) a residue spectrum was observed with a high g-value of 2.0064 and ΔHp-p = 18G (cf. Figure 3.9, spectrum 3).

This difference in spectrum closely resembles that of a phenoxy or substituted phenoxy, such as a hydroxyphenoxyl (neutral semiquinone radical) [14]. Indeed, the radicals from phenol and hydroquinone/catechol pyrolysis (and photolysis), produced as molecular products from lignin decomposition, have previously been identified as phenoxy and semiquinone radicals,

respectively [6, 12, 14-17]. These EPR spectra were structureless singlet lines detected by the LTMI-EPR technique at 77 K. The phenoxy radical spectrum exhibited a broader (ΔHp-p = 16G) than semiquinone radical (ΔHp-p = 12G) [13].

3.2. Molecular products from pyrolysis and oxidative pyrolysis of tyrosine[8]

3.2.1. Fraction pyrolysis of tyrosine

This investigation revealed the principal products of tyrosine pyrolysis in a N_2 atmosphere were phenolic compounds (phenol, *p*-cresol, and *o*-cresol), acetonitrile, benzaldoxime, ethyl benzene, and toluene. The maximum release of phenolic compounds and nitrogen containing compounds of low molecular weight occurred between 350 and 450˚C, while the maximum concentration of aromatic hydrocarbons and nitrogen containing compounds of high molecular weight occurred between 550 and 650 ˚C. Phenol and *p*-cresol reached maximum concentrations at 450 ˚C, Figure 3.10 A. Acetonitrile and benzaldoxime reached a maximum concentration at ~ 400 ˚C, (cf. Figures 3.10 B, and 3.10 **C**). Hydrogen cyanide was formed in significant amounts throughout the entire pyrolysis temperature range and appears to exhibit constant concentration as the pyrolysis temperature is increased, (cf. Figure 3.10 B). The behavior demonstrated by hydrogen cyanide is remarkable and needs further investigation. This behavior is not only manifested in pyrolysis but also in oxidative pyrolysis. The major hydrocarbon products: ethylbenzene, toluene, and benzene, peaked between 600 and 650 ˚C respectively, (cf. Figure 3.11 B).

The hydrocarbon products are believed to be the result of thermal cracking and concerted rupture of the C-C chain followed by molecular growth to form aromatic species [18]. Generally, product profile concentrations first increased with increase in pyrolysis temperature before falling off at high temperatures due to decomposition. Low molecular weight hydrocarbons
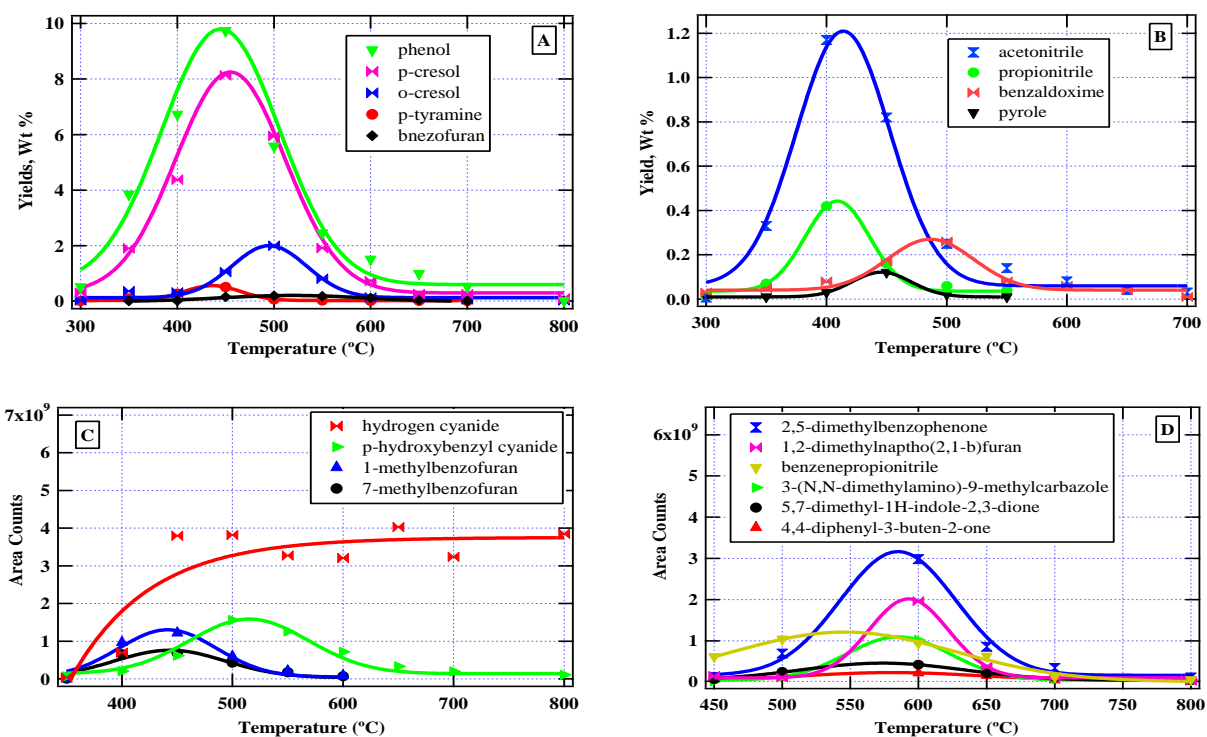
Figure 3.10. Wt % yields of the major phenol and nitrogen containing products (A and B) yields (based on GC area counts) of other major products (C and D) from the pyrolysis of tyrosine in N_2 at 1 atm.

(propene, 1-butene) yields were the lowest. High molecular weight polynuclear aromatic compounds (PAHs), were formed at high temperatures (450-800 °C). Substituted PAHs included: 1,2-dimethylnaptho[2,1-b]furan, 2,5-dimethylbenzophenone, 3-(N,N-dimethylamino)-9-methylcarbazole, 5,7-dimethyl-1H-indole-2,3-dione, and 4,4-diphenyl-3-buten-2-one. A summary of the quantified compounds are presented in Table 3.6.
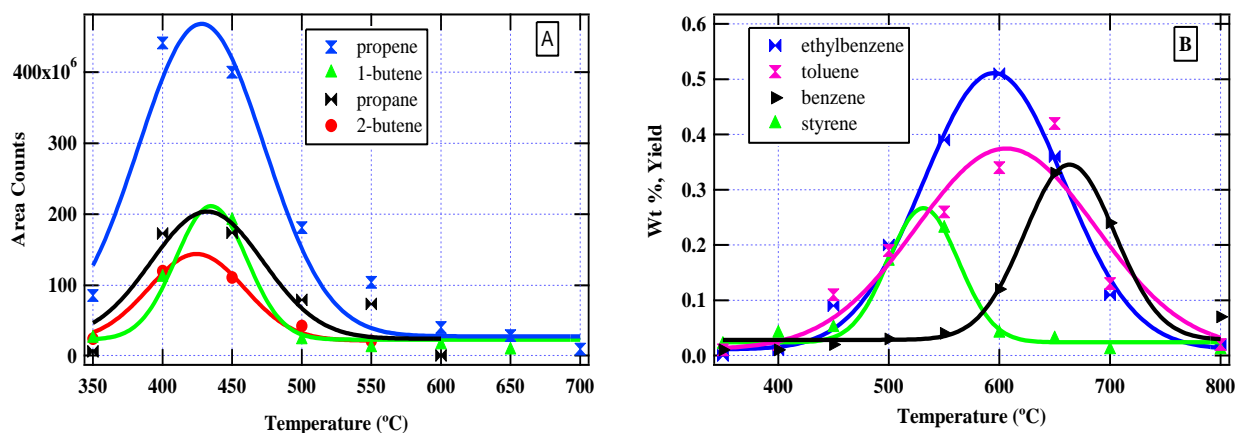
Figure 3.11. Yields (based on GC area counts) of low molecular weight hydrocarbon products (A) and Wt % yields aromatic hydrocarbons (B) from the pyrolysis of tyrosine in N_2 at 1 atm.

Table 3.6. Quantified yields of fractional pyrolysis of tyrosine at different temperatures (Wt % yields) in N_2 at 1 atm.

Quantified Compounds	Pyrolysis Temperature (˚C)									
	300	350	400	450	500	550	600	650	700	800
phenol	0.51	3.85	6.72	9.73	5.58	2.45	1.51	0.99	0.53	0.02
p-cresol	0.31	1.90	4.28	8.31	5.95	1.95	0.72	0.26	0.25	0.10
o-cresol	0.01	0.36	0.32	1.05	2.00	0.81	0.14	0.13	0.07	0.03
p-tyramine	0.01	0.10	0.27	0.57	0.51	0.07	0.03	0.02	0.02	0.01
benzaldoxime	0.00	0.03	0.05	0.08	0.17	0.26	0.08	0.06	0.04	0.01
benzofuran	0.01	0.02	0.16	0.20	0.18	0.12	0.04	0.01	0.00	0.00
acetonitrile	0.00	0.33	1.17	0.82	0.25	0.14	0.08	0.04	0.03	0.00
propionitrile	0.01	0.07	0.42	0.16	0.06	0.04	0.00	0.00	0.00	0.00
pyrrole	0.00	0.00	0.01	0.03	0.12	0.01	0.00	0.00	0.00	0.00
benzene	0.00	0.01	0.01	0.02	0.03	0.04	0.12	0.33	0.24	0.07
toluene	0.00	0.01	0.02	0.11	0.19	0.26	0.34	0.42	0.13	0.02
p-xylene	0.00	0.02	0.04	0.05	0.17	0.23	0.04	0.03	0.01	0.01
styrene	0.00	0.00	0.01	0.09	0.20	0.39	0.51	0.36	0.11	0.02
Wt % Total	**0.86**	**6.7**	**13.48**	**21.22**	**15.41**	**6.77**	**3.61**	**2.65**	**1.43**	**0.29**

3.2.2. Fractional oxidative pyrolysis of tyrosine

The principal products in this experiment were *p*-tyramine and phenolic compounds with a combined percent yield of over 80%. The formation of *p*-tyramine, with a maximum yield at 370 ˚C, (cf. Figure 3.12 A) was a very important observation. This compound has been known to

57

have a low volatility and is not easily transported for detection. Li et al. concedes that the low volatility behavior of *p*-tyramine/4-(2-aminoethyl) phenol was responsible for eluding detection in their experiments [18]. *p*-tyramine should be an important signature of tyrosine pyrolysis
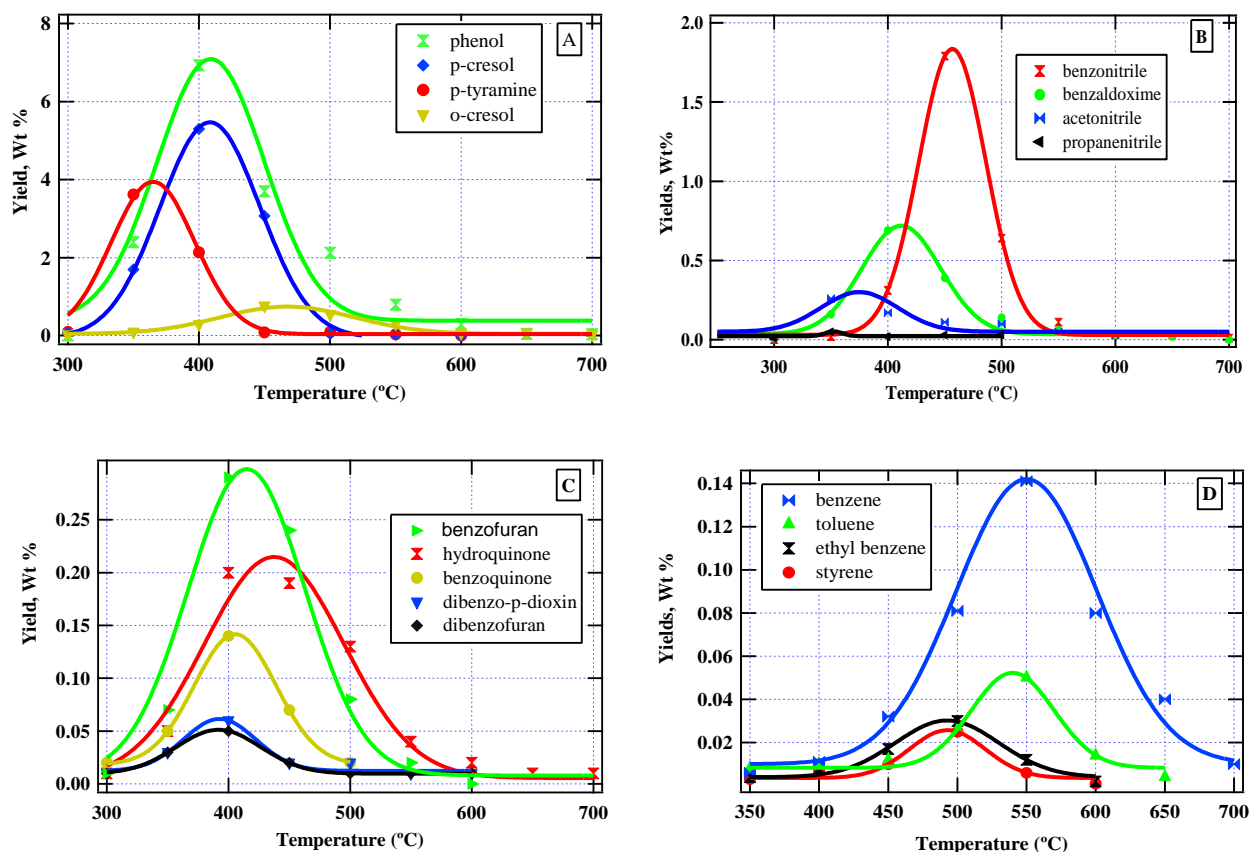
Figure 3.12. Wt % Yields of major products (A-D) from the oxidative pyrolysis of tyrosine in 4% O_2 in N_2 at 1 atm.

formed from decarboxylation reactions. In our study, *p*-tyramine was observed in high concentration under oxidative pyrolysis conditions and low concentrations from pyrolysis (cf. Figures 3.12 A and 3.12 A respectively). Oxidative pyrolysis also formed compounds of biological interest: hydoquinone, benzofuran, dibenzofuran, and dibenzo-*p*-dioxin, as well as phenolic compounds (phenol, *p*-cresol, and *o*-cresol). The maximum release of hydroquinone, benzofuran, dibenzo-*p*-dioxin, phenol, *p*-cresol, benzonitrile, and benzaldoxime occurred

between 400 and 450 ˚C (cf. Figure 3.12 A, 3.10 B and 3.12 C). Hydrogen cyanide was formed in low amounts throughout the entire temperature range, (cf. Figure 3.12 B).

Table 3.7. Quantified yields of fractional oxidative pyrolysis of tyrosine at different temperatures (Wt % yields) in 4% O_2 in N_2 at 1 atm.

Quantified Compounds	Pyrolysis Temperature (˚C)								
	300	350	400	450	500	550	600	650	700
*p*henol	0.01	2.40	6.93	3.70	2.13	0.80	0.30	0.05	0.04
p-cresol	0.18	1.70	5.30	3.07	0.05	0.03	0.01	0.00	0.00
o-cresol	0.03	0.1	0.3	0.77	0.55	0.31	0.38	0.08	0.03
p-tyramine	0.10	3.62	2.14	0.10	0.10	0.04	0.03	0.01	0.00
benzaldoxime	0.01	0.16	0.69	0.39	0.14	0.06	0.03	0.02	0.00
p-benzoquinone	0.02	0.05	0.14	0.07	0.02	0.00	0.00	0.00	0.00
hydroquinone	0.01	0.05	0.20	0.19	0.13	0.04	0.02	0.00	0.00
benzofuran	0.01	0.07	0.29	0.24	0.08	0.02	0.00	0.00	0.00
dibenzofuran	0.01	0.03	0.05	0.02	0.01	0.01	0.01	0.00	0.00
dibenzo-*p*-dioxin	0.01	0.03	0.05	0.02	0.02	0.02	0.01	0.01	0.00
benzonitrile	0.00	0.02	0.31	1.79	0.64	0.11	0.03	0.03	0.01
acetonitrile	0.02	0.26	0.17	0.11	0.10	0.05	0.03	0.00	0.00
pyrrole	0.01	0.02	0.02	0.02	0.00	0.00	0.00	0.00	0.00
benzene	0.00	0.01	0.01	0.03	0.08	0.14	0.08	0.04	0.01
toluene	0.00	0.01	0.01	0.01	0.03	0.05	0.01	0.00	0.00
p-xylene	0.00	0.00	0.01	0.02	0.03	0.01	0.00	0.00	0.00
styrene	0.00	0.00	0.01	0.01	0.02	0.01	0.00	0.00	0.00
Wt % Total	**0.42**	**8.53**	**16.63**	**10.56**	**4.13**	**1.69**	**0.93**	**0.24**	**0.09**

Benzene was the dominant product among the aromatic compounds, with a maximum concentration being observed at 550˚C. Ethylbenzene, which was one of the main products in pyrolysis experiments, was formed in nearly trace amounts under oxidative pyrolysis conditions and exhibited a maximum yield at about 450 ˚C (cf. Figure 3.12 D). Quantified yields of products from the thermal degradation of tyrosine are listed in Table 3.7. The concentration of the major reaction products pass through a maximum within a narrow temperature range of 400 and 450 ˚C.

3.2.3. Decomposition profile for tyrosine

Up to 300˚C, the weight loss of tyrosine for both pyrolysis and oxidative pyrolysis was negligible, however; a rapid weight loss of more than 50% occurred between 300 and 400 ˚C (cf.
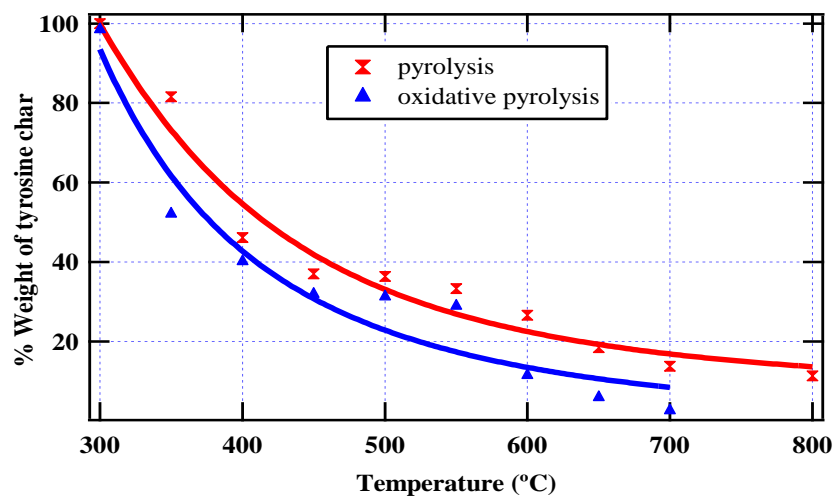
Figure 3.13. Wt % yield of tyrosine char as a function of temperature at 1 atm.

Figure 3.13). This coincided with the formation of the majority of the volatile components. The second stage of weight loss occurred at between 450 and 800 ˚C and was accompanied by release of hydrocarbons and nitro-PAHs. This implies a two stage decomposition process in the thermal degradation of tyrosine. The Char yields from thermolysis of tyrosine are shown in Table 3.8.

Table 3.8. Wt % yields of char from the thermal degradation of tyrosine at 1 atm.

Temp. (˚C)	300	350	400	450	500	550	600	650	700	800
Fractional Pyrolysis	99.91	81.52	46.11	37.00	36.42	33.33	26.64	18.47	13.78	11.42
Oxidative Fractional Pyrolysis	98.43	52.00	40.10	31.92	31.24	28.91	11.55	5.94	2.65	-

Both the pyrolysis and oxidative pyrolysis decomposition curves were similar in behavior but only differed in the rate of decomposition. The oxidative pyrolysis curve assumed a faster

decomposition rate and approached zero at about 700˚C, while the decomposition curve for pyrolysis reached 11.4% degradation at 800 ˚C. This contrasts markedly with the work of Li and his co-workers in which tyrosine decomposed to 19.4% during pyrolysis at 800 ˚C [18]. This difference can be attributed to the experimental conditions employed by Li [18]. While Li and his co-workers used a furnace of heating rate 20 ˚C/min and a constant flow rate of 100 mL/min in a TGA coupled to FT-IR, we used a furnace of heating rate˜ 10˚C/s at a constant residence time of 0.2s.

3.3. Molecular products from pyrolysis and oxidative pyrolysis of glutamic acid[9]

3.3.1. Fractional pyrolysis

A series of nitrogen containing products as well as hydrocarbon products were formed during pyrolysis of glutamic acid in an inert atmosphere. Accordingly, the reaction products from pyrolysis of glutamic acid can be grouped into five classes according to their maximum release temperature (cf. Figure 3.14):

Group 1. The maximum release of these products was between 300 and 400 ˚C with succinimide as the major product peaking at 350 ˚C (cf. Figure 3.14 A). The compounds in this class peak early and decrease sharply as the pyrolysis temperature is increased, implying a short release temperature range.

Group 2. This class of compounds included pyrrole, HCN and acrylonitrile and were generally peaked at about 450 ˚C (cf. Figure 3.14 B). The compounds appeared to be either formed from the decomposition of products in group 1 or breakdown of other intermediates such

---

[9] Reproduced in part with permission from Kibet J. K.; Lavrent K., and Dellinger, B. *Molecular Products from the Pyrolysis and Oxidative Pyrolysis of Glutamic Acid in a Tubular-Flow Reactor*, Energy & Fuels, 2013. Copyright American Chemical Society. (Submitted for Publication).

as pyroglutamic acid and diketo piperazine (cf. Scheme 2). The production of pyrrole from glutamic acid clearly indicates one carboxyl group is lost as carbon dioxide (cf. Scheme 2) whereas the second carboxyl group is incorporated into 2-pyrrolidone ring before converting to pyrrole via the loss of a water molecule [19, 20].

It is notable amino acids are capable of forming a relatively stable nitrogen-aromatic ring in the early stages of thermolysis yielding large amounts of hydrogen cyanide [19]. Nitrogen-containing rings are known to break down at high temperatures to give high levels of hydrogen cyanide [19-21]. Previous pyrolysis of intermediates such as pyrrolidine and 2-pyrrolidone led to
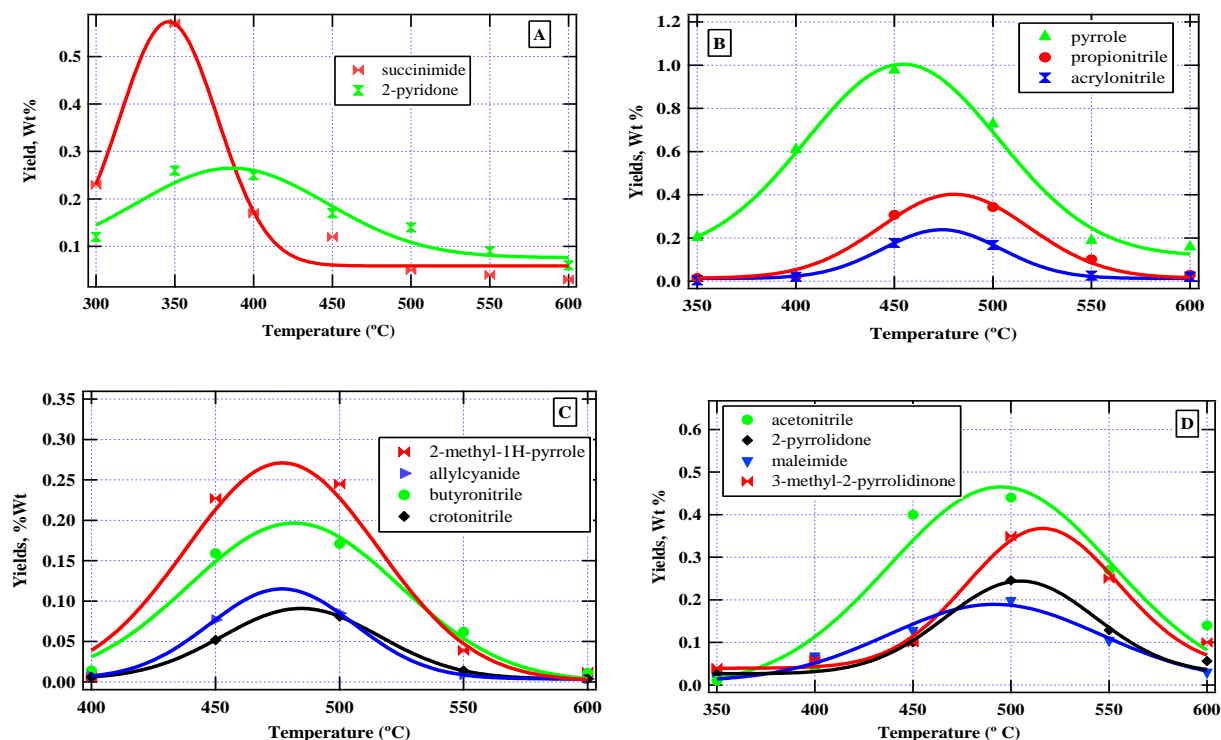
Figure 3.14. Wt % Yields of the major products from the pyrolysis of glutamic acid in N_2 at 1 atm.

observation of high yields of HCN [21]. This observation can be noted from Figure 3.14 B which shows the concentration of HCN increases sharply as the concentrations of succinimide, 2-pyrrolidone, pyridine, and pyrrole decreased.

Group 3. These reaction products have similarities to the products discussed in group 2 and have nearly the same maximum release temperature and concentration (cf. Figure 3.14 C). While the maximum release temperature for compounds in group 2 was 450 ˚C, the maximum release temperature for those in group 3 was about 475 ˚C with the major compound being 2-methyl-1H-pyrrole and allyl cyanide.

Group 4. These products include acetonitrile and 2-pyrrolidone as the major products (cf. Figure 3.14 D, *vide supra*). Acetonitrile is known to peak at high pyrolysis temperatures because it is thought to be formed from thermal decomposition of succinimide, pyrrole, and other heterocyclic products such as indole [22]. This observation can be noted from Figure 3.14 C which shows the concentration of acetonitrile increased sharply as the concentrations of succinimide, 2-pyrrolidinone, pyridine, and pyrrole decreased. It is remarkable that the concentration of acetonitrile and that of HCN both reached a maximum above 400 ˚C (425 and 440 ˚C respectively) suggesting they may be formed from further decomposition of nitrogen-containing aromatic rings in addition to being formed from decomposition of diketo piperazine. Nevertheless, the high concentration of five-membered ring nitrogen-containing compounds including pyrrole, and succinimide at temperatures ≤ 400 ˚C suggest that heterocyclic compounds are favored at low temperatures as compared to low molecular weight nitrogen-containing compounds such as acetonitrile, hydrogen cyanide, and propionitrile (cf. Figure 3.14 A and 3.14 D, *vide supra*).

Group 5. This group of products was exclusively hydrocarbons, with the major products being propene and propane. The Major hydrocarbon products in order of decreasing importance were toluene > benzene (cf. Table 3.9, *vide infra*). Hydrocarbon products are believed to form from homolysis of carbon-carbon bond α to the amino acid group (minor decomposition pathway

for amino acids) to yield an alkyl radical that decomposes to an olefin and an H radical [22]. This explains why alkene products predominate over alkane products [22]. Generally, the principal products in order of decreasing abundance were: Succinimide > pyrrole > acetonitrile > 2-pyrrolidone >3H-pyrrolo[2,3-d]pyrimidin-4(7H)-one   2-methyl-1H-pyrrole > 2-pyridone > maleimide > *p*-formylaniline > 3-methyl-2-pyrrolidinone.

Table 3.9. Quantified yields of fractional pyrolysis of glutamic acid at different temperatures (Wt % Yields) in N_2 at 1 atm.

Quantified Compounds	Pyrolysis Temperature (˚C)						
	300	350	400	450	500	550	600
acetonitrile	0.00	0.01	0.04	0.40	0.44	0.27	0.14
acrylonitrile	0.00	0.01	0.02	0.18	0.17	0.03	0.02
propionitrrle	0.00	0.02	0.02	0.31	0.34	0.10	0.03
crotononitrile	0.00	0.00	0.01	0.05	0.08	0.01	0.01
allyl cyanide	0.00	0.00	0.01	0.08	0.08	0.01	0.01
butyronitrile	0.00	0.00	0.01	0.16	0.17	0.06	0.01
pyrrole	0.01	0.20	0.61	0.98	0.73	0.19	0.16
2-methyl pyrrole	0.00	0.00	0.01	0.23	0.25	0.04	0.01
2-pyridone	0.12	0.26	0.25	0.17	0.14	0.09	0.06
2-pyrrolidone	0.01	0.03	0.04	0.10	0.25	0.13	0.06
3-methyl-2-pyrrolidone	0.01	0.04	0.06	0.10	0.35	0.25	0.10
maleimide	0.01	0.01	0.07	0.13	0.20	0.11	0.03
succinimide	0.23	0.57	0.17	0.12	0.05	0.04	0.03
benzene	0.00	0.00	0.00	0.01	0.01	0.02	0.02
toluene	0.00	0.00	0.01	0.01	0.05	0.03	0.02
Wt % Total	**0.39**	**1.15**	**1.33**	**3.03**	**3.31**	**1.38**	**0.71**

A list the quantified reaction products from fractional pyrolysis of glutamic acid are presented in table 3.9. Clearly, the yields of most reaction products peak between 400 and 500 ˚C. The Wt% yields of the compounds identified were very low. This observation may suggest that the bulky of products from glutamic acid pyrolysis may indeed be thermally stable and are possibly not carried over to the gas-phase for detection.

A representative GC-MS spectrum analysis of the principal products detected during the thermal degradation of glutamic acid at 500 ˚C (obtained using a DB5-MS column) are shown in Figure 3.15. Most hydrocarbon products discussed in this study were determined using a Gas-Pro column and consequently not indicated in Figure 3.15, *vide infra*. Similar products to those shown in Figure 3.15 were detected during oxidative pyrolysis of glutamic acid, with exception of few reaction products such as α-propionlactone, ethanol, acetaldehyde, and 5,6-dihydro-6-methyl uracil.
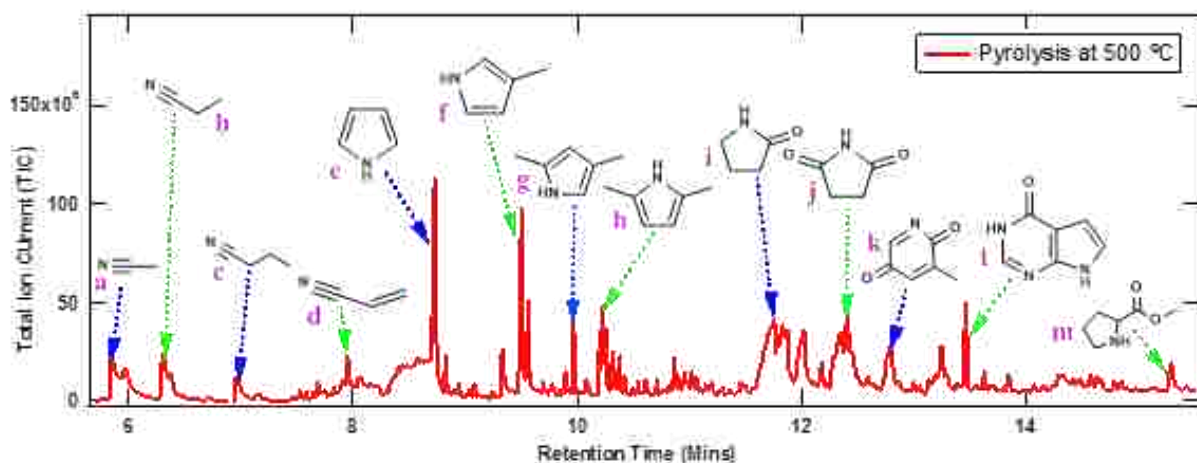
Figure 3.15. GC-M chromatogram (DB5-MS column) of products from pyrolysis of glutamic acid in N_2 at 500 ˚C. Compounds **a-m** are respectively, acetonitrile, propanenitrile, butyronitrile, acrylonitrile, pyrrole, 2,4-dimethyl pyrrole, 2,5-dimethyl pyrrole, 2-pyrrolidone,succinimide, 3-methyl-2,5-pyridinedione, 3H-pyrrolo[2,3-d]pyrimidin-4(7H)-one, and methyl pyrrolidine-2-carboxylate.

3.3.2. Fractional oxidative pyrolysis

The principal reaction products from oxidative pyrolysis of glutamic acid can be classified into three major groups.

65

Group 1. The major product in this class of compounds was exclusively succinimide which peaked at about 365 ˚C. Other products in this group included pyrrole and acetaldehyde (cf. Figure 3.17A, *vide infra*). Pyrrole, a major product in pyrolysis was formed in low amounts under oxidative pyrolysis because an oxidizing atmosphere may retard the formation of pyrrole while enhancing the release of CO_2 [19, 23]. Previously, intra-molecular reactions involving α-lactone followed by decarbonylation were proposed to account for the observed aldehydes [22, 24], although aldehydes (acetaldehyde) were observed as minor products in our experiments (only detected under oxidative pyrolysis).

Group 2. Many of the reaction products detected in this group were mainly oxygenated products with the major product being α-propiolactone (reached maximum concentration at
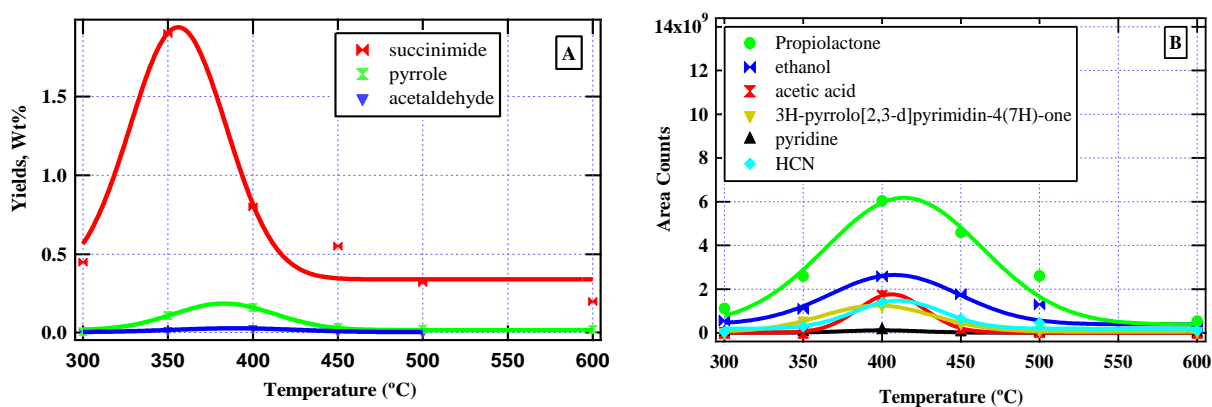
Figure 3.16. Wt % yields of major products (A) and yields (based on GC area counts) of other major products (B) from the pyrolysis of glutamic acid in 4% O_2 in N_2 at 1 atm.

about 400 ˚C), Figure 3.16 B. Direct deamination of the intermediate 4-aminobutanoic acid yields ammonia and α-propiolactone. An analogous reaction in presence of water suggest direct deamination occurs via and internal S_N2 mechanism yielding ammonia and α-propiolactone [25] .Ethanol and acetic acid were the other oxygenated products observed in this group.

Group 3. This comprises the products that were formed between above 400 °C and 450°C (cf. Figure 3.17, *vide supra*) and include 5-methyl pyrimidine, and acetonitrile as the principal products. These products appear to be formed from the thermal decomposition of major products such as succinimide. Early studies postulated pyrolysis of succinimide yielded mainly CO, H_2O and acetonitrile [26]. This may suggest a secondary route for the formation of acetonitrile. Choudhar et al. proposed an activation energy of 52 kcal/mol for the ring opening of succinimide [26]. Subsequently, the ring opening of succinimide facilitates its decomposition to other poducts including acetonitrile and HCN. Table 3.10 shows a list of the quantified compounds from the fractional oxidative pyrolysis of glutamic acid at 1 atmosphere.
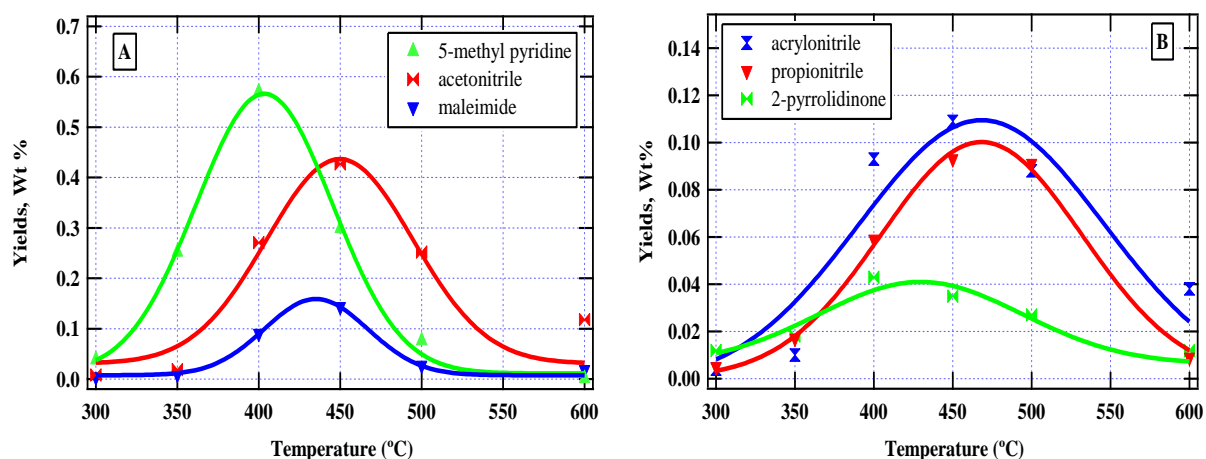
Figure 3.17. Yields (based on GC area counts) of other major products from the pyrolysis of glutamic acid in 4% O_2 in N_2

Succinimide was the most abundant product contributing over 40% of the total products quantified from oxidative pyrolysis attaining a maximum concentration at~365 °C. The order of abundance for the major reaction products in decreasing order was: succinimide > propiolactone > ethanol > HCN > acetic acid > 5-methylpyrimidine.

Table 3.10. Quantified yields of fractional oxidative pyrolysis of glutamic acid at different temperatures (Wt % yields) in 4% O_2 in N_2 at 1 atm.

Quantified Compounds	Pyrolysis Temperature (˚C)						
	300	350	400	450	500	550	600
acetaldehyde	0.00	0.01	0.02	0.03	0.01	0.01	0.00
acetonitrile	0.00	0.01	0.02	0.27	0.43	0.25	0.12
acrylonitrile	0.00	0.01	0.02	0.06	0.09	0.09	0.01
propionitrrle	0.00	0.01	0.01	0.09	0.11	0.09	0.04
pyrrole	0.00	0.01	0.11	0.16	0.04	0.03	0.02
pyridine	0.00	0.01	0.01	0.04	0.01	0.01	0.01
5-methyl pyrimidine	0.01	0.04	0.25	0.57	0.30	0.08	0.00
2-pyrrolidone	0.01	0.01	0.02	0.04	0.03	0.03	0.01
maleimide	0.00	0.01	0.01	0.09	0.14	0.03	0.02
succinimide	0.04	0.45	1.90	0.80	0.55	0.32	
Wt % Total	**0.06**	**0.57**	**2.37**	**2.15**	**1.71**	**0.94**	**0.43**

As can be observed from Figure 3.18 (overlay spectra for pyrolysis and oxidative pyrolysis at 400 ˚C), pyrolysis and oxidative pyrolysis yielded similar reaction products of
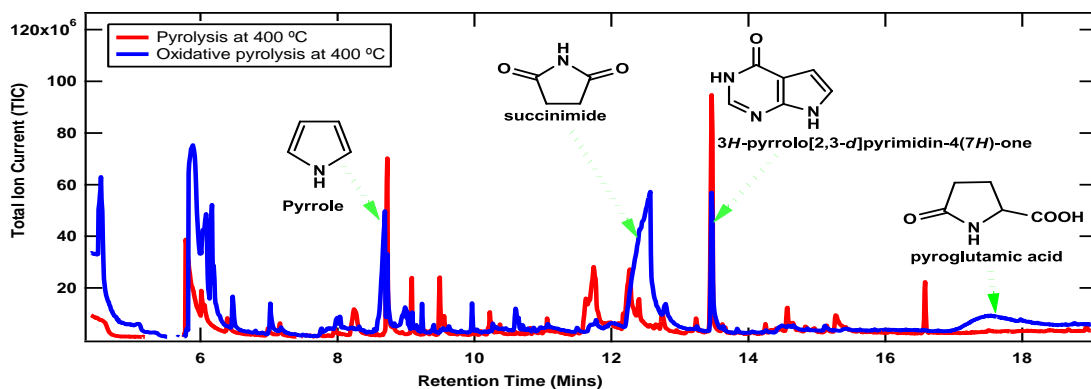
Figure 3.18. GC-MS Spectra for Pyrolysis (Red Line) and Oxidative Pyrolysis (Blue Line) of glutamic acid in N_2 and 4 % O_2 in N_2 at 400 ˚C.

different intensities. It is clear from the spectra that while some products were favored by an

inert regime, some were favored by a reactive regime. Therefore, a comparison between three

68

major compounds, pyrrole, succinimide, and 3H-pyrrolo[2,3-d]pyrimidin-4(7H)-one reveal interesting results. Under pyrolysis, 3H-pyrrolo[2,3-d]pyrimidin-4(7H)-one, and pyrrole are exclusively the major products while for oxidative pyrolysis, succinimide is the principal component. Noteworthy was the formation of a product during oxidative pyrolysis which exhibited a broad peak at Retention Time (RT) 17.5 minutes. The compound was identified as pyroglutamic acid and has never been previously identified during the thermal degradation of glutamic acid.

3.3.3. Decomposition profile for glutamic acid

The decomposition profiles for glutamic acid for both pyrolysis and oxidative experiments were similar (cf. Figure 3.19). Accordingly, glutamic acid appears to exhibit a
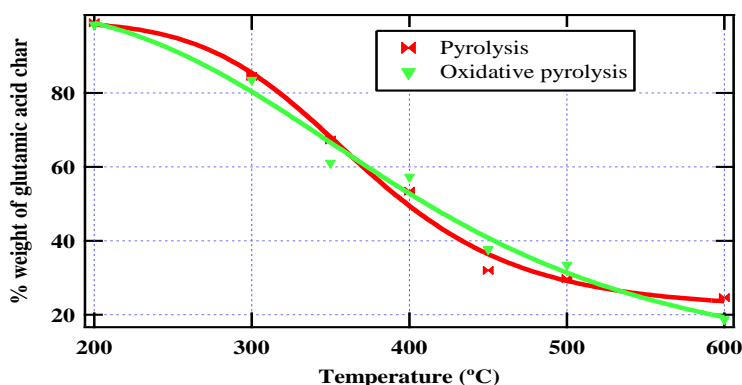
Figure 3.19. Wt % of glutamic acid char as a function of temperature at 1 atm.

single decomposition regime, starting at 300 ˚C and ending at 600 ˚C. The highest rate of decomposition for oxidative pyrolysis was realized between 300 and 350 ˚C with a mass loss of 22.4% while the highest rate of decomposition for pyrolysis was achieved between 400 and 450 ˚C with a mass loss of 21.4%. At the end of the experiment (600 ˚C), the mass loss for pyrolysis and oxidative pyrolysis was 75.4 and 81.3% respectively. This suggests that glutamic acid has high residue content than most biomass materials such as tyrosine, pectin, and cellulose [18, 27].

An observation of glutamic acid after heat treatment revealed a waxy substance (may be polyglutamic acid) that stuck to the walls of the reactor. Accordingly, it would imply the gas-solid interface changes during heat treatment and any pores present in the sample disappears so that oxygen acts only on the surface but does not penetrate into the matrix of the (polymer) sample [27, 28]. Thus the degradation of glutamic acid is independent of oxidative reactions [27]. Consequently, the mass loss due to an oxidizing environment will certainly not vary significantly compared to that due to an inert environment. This may explain why the variation in mass due to pyrolysis is similar to that due to oxidative pyrolysis in the entire temperature range of this experiment. Compared to cellulose decomposition, it is speculated that mass loss below 300 ˚C was due to oxidative reactions but at temperatures above 300 ˚C, the rate of pyrolysis was essentially the same in both air and nitrogen, indicating thermal degradation is independent of oxidative reactions [27, 28]. This observation is remarkable and agrees well with observations made during the thermal degradation of glutamic acid. The percent yields of char from the thermal degradation of glutamic acid are presented in Table 3.11.

Table 3.11. Wt % Yields of char from the thermal degradation of glutamic acid at 1 atm.

Temp. (˚C)	200	300	350	400	450	500	600
Fractional Pyrolysis	99.04	84.50	67.29	53.44	32.01	29.78	24.62
Oxidative Fractional Pyrolysis	98.41	83.52	61.13	57.36	37.67	33.54	18.70

3.4. Modeling of biomass pyrolysis

Combustion is a complex sequence of chemical reactions between a fuel and an oxidant [29, 30] while pyrolysis is described as the direct degradation of a biomass matrix to obtain an array of solid, liquid, and gaseous products under inert conditions. It is therefore necessary that the input parameters and physical properties chosen by researchers are simplified in order to

provoke the greatest possible influence on the overall kinetic parameters. Large number of chemical reactions and the species involved increases the complexity of the thermal degradation of biomass [29, 30]. Consequently, there is need for a detailed kinetic scheme of biomass pyrolysis that considers the distribution of molecular weight and the solution of a high-dimensional system of differential equations. Fortunately, the current state of knowledge in computation allows individual yield predictions of biomass pyrolysis products through mathematical modeling [31]. To make computation more fluent, some combustion computation tools have been developed [30].

Degradation kinetics of biomass materials can be studied in either dynamic or static conditions [30, 32, 33]. This study employed static conditions in which the temperature and the residence time inside the reactor was held constant. Pyrolysis gas, however; was varied with temperature as the residence time remained constant during the entire pyrolysis temperature range. Numerical simulations using CHEMKIN combustion package to model the major products of lignin was applied in this work. Previously, a number of mechanisms have been proposed for the pyrolysis of wood [30, 32-36]. The models are classified into three categories: one stage global models; one-stage multi-reaction models; and two-stage semi global-models [30]. The first category of models considered pyrolysis as a single-step first order reaction described by the following parallel reactions [30]:

$$Virgin\ Biomass \rightarrow (Volatiles + Gases)_1 \qquad\qquad Equation\ 3.1$$

$$Virgin\ Biomass \rightarrow (Char)_1 \qquad\qquad Equation\ 3.2$$

The secondary reactions for the above system are considered thus [30]:

$$(Volatiles + Char)_1 + (Char)_1 \rightarrow (Volatiles + Char)_2 + (Char)_2 \qquad Equation\ 3.3$$

The secondary interaction model describe simultaneous and first order competing reaction mechanisms in which virgin biomass decompose to pyrolysis products: tar, char, and gases [30]. The third class of model considers pyrolysis to be a two stage reaction in which the products of the first stage break up further in presence of each other to yield secondary pyrolysis products [30]. It is reported pyrolysis of biomass materials of size less than 1mm is kinetically controlled whereas for large particles, kinetic equations are coupled to describe the transport phenomena [30, 37, 38]. In these kinetic models, an exponential decay of solid reactivity with respect to conversion level is proposed and the rate expression based on first-order degradation of the reactive solid is defined in terms of fraction change [30, 32, 39]. The reaction rate constant is expressed as a function of the extent of reaction, which has replaced the Arrhenius expression of the rate constant with temperature [30]. The kinetic model suggested by Koufopanos *et al.* for the pyrolysis of biomass based on the two-stage model has been accepted and corroborated [30, 37, 38].

The differential equations *3.5 - 3.12* (Scheme 3.1, *vide infra*) will be discussed in detail in in this chapter. These equations describe the rate of formation of volatile products and char from biomass pyrolysis, and the rate of disappearance of the volatile products and the char as presented in equations 3.*1-3.3* above. Similarly, equations 3.4, 3.13, and 3.14 will be discussed in detail in order to elucidate the residual weight fraction (W) and describe the Arrhenius relation of the kinetic rate constant with temperature. The formation kinetics of intermediates and their subsequent destruction are critical in designing a model for lignin pyrolysis. The char kinetics are also important towards understanding the parallel reactions that occur in biomass pyrolysis reactions.

Koufopanos *et al.* (1991) mechanism

Virgin Biomass B (n_1 order decay)

Reaction 3.1   Reaction 3.2

$$\text{(Volatile + Gases)}_1 \quad + \quad \text{(Char)}_1 \xrightarrow{\text{Reaction 3.3}} \text{(Volatile + Gases)}_2 \quad + \quad \text{(Char)}_2$$

(n_2 order decay)   (n_3 order decay)
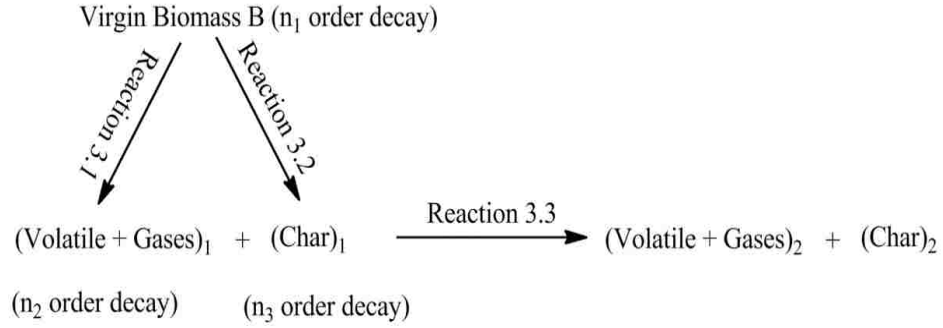
Residual weight fraction (W) calculation $n_1 = n_2 = n_3$

$$W = B + C_1 \tag{3.4}$$

$$\frac{dB}{dt} = -(k_1 + k_2)B \tag{3.5}$$

$$\frac{dC_1}{dt} = k_1 B \tag{3.6}$$

$$\frac{dW}{dt} = -k_1 B \tag{3.7}$$

$$\frac{dC_B}{dt} = -k_1 C_B^{n_1} - k_2 C_B^{n_1} \tag{3.8}$$

$$\frac{dC_{G_1}}{dt} = k_1 C_B^{n_1} - k_3 C_{G_1}^{n_2} C_{C_1}^{n_3} \tag{3.9}$$

$$\frac{dC_{C_1}}{dt} = k_2 C_B^{n_1} - k_3 C_{G_1}^{n_2} C_{C_1}^{n_3} \tag{3.10}$$

$$\frac{dC_{G_2}}{dt} = k_3 C_{G_1}^{n_2} C_{C_1}^{n_3} \tag{3.11}$$

$$\frac{dC_{C_2}}{dt} = k_3 C_{G_1}^{n_2} C_{C_1}^{n_3} \tag{3.12}$$

$$k_1 = A_1 \exp\left(-\frac{E_1}{RT}\right) \tag{3.13}$$

$$k_2 = A_2 \exp\left(-\frac{E_2}{RT}\right) \tag{3.14}$$

Scheme 3.1. Char (C1) and volatiles (G1) are considered to have been formed in an intermediate stage and converted to char (C2) and volatile (G2) of different types [30, 37].

A pyrolysis phenomenon is stimulated by a scheme consisting of three reactions [37, 40, 41].

- Two parallel reactions and

- A third reaction for the secondary interactions between charcoal and volatiles

An approach to construct a detailed mechanism for biomass decomposition was initiated recently in which a simplified model of combining products depending on their release temperature, properties, and distribution was developed to handle the large amounts of initial, intermediate, and final products [30, 42]. For instance, 100 molecular and radical species in 500 elementary and lumped reactions for lignin and more than 500 species and 8000 reactions for cellulose pyrolysis processes have previously been considered [30, 42]. The model predictions, in the case of cellulose pyrolysis generally agreed for the experimental concentration profiles of major species such as H_2, CO, CO_2, CH_4, and C_2H_4 [43]. However, the agreements for minor products such as acetaldehyde, acetic acid, acetone, hydroxyl acetone, furan, benzene, and toluene were fair at best [43].

Based on literature survey as well as the fact that the detailed modeling requires much more computational effort, we have preferred to consider simplified modeling procedure for lignin pyrolysis. Similar approaches were widely used for the kinetic modeling of thermal cracking of petroleum residues although detailed kinetic modeling of petroleum residues initially, did not get due attention in literature [44].

3.5. Modeling of lignin pyrolysis

3.5.1. Creation of lignin pseudo 1st order decomposition model

A 15 reaction model for lignin decomposition is presented in Figure 3.20 below. It contains:

1. 6 parallel pseudo-first order reactions for decomposition of lignin (assigned **L**) to formation of intermediate products (with rate constants of $k_{1f} - k_{6f}$) grouped by similarity of accumulation (cf. Figure 3.21, *vide infra*) where:

[Syr + Gua] represents a group of products peaked at ~ 400 $^{\circ}$C: syringol, guaiacol, eugenol, 5-methyl guaiacol, 4-ethylguaiacol
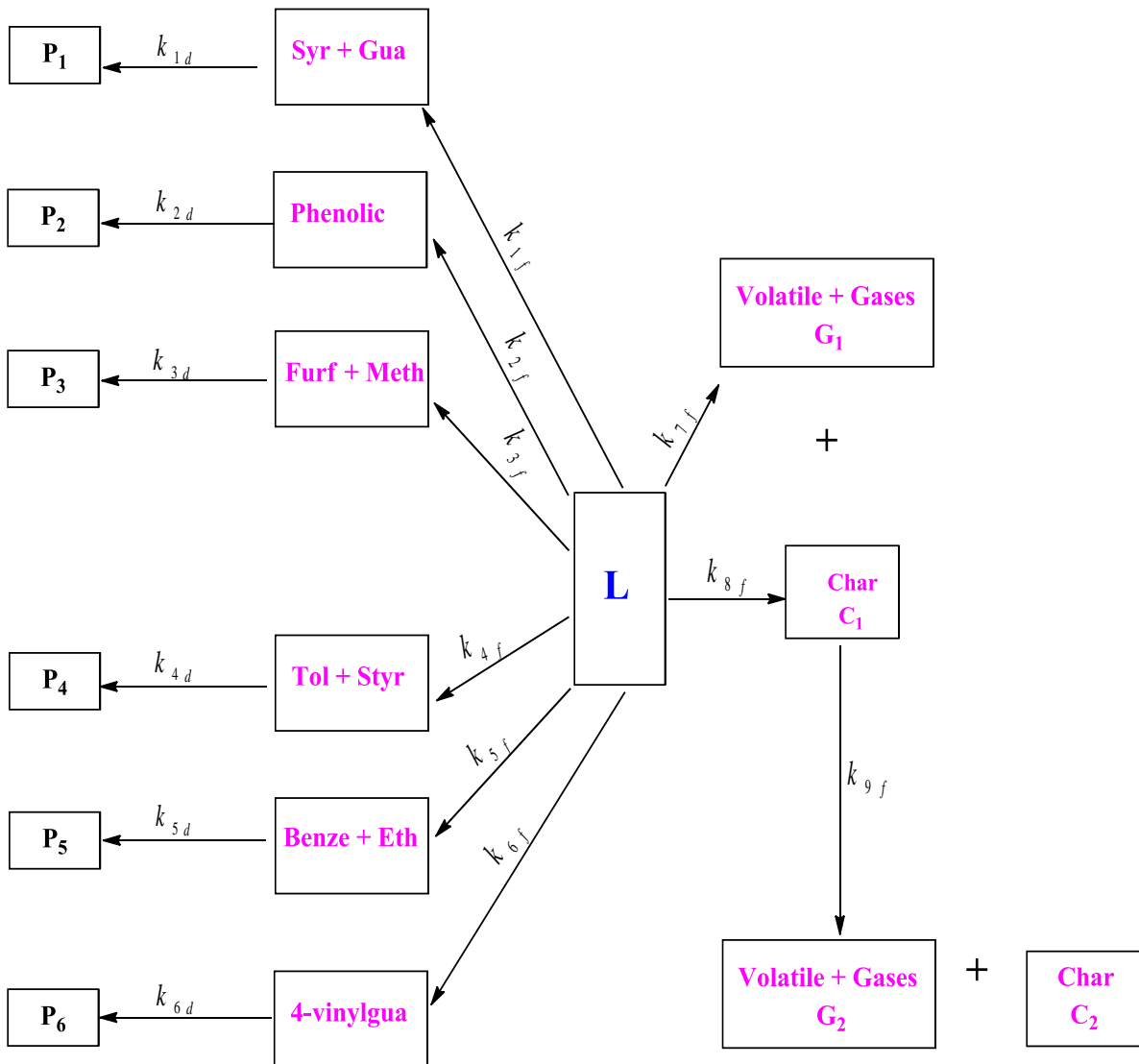
Figure 3.20. Formation reactions of products from Lignin (L) with rate constants $k_{1f} - k_{6f}$, and decomposition reactions with rate Constants $k_{1d} - k_{6d}$. Reactions 7-9 are adapted from literature [37].

[Phenolic] represents a group of products peaked at ~ 400 $^{\circ}$C: catechol, phenol, 3-methoxycatechol, *p*- cresol,

[Furf+Meth] represents a group of products peaked at ~ 400 $^{\circ}$C: furfural, methanol, 2-methylfuran, furan, 2,5-dimethylfuran,

[Tol+Styr] represents a group of products peaked at ~ 500 $^{\circ}$C: toluene, styrene, propene, p-xylene, propane, ethene and 3,4 dimethoxyphenol

[Benz+Eth] represents a group of products peaked at ~ 600 $^{\circ}$C: benzene and ethane

[4-Vinylgua] represents a group of products peaked at ~ 300 $^{\circ}$C: 4-vinylguaiacol, 4-propenylsyringol, acetic acid, furfuryl alcohol

2. Two reactions representing the pseudo first order decomposition of lignin to formation of volatiles/gases and char (with rate constants of $k_{7f} - k_{8f}$) Figure 3.26 *vide infra*, along with secondary reaction 9 [37].

3. Decomposition reactions all of 6 grouped products (with rate constants of $k_{1d} - k_{6d}$) are also included as secondary reactions for intermediate products.

The model consists of 15 reactions; 8 parallel (pseudo 1st order decomposition reactions of lignin with rate constants of $k_{1f} - k_{8f}$), 6 pseudo 1st order decomposition (secondary reactions of intermediate products with rate constants of $k_{1d} - k_{6d}$) as well one secondary reaction, k$_{9d}$ of char decomposition adapted from literature [37]. In order to run CHEMKIN for the assumed pseudo first order decomposition model for Lignin (cf. Figure 3.20, *vide infra*), the rate constants for formation (k$_{if}$) and decomposition (k$_{id}$) of intermediate products are needed. The approximate procedures to determine these rate constants values are discussed in detail in this chapter.

Group [Syr + Gua]
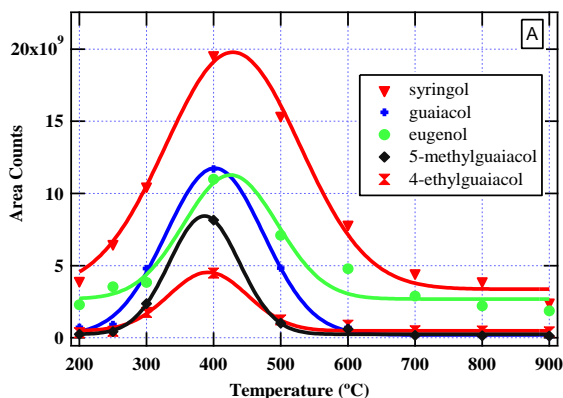
Group [Phenolic]
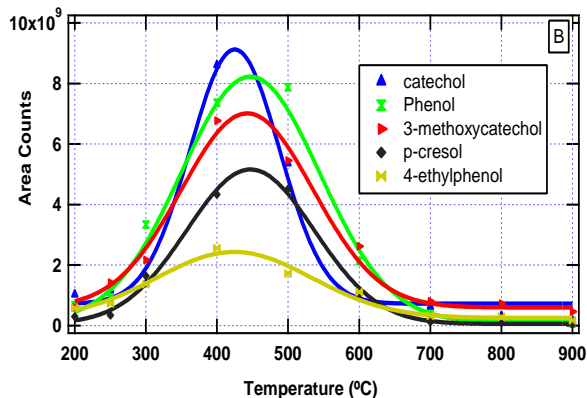
Group [Furf + Meth]
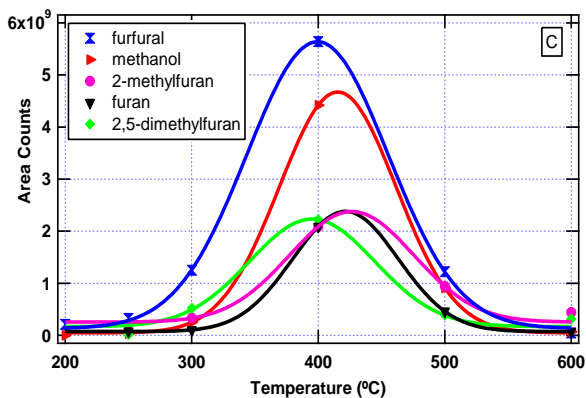
Group [Tol + Styr]
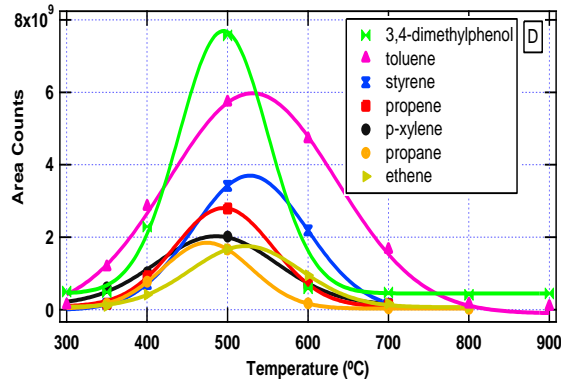
Group [4-Vinylgua]
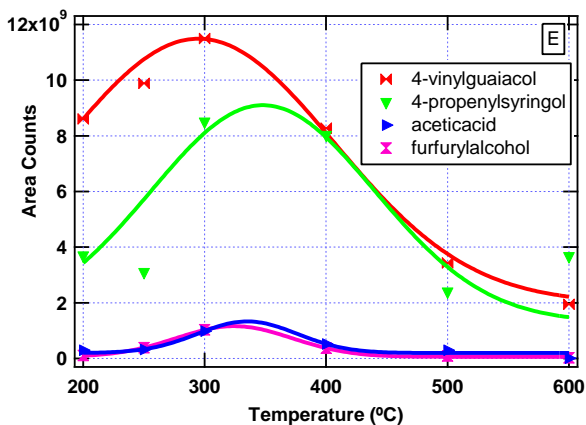
Group [Benz + Eth]
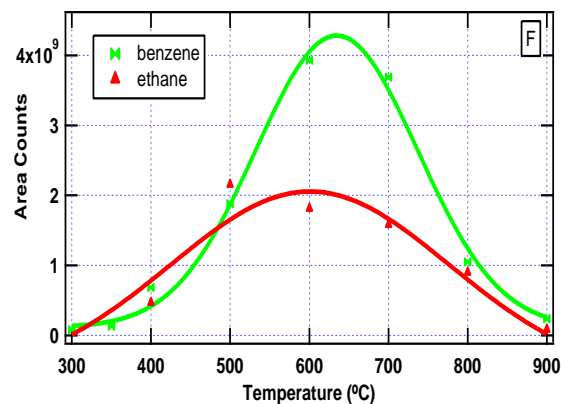
Figure 3.21. Yields (Based on GC Area Counts) of major products from partial pyrolysis of lignin in N_2 grouped according to the temperature at which maximum concentrations was achieved.

77

3.5.2. Constructing the model for lignin pyrolysis

3.5.2.1. Formation vs. destruction of intermediate products

The experimental results from lignin fractional pyrolysis are presented, in Figure 3.21, *vide supra* (Major products are grouped into 6 categories).

3.6. Formation of intermediate products

As can be seen from the model, *vide supra,* Figure 3.20, the intermediate products form during parallel decomposition reactions of lignin. For simplicity purposes, two parallel reactions 3.15 and 3.16 with rate constants k_1 and k_2 are considered.

$$A \rightarrow B \qquad\qquad\qquad \textit{Equation 3.15}$$

$$A \rightarrow C \qquad\qquad\qquad \textit{Equation 3.16}$$

The rate expressions are

$$\frac{d[A]}{dt} = -\left(\frac{k_1 + k_2}{[A]} \right) \qquad\qquad \textit{Equation 3.17}$$

$$\frac{d[B]}{dt} = k_1[A] \qquad\qquad \textit{Equation 3.18}$$

$$\frac{d[C]}{dt} = k_2[A] \qquad\qquad \textit{Equation 3.19}$$

Equation 4.4 is an ordinary first order decay given by:

$$\ln A = A_0 \exp\left[\left(-k_1 + k_2 \right) \right] t \qquad\qquad \textit{Equation 3.20}$$

Substituting equations that result into the equations 3.19 and 3.20 the solutions for B and C will be:

$$[B] = A_0 \left(\frac{k_1}{k_1 + k_2} \right) x \left\{ 1 - \exp\left[-(k_1 + k_2) \right] t \right\} \qquad \text{Equation 3.21}$$

$$[C] = A_0 \left(\frac{k_2}{k_1 + k_2} \right) x \left\{ 1 - \exp\left[-(k_1 + k_2) t \right] \right\} \qquad \text{Equation 3.22}$$

The important conclusion from equations 3.21 and 3.22 is that the temporal behavior of both B and C are the same; their time dependence is determined by the sum of the two elementary rate coefficients. By dividing equation 3.21 by equation 3.22, the concentrations of B and C can be determined as a ratio of the individual rate constants, yielding equation 3.23,

$$\frac{[B]}{[C]} = \frac{k_1}{k_2} \qquad \text{Equation 3.23}$$

Equation 3.23 is for the parallel reactions (1) and (2) and in combination with the equation 3.17 the constants k_1 and k_2 can be determined. For finite times of reaction equation 3.23 can be written as:

$$k_1 + k_2 = -\left(\frac{\Delta A}{A \Delta t} \right) \qquad \text{Equation 3.24}$$

It is obvious that by comparison of equations 3.23 and 3.24 k_1 and k_2 can be determined based on experimental measurements of ΔA, A, B and C at a known time interval of Δt for a given temperature, T. The rate constants for the reaction products were then tabulated at various pyrolysis temperatures to assist in computing the kinetic parameters; activation energy, Ea and the Arrhenius factor, A. The kinetics of lignin pyrolysis in this study considers that the initial time $t = 0$ and $t = 0.2$ so that $\Delta t = 0.2$.

3.6.1. Destruction of intermediate products

As it can be seen from the example for formation of first group of products, [Syr +
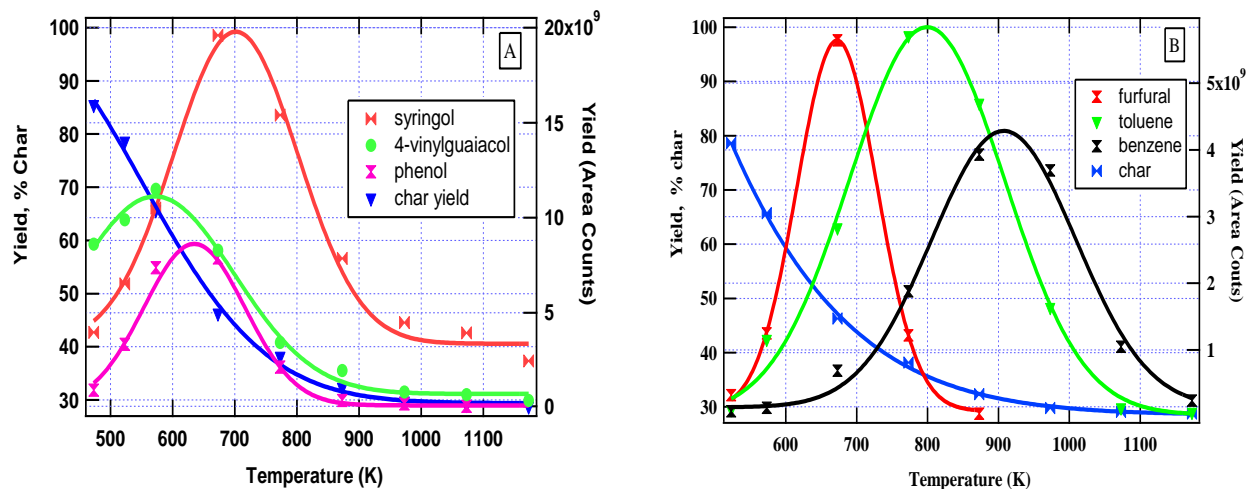
Figure 3.22. The percent yields of lignin char relative to the yields of major products (A and B) from pyrolysis of lignin in N_2

Gua], the yields of intermediate products grow up to $400 - 425$ $^{\circ}$C, i.e. the formation rate of products prevails over destruction rates, *vide supra* Figure 3.22. At peak temperatures these two rates are very close, while at higher than 425 $^{\circ}$C the yields of intermediate products drops significantly over a very narrow temperature region, from 425 to 500 $^{\circ}$C for most products (cf. Figure 3.22). There are two possible reasons for this observation;

1. The continuously decreased amount of initial lignin provides continuously slow generation of intermediate in duration of pyrolysis

2. The rate of destruction of product increases drastically with increasing temperature in comparison with the rate of formation.

The analysis for the destruction curve of lignin, Figure 3.22, indicates lignin is not significantly consumed from~ 700 to 773 K (note that the destruction curve for the lignin
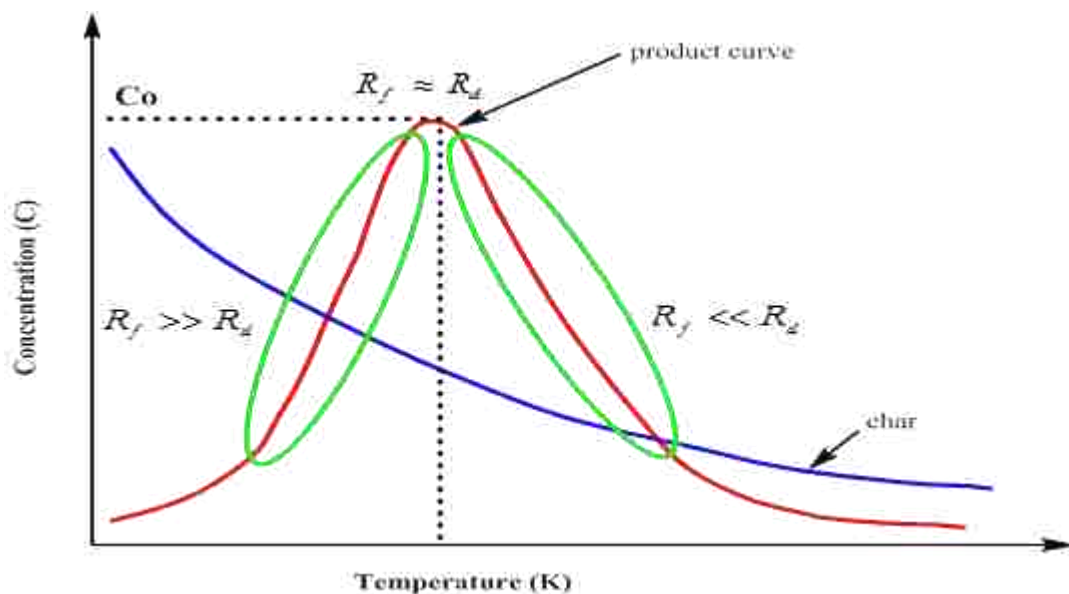
Figure 3.23. A schematic representation of consumption of initial component A and accumulation of intermediate B for hypothetical consecutive first order reaction $A \rightarrow B \rightarrow C$. R_f and R_d represents formation and destruction rates for B.

represents the char mass dependence vs. temperature, where char is defined as residue lignin + charred material) [45]. The intermediate product concentration for instance syringol drops substantially in the same temperature region (cf. Figure 3.22). Thus at high temperatures the destruction rate of products is higher than the rate of their formation and the drop of concentration may be mostly explained by further decomposition reactions of the intermediate product.

Generally, the relation of the rate of formation of intermediate product (R_f) vs. the rate of destruction (R_d) is represented in Figure 3.23. For hypothetical consecutive first order reaction as shown in equation 3.25:
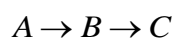
$$A \rightarrow B \rightarrow C \qquad\qquad\qquad Equation\ 3.25$$

Based on these rough assumptions, it is possible to calculate the apparent kinetic parameters for destruction of intermediate products from the temperature dependence of the yields of products.

Pseudo-unimolecular kinetics might be applied, in which the empirical rate of decomposition of intermediate product is first-order and expressed by equation 3.26 at given temperature:

$$C_0 = C \exp\left(-kt\right)$$
Equation 3.26

where Co and C are initial and current concentrations, respectively and k is the pseudo-unimolecular reaction rate coefficient in the Arrhenius equation (Equation 3.27),:

$$\ln k = A \exp\left(-\frac{Ea}{RT}\right)$$
Equation 3.27

In this case, Co is the concentration of intermediate B (cf. Equation 3.20, *vide supra*) at the time when it reaches the maximum concentration and $R_f \sim R_d$, Figure 3.23 *vide supra*. The activation energy *Ea* and pre-exponential A factor will be determined based on the dependence of an Arrhenius plot of ln k vs 1/T (Equation 3.28).

$$\ln k = \ln A - \frac{Ea}{R} \cdot \frac{1}{T}$$
Equation 3.28

3.7. Char formation

The char formation reactions were adapted from the literature known as 1st order lignin decomposition model, or char/volatile formation [37, 38, 40, 41] consisting of two parallel reactions 7 and 8 and a third reaction for the secondary interactions between charcoal and volatiles, reaction 9, Figure 3.20, *vide supra*. Kinetic parameters for the reactions 7 and 8 have

been determined [37] based on modified Arrhenius equation known as the Landau-Teller (LT) expression, equation 3.29 and are presented in Table 3.12.

$$k_{fi} = A_i \exp\left(-\frac{B_i}{T^{\frac{1}{3}}} + \frac{C_i}{T^{\frac{2}{3}}}\right)$$

Equation 3.29

Table 3.12. Best fit values for the kinetic parameters of the primary pyrolysis reactions 7 and 8 from ref. [37].

Reactions	A, sec^{-1}	B	C
7	9.973 x 10-5	17254.4	-9061227
8	1.068 x 10-3	10224.4	-6123081

In the case of using modified Arrhenius equation CHEMKIN could be afforded by using special auxiliary keyword **LT** to be able to use equation 3.29 for certain reactions. Finally, volatiles and gases (as G_1, Figure 3.20, *vide supra*) may further react with char (C_1), reaction 9 (as secondary reaction) and produce also volatile, gases (G_2) and char (C_2) of different composition. The rate of char reaction with the primary gaseous products (G_1) of pyrolysis can be expressed according to a first-order kinetic scheme [79], equation 3.30:

$$\frac{dC_2}{dt} = \delta k_3 C_1$$

Equation 3.30

where δ is the coefficient of deposition and represents the fraction of volatiles and gases (G_1) deposited on the char sites because of the secondary reaction 9. The fitting procedure suggests the best values for reaction 9, [37]:

$A_9 = 5 x\, 10^5\, s^{-1}$, $E_9 = 19.38\, kcal\, mol^{-1}$, $\delta = 1.45$. These values for reaction 9 (i.e.

$$k_9 = 8.26 \; x \; 10^5 \exp\left(-\frac{20000\, cal\, mol^{-1}}{RT} \right) \qquad\qquad \textit{Equation 3.31}$$

as well as for rxns 7 and 8 (cf. Table 3.12, *vide supra*) will be used in the CHEMKIN calculations.

3.8. Pseudo-unimolecular kinetics for formation of intermediates

The pseudo-unimolecular rate constant calculations for the intermediate products have been performed according to equations 3.23 and 3.24 discussed above:

For instance, syringol from the group of products [Syr+Gua] and phenol from the [Phenolic] group were chosen as representative products B and as C, respectively. The experimental data for the formation of these products (cf. Table 3.14, *vide infra*) have been extracted from the corresponding curves of accumulation in (cf. Figure 3.22, *vide supra*). The Arrhenius dependence of the pseudo-unimolecular reaction rate constants of phenol and syringol formation is represented in Figure 3.24, *vide infra*.

Table 3.13. The temperature dependence of the pseudo-unimolecular rate constants for formation of syringol (k_1) and phenol (k_2) using equations 3.26 and 3.27.

T (K)	1/T	% Char	Syr., B	Phen., C	B/C=k_1/k_2	ΔA	0.2xA	k_1+k_2	k_2	k_1	logk_2	logk_1
523	0.0019	78.64	6.51E+09	9.23E+08	7.05	21.36	15.73	1.36	0.169	1.19	-0.773	0.075
573	0.0017	65.7	1.05E+10	3.34E+09	3.14	34.3	13.14	2.61	0.630	1.98	-0.201	0.297
673	0.0015	46.3	1.96E+10	7.36E+09	2.66	53.7	9.26	5.80	1.583	4.22	0.1995	0.625

For the subsequent couples, product B was always chosen as syringol and product C was toluene, furfural, benzene, or 4-vinylguaciacol. Similarly, the final results for the pseudo-unimolecular rate constants of toluene, furfural and benzene, 4-vinylguaiacol were calculated in the same manner and Arrhenius dependence of the pseudo-unimolecular reaction rate constants are presented in Figure 3.23 *vide supra*, and 3.24 *vide infra*.

The pseudo-unimolecular formation reaction rate constants calculated for the representative intermediate products during lignin pyrolysis are summarized in Table 3.13, *vide supra*. These data will be used in CHEMKIN modeling calculations.
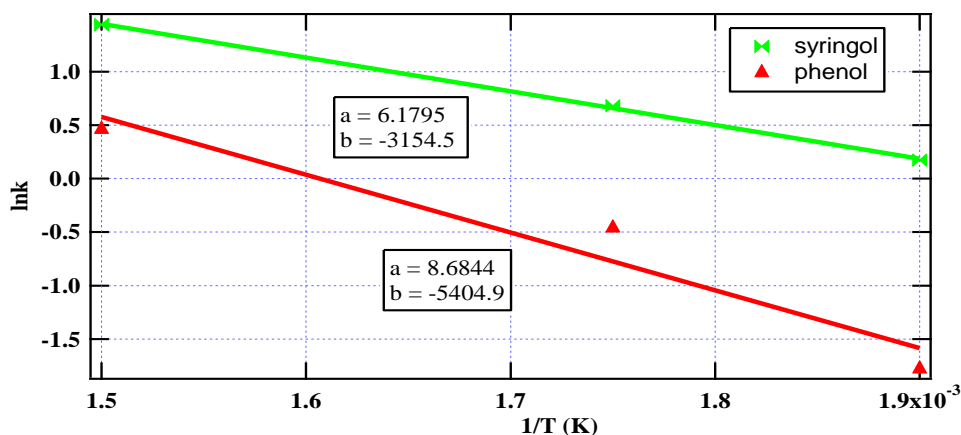
Figure 3.24. The Arrhenius dependence of the pseudo-unimolecular reaction rate constant for the formation of syringol from the pyrolysis of lignin in N_2.

Table 3.14. The Arrhenius parameters for the formation rate constants for selected products from lignin pyrolysis.

product	Ea (cal/mol)	A (s^{-1})
syringol	6000.0	3.47E+02
phenol	10000.0	3.55E+03
furfural	5600.0	5.75E+01
toluene	17000.0	8.32E+05
4- vinylguaiacol	4200.0	4.90E+01
benzene	22400.0	6.31E+06

3.9. Pseudo-unimolecular kinetics for decomposition of intermediates

The pseudo-unimolecular rate constant calculations for the destruction of intermediate, representative products have been performed according the equation:

$$k = \ln\frac{[A_0]}{[A]}\frac{1}{t} \qquad\qquad \textit{Equation 3.32}$$

where t = 0.2 sec residence time:

$$k = 11.5\ln\frac{[A_0]}{[A]} \qquad\qquad \textit{Equation 3.33}$$

where Ao is the maximum concentration of intermediate product and A is the current concentration in case of syringol accumulation.

The data of temperature dependence of the rate constant for syringol destruction is represented in Table 3.15 while the corresponding Arrhenius dependence is presented in Figure 3.25, *vide infra*. The Arrhenius dependence of the pseudo-unimolecular reaction rate constants of destruction for phenol, toluene and benzene as well for furfural and 4-vinylguaiacol were built in the same manner as that of syringol.

Table 3.15. The temperature dependence of the pseudo-unimolecular rate constants for destruction of syringol.

T (K)	1/T	As	Ap	Ao/As	Ao/Ap	lnAo/As	lnAo/Ap	ks	kp	lnks	lnkp
673	0.0015	98.0	57.2	1.02	1.75	0.02	0.56	0.23	6.44	-1.47	1.86
773	0.0013	82.4	37.6	1.21	2.64	0.19	0.97	2.19	11.12	0.78	2.41
873	0.0011	56.6	29.4	1.77	3.40	0.57	1.22	6.79	14.03	1.92	2.64
973	0.0010	45.3	28.1	2.21	3.56	0.79	1.27	9.09	14.61	2.21	2.68
1073	0.0009	42.1	27.9	2.38	3.58	0.87	1.28	10.00	14.72	2.30	2.69

The Arrhenius parameters (*A*) and calculated activation energies (*Ea*) for the destruction of representative intermediate products during lignin pyrolysis are summarized in Table 3.16, *Vide infra*.
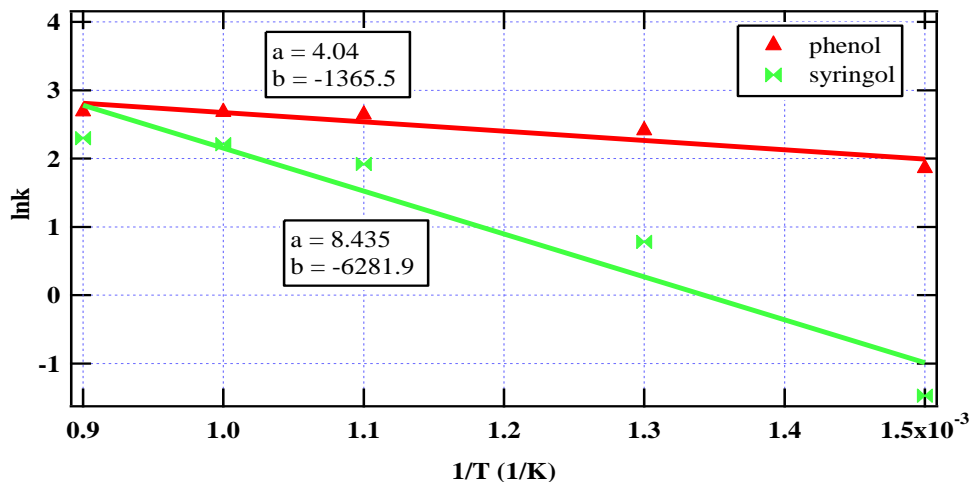
Figure 3.25. The Arrhenius dependence of the rate constant of destruction of phenol and syringol from the pyrolysis of lignin in N_2

The data for the last component (gases), has been estimated, Table 3.16. This will represent gases such as CO, CO_2, methane etc.

Table 3.16. The Arrhenius parameters for the rate constants of destruction reactions for selected products from lignin pyrolysis.

product	Ea (cal/mol)	A (s^{-1})
syringol	19000.0	1.98E+05
phenol	6300.0	4.00E+02
furfural	9000.0	5.60E+03
benzene	7000.0	4.10E+02
toluene	7500.0	7.20E+02
4-vinylguaiacol	5000.0	2.10E+02
gases	4600.0	1.10E+02

3.10. References

1. Sharma, R.K. and M.R. Hajaligol, *Effect of pyrolysis conditions on the formation of polycyclic aromatic hydrocarbons (PAHs) from polyphenolic compounds.* Journal of Analytical and Applied Pyrolysis, 2003. **66** (1-2): p. 123-144.

2. Sharma, R.K. and M.R. Hajaligol, *Polycyclic aromatic hydrocarbon formation in pyrolysis of polyphenolic compounds.* Abstracts of Papers of the American Chemical Society, 2001. **221**: p. U509-U509.

3. Qu, T.T., et al., *Experimental study of biomass pyrolysis based on three major components: hemicellulose, cellulose, and lignin.* Industrial & Engineering Chemistry Research, 2011. **50** (18): p. 10424-10433.

4. Jakab, E., O. Faix, and F. Till, *Thermal decomposition of milled wood lignins studied by thermogravimetry mass spectrometry.* Journal of Analytical and Applied Pyrolysis, 1997. **40-1**: p. 171-186.

5. Carlier, M., Pauwels, J.P., and Sochet, L-R., *Application of ESR techniques to the study of gas-phase oxidation and combustion phenomena.* Oxidation Communication, 1984. **6** (1-4): p. 141-156.

6. Khachatryan, L., J. Adounkpe, and B. Dellinger, *Radicals from the gas-phase pyrolysis of hydroquinone: 2. Identification of alkyl peroxy radicals.* Energy & Fuels, 2008. **22** (6): p. 3810-3813.

7. Sharma, R.K., et al., *Characterization of char from the pyrolysis of tobacco.* Journal of Agricultural and Food Chemistry, 2002. **50** (4): p. 771-783.

8. Zhou, S., et al., *Pyrolysis behavior of pectin under the conditions that simulate cigarette smoking.* Journal of Analytical and Applied Pyrolysis, 2011. **91** (1): p. 232-240.

9. Pryor, W.A., Prier, D.G., and Church, D.F., *ESR Study of mainstream and sidestream cigarette smoke: Nature of free radicals in gas-phase smoke and in cigarette tar.* Environmental Health Perspectives, 1983. **47**: p. 345-355.

10. Flicker, T.M. and S.A. Green, *Comparison of gas-phase free radical populations in tobacco smoke and model systems by HPLC* Environmental Health Perspectives, 2001. **109**: p. 765-771.

11. Valavanidis, A., Haralambous, E., *A comparative study by EPR of free radical species in the mainstream and sidestrem smoke of sigarettes with conventional acetate filters and 'bio-filters".* Redox.Report, 2001. **6** (3): p. 161-171.

12. Adounkpe, J., et al., *Radicals from the Atmospheric Pressure Pyrolysis and Oxidative Pyrolysis of Hydroquinone, Catechol and Phenol.* Energy and Fuels, 2009. **23**: p. 1551-1554.

13.   Khachatryan, L., J. Adounkpe, and B. and Dellinger, *Radicals from the gas-phase pyrolysis of hydroquinone 2. Identification of alkyl peroxy radicals* Energy & Fuel, 2008. **22**: p. 3810-3813.

14.   Khachatryan, L., Adounkpe, J., and Dellinger, B., *Formation of phenoxy and cyclopentadienyl radicals from the gas-phase pyrolysis of phenol.* J.Phys. Chem., A, 2008. **112**: p. 481-487.

15.   Khachatryan, L., et al., *Radicals from the gas-phase pyrolysis of catechol. 2. Comparision of the pyrolysis of catechol and hydroquinone.* J. Phys. Chem., A 2010. **114**: p. 10110-10116.

16.   Khachatryan, L., et al., *Radicals from the gas-phase pyrolysis of catechol: 1. o-semiquinone and ipso-catechol radicals.* J.Phys. Chem., A, 2010. **114** (6): p. 2306-2312.

17.   Adounkpe, J., L. Khachatryan, and B. and Dellinger, *Radicals from the gas-phase pyrolysis of hydroquinone 1. Temperature dependence of the total yields of Radicals.* Energy & Fuels, 2008. **22**: p. 2986-2990

18.   Li, J., et al., *The investigation of thermal decomposition pathways of phenylalanine and tyrosine by TG-FTIR.* Thermochimica Acta, 2008. **467** (1-2): p. 20-29.

19.   Haidar, N.F., et al., *Effects of structure on pyrolysis gases from amino-acids.* Journal of Agricultural and Food Chemistry, 1981. **29** (1): p. 163-165.

20.   Patterso.Jm, et al., *Pyrolysis of phenylalanine, 3,6-dibenzyl-2,5-piperazinedione, and phenethylamine.* Journal of Organic Chemistry, 1973. **38** (4): p. 663-666.

21.   Johnson, W.R. and J.C. Kang, *Mechanisms of hydrogen cyanide formation from pyrolysis of amino acids and related compounds.* Journal of Organic Chemistry, 1971. **36** (1): p. 189-&.

22.   Simmonds, P.G., et al., *Thermal-Decomposition of aliphatic monoamino-monocarboxylic acids.* Analytical Chemistry, 1972. **44** (12): p. 2060-&.

23.   Patterso.Jm, et al., *Thermally induced side-chain to ring migrations in aromatic systems.* Journal of Organic Chemistry, 1973. **38** (17): p. 3052-3054.

24.   Ratcliff, M.A., E.E. Medley, and P.G. Simmonds, *Pyrolysis of amino-acids - mechanistic considerations.* Journal of Organic Chemistry, 1974. **39** (11): p. 1481-1490.

25.   Alexandrova, A.N. and W.L. Jorgensen, *On the mechanism and rate of spontaneous decomposition of amino acids.* Journal of Physical Chemistry B, 2011. **115** (46): p. 13624-13632.

26.   Choudhar.G, A.M. Cameron, and R.A. Back, *Photolysis and pyrolysis of succinimide vapor.* Journal of Physical Chemistry, 1968. **72** (7): p. 2289-&.

27.   Mamleev, V., S. Bourbigot, and J. Yvon, *Kinetic analysis of the thermal decomposition of cellulose: The main step of mass loss.* Journal of Analytical and Applied Pyrolysis, 2007. **80** (1): p. 151-165.

28.   Mamleev, V., et al., *Model-free method for evaluation of activation energies in modulated thermogravimetry and analysis of cellulose decomposition.* Chemical Engineering Science, 2006. **61** (4): p. 1276-1292.

29.   Blondeau, J. and H. Jeanmart, *Biomass pyrolysis at high temperatures: Prediction of gaseous species yields from an anisotropic particle.* Biomass & Bioenergy, 2012. **41**: p. 107-121.

30.   Babu, B.V., *Biomass pyrolysis: A state-of-the-art review.* Biofuels Bioproducts & Biorefining-Biofpr, 2008. **2** (5): p. 393-414.

31.   Pou, J.O., et al., *Co-primary thermolysis molecular modeling simulation of lignin and subbituminous coal via a reactive coarse-grained simplification.* Journal of Analytical and Applied Pyrolysis, 2012. **95**: p. 101-111.

32.   Babu, B.V. and A.S. Chaurasia, *Modeling, simulation and estimation of optimum parameters in pyrolysis of biomass.* Energy Conversion and Management, 2003. **44** (13): p. 2135-2158.

33.   Babu, B.V. and A.S. Chaurasia, *Modeling for pyrolysis of solid particle: kinetics and heat transfer effects.* Energy Conversion and Management, 2003. **44** (14): p. 2251-2275.

34.   Diblasi, C., *Modeling and simulation of combustion processes of charring and non-charring solid fuels.* Progress in Energy and Combustion Science, 1993. **19** (1): p. 71-104.

35.   Di Blasi, C., *Modeling chemical and physical processes of wood and biomass pyrolysis.* Progress in Energy and Combustion Science, 2008. **34** (1): p. 47-90.

36.   Thurner, F. and U. Mann, *Kinetic investigation of wood pyrolysis.* Industrial & Engineering Chemistry Process Design and Development, 1981. **20** (3): p. 482-488.

37.   Koufopanos, C.A., et al., *Modeling of the pyrolysis of biomass particles - studies on kinetics, thermal and heat-transfer effects.* Canadian Journal of Chemical Engineering, 1991. **69** (4): p. 907-915.

38.   Koufopanos, C.A., G. Maschio, and A. Lucchesi, *Kinetic modeling of the pyrolysis of biomass and biomass components.* Canadian Journal of Chemical Engineering, 1989. **67** (1): p. 75-84.

39.   Demirbas, A., *Mechanisms of liquefaction and pyrolysis reactions of biomass.* Energy Conversion and Management, 2000. **41** (6): p. 633-646.

40. Srivastava, V.K. and R.K. Jalan, *Predictions of concentration in the pyrolysis of biomass materials .1.* Energy Conversion and Management, 1994. **35** (12): p. 1031-1040.

41. Srivastava, V.K., Sushil, and R.K. Jalan, *Prediction of concentration in the pyrolysis of biomass material .2.* Energy Conversion and Management, 1996. **37** (4): p. 473-483.

42. Faravelli, T., et al., *Detailed kinetic modeling of the thermal degradation of lignins.* Biomass & Bioenergy, 2010. **34** (3): p. 290-301.

43. Martinez, M.T., A.M. Benito, and M.A. Callejas, *Thermal cracking of coal residues: Kinetics of asphaltene decomposition.* Fuel, 1997. **76** (9): p. 871-877.

44. Singh, J., S. Kumar, and M.O. Garg, *Kinetic modelling of thermal cracking of petroleum residues: A critique.* Fuel Processing Technology, 2012. **94** (1): p. 131-144.

45. Nunn, T.R., et al., *Product compositions and kinetics in the rapid pyrolysis of milled wood lignin.* Industrial & Engineering Chemistry Process Design and Development, 1985. **24** (3): p. 844-852.

CHAPTER 4: DISCUSSION

4.1. Decomposition mechanism of lignin [10]

During combustion, lignin undergoes pyrolysis and oxidation to form many gaseous products which influence the chemical composition of the smoke [1]. In view of its chemical composition, lignin may serve as an interesting basic material for the study of formation of phenolic compounds with high yields, i.e. the phenoxy linkages are important structural units in lignin [2]. Nuclear Magnetic Resonance (NMR) studies have revealed various monolignol derivatives, e.g., *p*-hydroxyphenyls, guaiacyls, syringyls [3, 4]. Analyses of methoxy groups by quantitative ^{13}C NMR spectroscopy correlate well with published data from wet chemical methods [5].

Lignin decomposition occurs by several competing, bond-cleavage reactions at different temperatures depending on the bond energies [6]. The most frequently studied reaction is the thermal scission of the α- and β- alkyl-aryl ether bonds (cf. Figure 4.1 and Scheme 4.1) due to
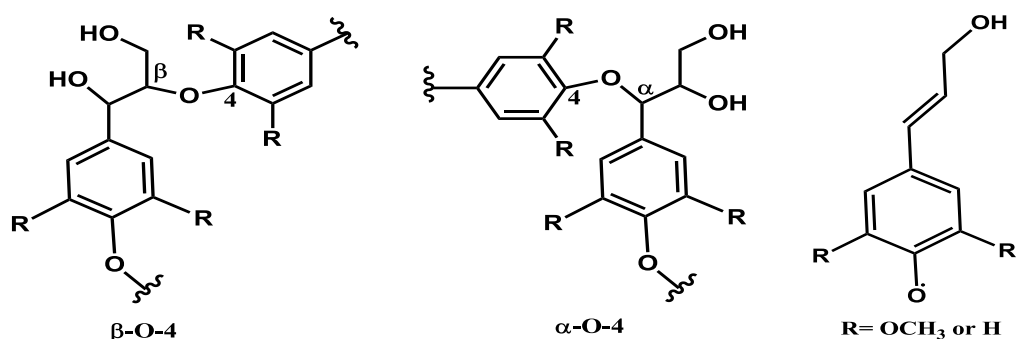
Figure 4.1. The main linkages in lignin polymer (β-O-4 and α-O-4) and substituted phenoxy radical from monolignols.

their prominent role in lignin chemistry [6]. Ether-linkages in lignin are cleaved in heat

---

treatment, leading to depolymerization of the lignin macromolecule, and formation of many products with ether linkages [7]. Lignin has a tendency to form volatile products when thermally decomposed between 200 and 500 ˚C [6, 8]. Thermogravimetric analysis of various lignin samples indicated the primary pyrolysis of lignin occurred between 200 and 400 ˚C [6, 9, 10], with the highest degradation rates occurring at~380 ˚C [3, 11]. This observation is attributed to the thermal scission of the α- and β- alkyl-aryl ether bonds, C-C and the C-O bonds that have lower bond dissociation energies (~346 and 358 kJmol^{-1}, respectively) than the C-OCH$_3$ bond (410 kJmol^{-1}), (cf. Figure 4.1) [6]. All these processes involve appearance of free radicals, elimination of water, formation of carbonyl, carboxyl and hydro peroxide groups (especially in air), evolution of CO and CO$_2$, and eventually production of a charred residue [12, 13]. Consequently, these findings point to the importance of interaction of various functional groups and their influence on the thermal decomposition of lignin [6]. Nevertheless, lignin is believed to thermally decompose via a free radical mechanism, Scheme 4.1 [13-15].

Pyrolysis of surface-immobilized model compounds revealed the thermal decomposition of lignins occurred primarily by free-radical mechanisms [15]. Phenoxy-type radicals (cf. Figure 4.1) have been implicated in lignin biosynthesis via coupling reactions and are considered the primary units of lignin [16], whereas semiquinone-type radicals are thought to be the minor linkages [17, 18]. The transient participation of phenoxy radicals is consistent with the structures of lignols isolated from the enzymatic polymerization of the lignin precursors, for instance, the participation of *p*-coumaryl alcohols have also been inferred by the detection of a weak, unresolved EPR signal during the initial stages of polymerization [16, 19]. Upon dehydrogenation, coniferyl alcohol is converted to phenoxy radical [19]. Moreover, photolysis of coniferyl alcohol in carbon tetrachloride suggested a radical mechanism and formation of a

phenoxy radical with a half-life of 0.5 s [16]. Therefore, the observation of phenoxy radicals has

led to the suggestion of a free radical mechanism of thermolysis of the alkyl-aryl ether linkages

in lignin [13, 20, 21]. Scheme 4.1 gives the proposed mechanism for lignin pyrolysis.

Studies using D-band EPR revealed a background singlet due to the natural Para
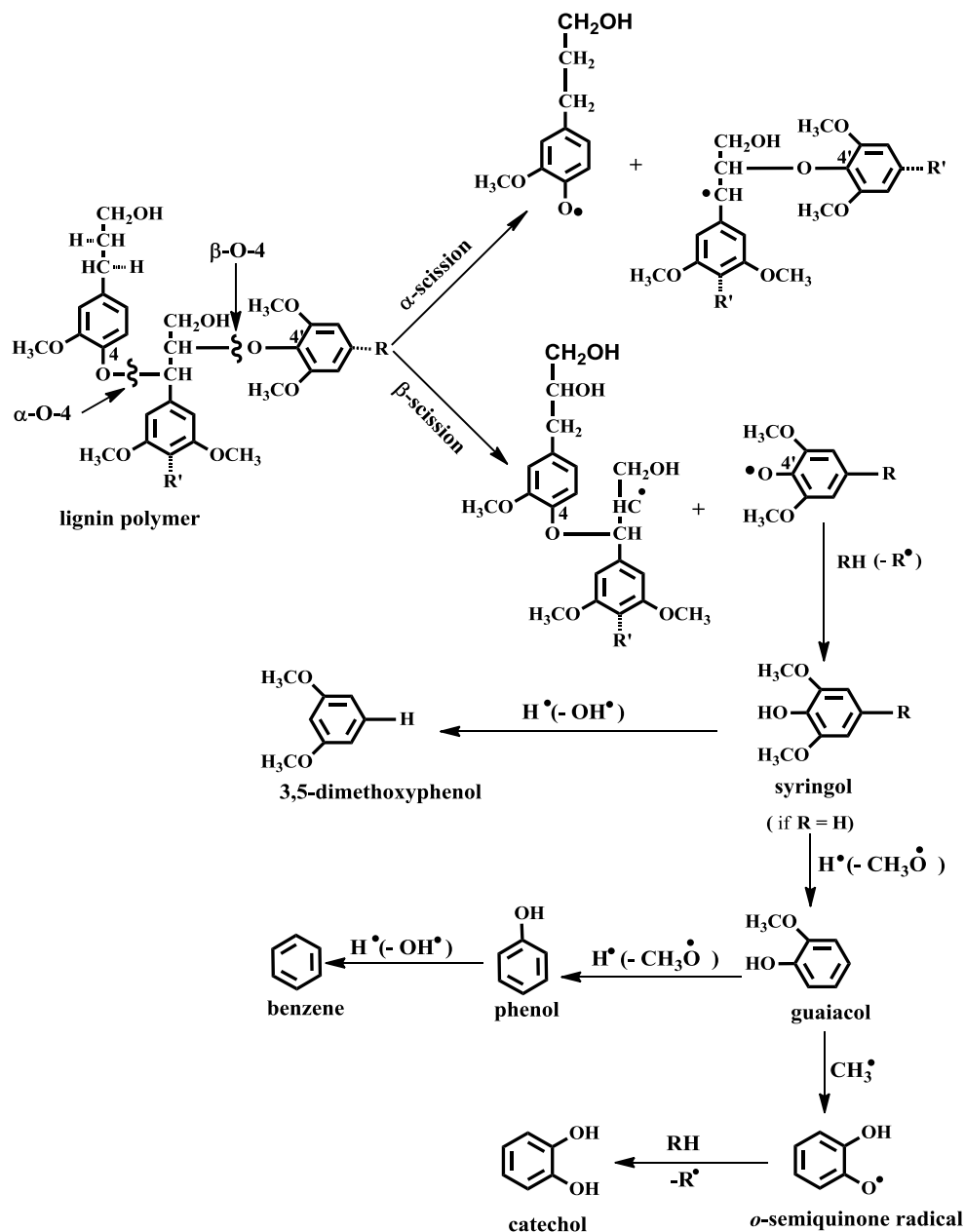
Scheme 4.1. Proposed mechanism for formation of major products from pyrolysis of lignin.

magnetism of wood at g = 2.000, which is consistent with radicals having conjugated carbon-

carbon bonds [22, 23]. Furthermore, in the lignin polymeric framework, some of the linkages are present as polyhydroxy derivatives, which can form semiquinone derivatives [18]. Such a matrix is mainly composed of hydroquinone-quinone type building blocks to stabilize effectively semiquinone-type free radicals [17, 18]. The observation of 2,6-dimethoxy-*p*-benzosemiquinone and 6-hydroxy-2-methoxy-*p*-benzosemiquinone radicals from oxidation of dioxane lignins in alkaline solutions has also been thought to be produced from syringyl end groups [14].

We here report on the pyrolytic decomposition of lignin using the System for Thermal Diagnostic Studies (SDTS) to analyze for molecular products and Low Temperature Matrix Isolation EPR (LTMI-EPR) to identify free radical intermediates. These data are discussed in relation to the mechanism of lignin decomposition and the toxicity of its decomposition by-products.

4.1.1. Radicals from pyrolysis of lignin

Because phenoxy linkages are key structural units while semiquinones are secondary linkages, phenoxy-type radicals may be higher in concentration than semiquinone radicals from lignin pyrolysis [16]. Accordingly, it can be concluded that intermediate radicals are mostly derived from phenolic linkages in lignin and are probable precursors for formation of phenolic compounds, i.e. 2,6 - dimethoxy phenoxy (syringyl groups), 2-methoxy phenoxy (guaiacyl groups), and phenols for (phenoxy goups) etc. For this to be true, these intermediate radicals should be present in the EPR spectrum. Additionally, this argument is supported by results from GC-MS analyses which indicate that phenolic compounds are the major reaction products of lignin pyrolysis. The yields of the principal phenol-type products drop significantly in the order: syringol > guaiacol > phenol > cresols~catechol, Figure 3.1, *vide supra*.

A key issue is the broad character of the EPR spectra detected from lignin pyrolysis. Comparing the broadening effect of substituent groups on EPR spectra of phenoxy radical is useful to understand this. For instance, the position and number of Cl atoms on the aromatic ring, as a typical electronegative (electron-withdrawing) substituent, slightly affects the total spectral width [24]. The g-value slowly increases from g = 2.0062 for mono -, to g = 2.0065 for di −, and g = 2.0076 for tri-chloro phenoxyl radicals (the g-value for pure phenoxy is g = 2.0053) [24]. In contrast to chlorine substituents, methyl group are electron-donating and broaden the EPR spectra of phenoxy groups [25]. Methoxy substituted phenoxy radicals, which form in lignin pyrolysis, may have dual impacts on total EPR line-width, because of their ability to be either electron-donating or electron − withdrawing, depending on the position of substitution [25, 26]. The spectral width of EPR spectra presented in the residue spectrum is broader (ΔHp-p = 18G) than the phenoxy radical EPR spectrum (ΔHp-p = 16G) detected from phenol pyrolysis using the same LTMI-EPR technique [27].

To determine if the observed spectra were of substituted phenoxy radiclas, additional experiments were initiated. Radicals were generated by UV photolysis of hydroquinone (HQ), catechol (CT), phenol (PhOH) and some substituted phenols from their frozen aquatic solutions. The UV photo excitation of phenol resulted in partial photo dissociation to phenoxy radical and a hydrogen atom [28, 29], and the photodecomposition of HQ/CT should occur similarly [30]. It was observed that the EPR spectra generated from these experiments were simple unstructured singlet lines as indicated in Table 4.1, *vide infra*. By comparing the g-factor and DHp-p for various species generated at various conditions, the radical parameters for the radicals in lignin were deduced.

96

Table 4.1. EPR Parameters of radicals generated by uv photolysis of hydroquinone (HQ), catechol (CT), phenol (PhOH) and some substituted phenols in frozen aquatic solution, pH = 7.0.

	HQ	HQ	HQ	HQ	CT	CT	PhOH	PhOH	Tyrosine[b]	4-Cl-PhOH
ΔH p-p, G	12.5	11.0	9.5	11.5	15.5	12.7	16.0-21.0[c]	21.0	21.0	19.0
g-value	2.0049	2.0049	2.0050	2.0042	2.0058	2.0049	2.0051	2.0050	2.0048	2.0063
Molarity, M	8.0×10^{-2}	Annealing[a]	Annealing[a]	**	1×10^{-1}	**	6.0×10^{-2}	**	5.0×10^{-3}	1×10^{-1}

[a] gradual annealing of the frozen solution of HQ at 8.0×10^{-2} M after UV irradiation.

** – radicals were generated from very low pressure, gas-phase photolysis of precursors and accumulated on the cold finger at 77 K.

[b] tyrosine: $(OH)C_6H_4CH_2CH(NH_2)CO_2H$.

[c] depending on irradiation time.

The common feature for all spectra was the high g-values characteristic for oxygen centered radicals [31] and broad singlet lines. The ΔHp-p for radicals produced from phenol, tyrosine and 4-chlorophenol were much broader (19-21 G) than for radicals from HQ or CT (10-15G) (cf. Table 4.1). The effect of concentration broadening on the EPR spectra of radicals (hydroxyphenoxyl or neutral semiquinone radical) produced by UV photolysis of frozen aquatic solutions of hydroquinone is clear from the data in Table 1 [32]. For instance, the ΔHp-p = 12.5 G for semiquinone radicals derived from stock solution of HQ (normalized intensity, I = 1.5, arbitrary units) dropped slowly by annealing procedure to ΔH p-p = 11.0 G (I = 0.14) and ΔH p-p = 9.5.0 G (I = 0.07) at almost the same g-value (cf. Table 4.1). The broad signals derived from phenol, tyrosine and 4-chlorophenol (ΔH p-p = 19-21 G) most resembled the signal produced from lignin pyrolysis (ΔH p-p = 18.0 G), with a high g-value of 2.0064.

Due to their high g-value and broad line-width, the EPR data strongly suggest the EPR spectra from lignin gas–phase pyrolysis are phenoxy and substituted phenoxy radicals. To the best of our knowledge, these EPR data supported by molecular product analysis are new and

successfully identify the intermediate character of radicals in the gas-phase pyrolysis of lignin. This establishes a critical base for further elucidation and modeling of the gas-phase pyrolysis of lignin.

4.2. Decomposition pathways for tyrosine[11]

4.2.1. Initial decomposition

The mechanistic considerations for pyrolysis experiments of amino acids have been extensively studied [20, 21, 33-37]. Consequently, this investigation will focus primarily on the mechanistic pathways of new, major products from oxidative pyrolysis of tyrosine (*p*-tyramine, phenol, and *p*-cresol), while elucidating critical concepts of pyrolysis. First, *p*-tyramine, one of the principal products from oxidative pyrolysis of tyrosine may be formed from simple decarboxylation pathway.

Previously, the decarboxylation of amino acids has been conducted using density functional theory in the gas phase, and found that the decarboxylation channel for high molecular weight amino acids including tyrosine proceeds from the higher-energy anti carboxylic hydrogen conformer and involves the direct heterolytic loss of CO_2 accompanied by direct proton transfer [38,39], Scheme 4.2. The calculated activation energy for direct decarboxylation in tyrosine was found to be 72 kcal mol^{-1} in absence of water [39]. While in the presence of water, the direct decarboxylation is catalyzed and the calculated energy barrier drops to an average of 45 kcal mol^{-1} [39].

---

[11] Reproduced in part with permission from Kibet J. K.; Lavrent K., and Dellinger, B. *Molecular Products from Pyrolysis and Oxidative Pyrolysis of Tyrosine*. DOI: 10.1016/j.chemosphere.2013.01.071. Chemosphere. Copyright Elsevier, 2013.

More recently, a statistical mechanical investigation (QM/MM) [39] indicated the most likely pathway for decomposition of amino acids in the presence of water occurs via direct decarboxylation, where CO_2 elimination is the first as well as the rate determining step [39]. For instance, the computed free energy of activation for decarboxylation of glycine in presence of water was found to be 45 kcal mol^{-1}, and the resultant rate constant was 10^{-21} s^{-1} at 25 ˚C [39] in agreement with experimental data [38]. The low activation energy and low pre-exponential
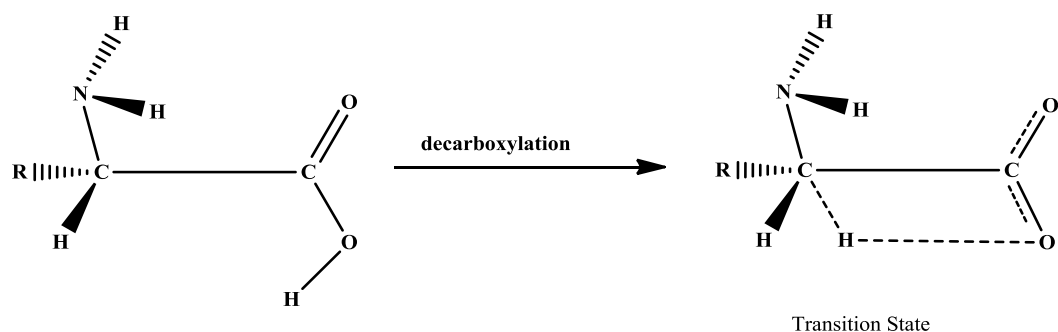
Scheme 4.2. Transition state during decarboxylation of high molecular weight amino acids in the gas phase [39]

factor for decarboxylation of amino acids results in a very slow process at room temperature which accelerates rapidly with increasing temperature.
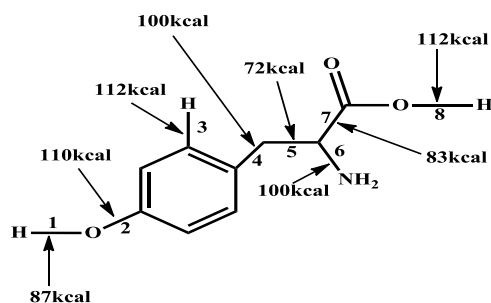
Figure 4.2. Estimated bond dissociation energies for important bonds in tyrosine [33-37]

The other competetive pathway to tyramine formation is the cleavage of bond # 5 with an

estimated bond strength of 72 kcal mol^{-1}, (cf. Figure 4.1) [40-46]. Cleavage of bond # 5 results in the formation of 4-methylene phenolic radical and subsequently *p*-cresol by donation of a hydrogen by a suitable donor, RH (Rxns. 1, 2).

Typically, the activation energy for simple bond cleavage reactions, such as Rxn 1 is closely related to the enthalpy of reaction, 72 kcal mol^{-1}. This is close to the activation energy

Rxn 1

Rxn2

p-methylene phenolic radical

p-cresol
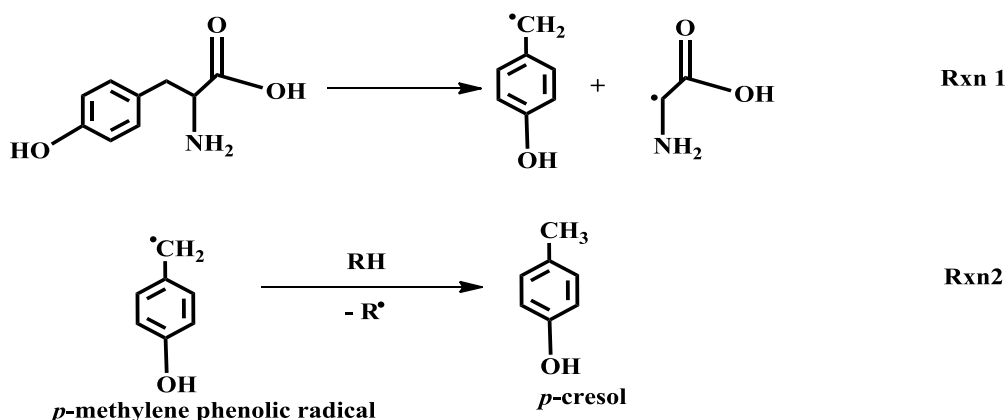
(72.6 kcal mol^{-1}) for decarboxylation of tyrosine which produces *p*-tyramine [39]. However, the steric hindrance for decarboxylation reaction is obvious. For instance, the pre-exponential factors for decarboxylation reactions of different amino acids span a wide range, from 10^{10} s^{-1} for met-amino acid (methionine amino acid) to 10^{16} s^{-1} for α-Aib (α-amino isobutyric) amino acid [39]. This difference may make the cleavage of bond # 5 (cf. Figure 4.2) favorable over decarboxylation reactions and as a result, *p*-cresol is one of the dominant products in tyrosine pyrolysis, *vide supra* Figure 3.10 A.

Phenol has been proposed to form from further decomposition of *p*-cresol via the formation of a phenoxy radical and subsequently to phenol via abstraction of an H radical [20]. Because the concentration of phenol is a little higher than that of *p*-cresol for both pyrolysis and oxidation experiments, *vide supra* Figure 3.10 A, it would appear there is an additional

mechanistic channel for the formation of phenol. For instance it may be the result of cleavage of

bond # 4 (cf. Figure 4.2) with a bond energy of 100 kcal mol^{-1}, leading to the formation of p-

hydroxylated phenyl radical (and latter to phenol by abstraction of hydrogen) or displacement of

the entire side-chain by H$^•$. This pathway may be feasible if we compare it with one of the

important channels, deamination of amino acids [39] which occurs by participation of the bond #

6 with exactly the same bond energy as bond # 4, 100 kcal mol^{-1} (cf. Figure 4.2).

4.2.2. The main channels from oxidative pyrolysis

Whereas p-tyramine is the major product during oxidative pyrolysis of tyrosine, it is
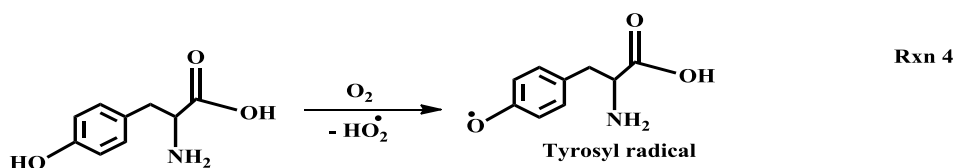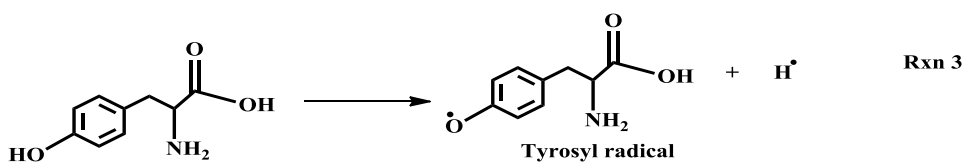
formed in low concentrations under pyrolysis, *vide supra* Figures 3.8 A and 3.10 A. This

phenomenon can be understood if a more favorable, free radical mechanism is considered in

presence of oxygen. For instance the initiation pathway presented in rxn 3 (assuming the

activation energy equal to the bond dissociation energy ~ 86.5 kcal mol^{-1}),

$k_3 = 3.2x10^{15} \exp\left(\dfrac{-86500\ cal\,mol^{-1}}{RT}\right)$ s^{-1} can be accelerated significantly in presence of oxygen,

rxn 4 (activation energy may be around 40-42 kcal mol^{-1}),

$k_4 = 10^{12}(10^{14})\exp\left(\dfrac{-41500\ cal\,mol^{-1}}{RT}\right)$ cm^3 mol^{-1} s^{-1} [47]. The concentration of oxygen in the

system was 4%, the equivalent of 4.50 x 10^{17} molecules/cm^3 at 400 ^{o}C. Therefore the ratio of the

rates $\dfrac{R_4}{R_3}$ can be computed and found to be in favor of rxn 4 ($\dfrac{R_4}{R_3} \sim 1.0$ x 10^5).

Reactions 3 and 4 form tyrosyl radical. The tyrosyl radical (Tyr•) is an intermediate radical that has been detected, identified and reported as a protein - derived tyrosyl radical from the fractional pyrolysis of bright tobacco [48]. It is remarkable that the observable amounts of Tyr• were produced at < 380 ^{o}C from tobacco pyrolysis, which matches well with the maximum yields of tyramine (370 ^{o}C) from tyrosine pyrolysis, *vide supra* Figure 3.10 A. Further

Tyraminyl radical

Rxn 5

Tyraminyl radical
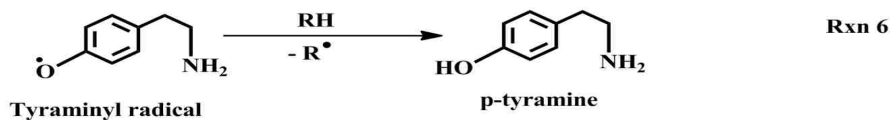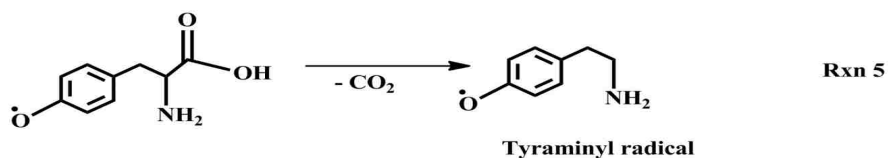
p-tyramine

Rxn 6

decarboxylation of Tyr• favors formation of tyraminyl radical, Rxn 5, and subsequent formation of *p*-tyramine via Rxn 6.

Note that in presence of water the decarboxylation of amino acids is more facile and the activation energy drops from 72 kcal mol^{-1} (without water) to 45 kcal mol^{-1} (in presence of water) [38, 39]. The •OH may have a similar effect towards decarboxylation as water. Furthermore the processes of formation Tyr• will be accelerated when •OH are the main chain carrier radicals (Rxn 4, abstraction of hydrogen from phenolic hydroxyl group). These reactions (4-6) are the main pathways that promote the formation of *p*-tyramine, which is the major product during oxidative pyrolysis. These as well some additional reactions for formation of

major products from tyrosine pyrolysis / oxidative pyrolysis, based also on literature data [20] are summarized in Scheme 4.3.

The formation of other major products (by decreasing yields after *p*-tyramine, phenols and cresols) such as benzonitrile, benzaldoxime, and acetonitrile are probably the result of
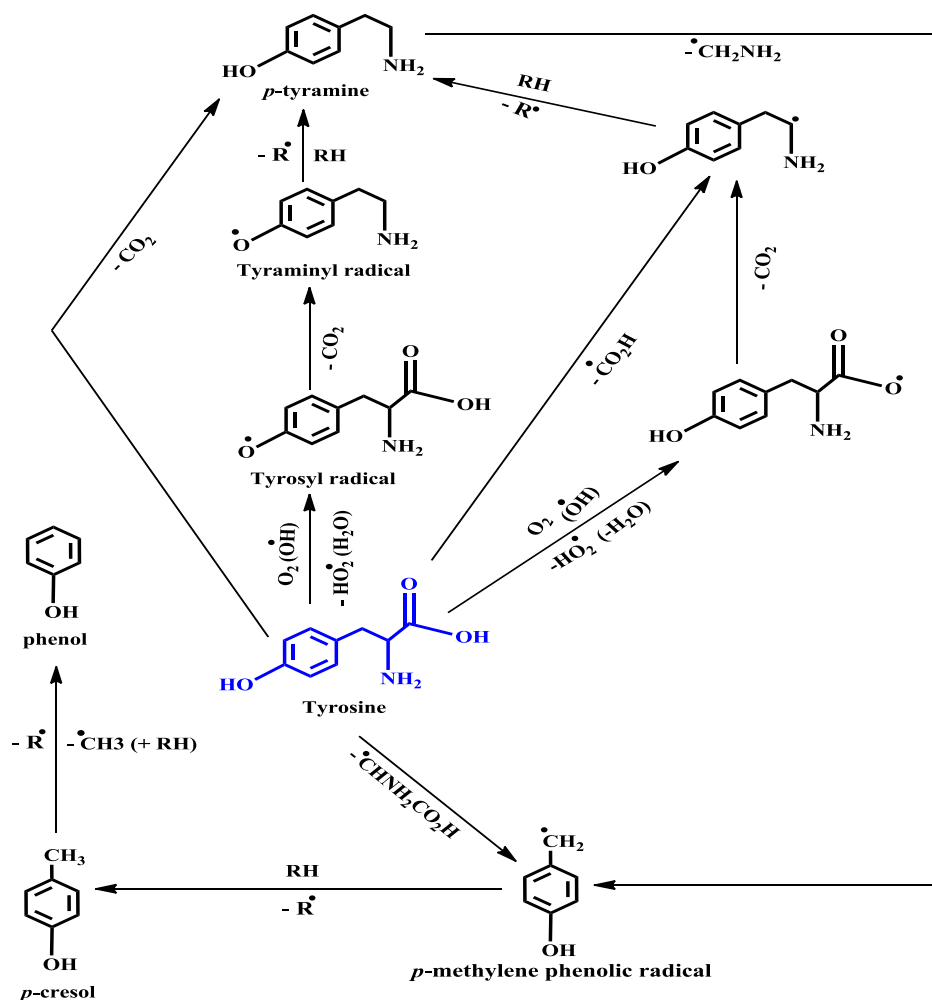
Scheme 4.3. Mechanistic Pathways for Formation of Major Phenolic Compounds from Decomposition of Tyrosine.

dipeptide or polypeptide decomposition reactions. Dipeptide forming reactions occur readily because they are simple dehydration reactions which are usually enhanced by increase in temperature [20, 36, 37, 49]. Although the concentration of dipeptide is considered low, it is

believed to play a critical role in the formation of many observed products of amino acid pyrolysis [33, 49]. For instance the formation of acetonitrile from pyrolysis of tyrosine may proceed via the decomposition of cyclic dipeptides [49]. This channel involves a molecular process, and a free radical mechanism in which acetonitrile is eventually formed from dehydration of acetamide.

The rate of decomposition of tyrosine is enhanced for oxidative pyrolysis because the process occurs under a reactive regime, in presence of O_2 and ${}^{\bullet}$OH. For this reason, decarboxylation reaction will also proceed via a free radical mechanism in additional to a molecular process under pyrolysis. This explains why the concentration of *p*-tyramine for oxidative pyrolysis experiments is much higher than that of pyrolysis experiments.

The direct decarboxylation of tyrosine yields 4-(2-amino ethyl) phenol as the major product (cf. Scheme 4.3, *vide supra*). As discussed above 4-(-amino ethyl) phenol subsequently undergoes deamination to form an ethyl phenolic radical and ultimately to 4-ethyl phenol. Alternatively, 4-ethyl-(-amino ethyl) phenol decomposes to a methylene phenolic radical via rupture of bond #2 to ultimately form *p*-cresol. Phenol may be formed in one of two ways: 1) via the decomposition of *p*-cresol or 2) via the rupture of bond #1 to form a phenolic radical and finally to phenol by addition of H from a suitable donor, RH, (cf. Figure 4.2 and Scheme 4.3).

This explains why the concentration of phenol is higher than the concentration of *p*-cresol for both pyrolysis and oxidative pyrolysis. The other phenolic compounds observed (*o*-cresol and 2,3-dimethyl phenol) are believed to be the result of methylation of phenol or the abstraction of ring hydrogen by a methyl radical. In the formation of *o*-cresol, a hydrogen *ortho* to the phenol is replaced by a methyl group while in the formation of 2,3-dimethyl phenol, a *meta* hydrogen in *o*-cresol is replaced by a methyl group.

The formation of aromatic hydrocarbon products is believed to proceed from displacement of OH radical from respective precursors (cf. Scheme 4.4). For instance, the formation of benzene proceeds from displacement of OH radical from phenol by hydrogen to form phenyl radical and subsequently to benzene by addition of H from an H donor species, RH. Similarly, toluene and ethyl benzene are formed as reported in Scheme 4.4. The formation of low molecular weight hydrocarbons may be the result of ring opening of benzene (minor route) or the
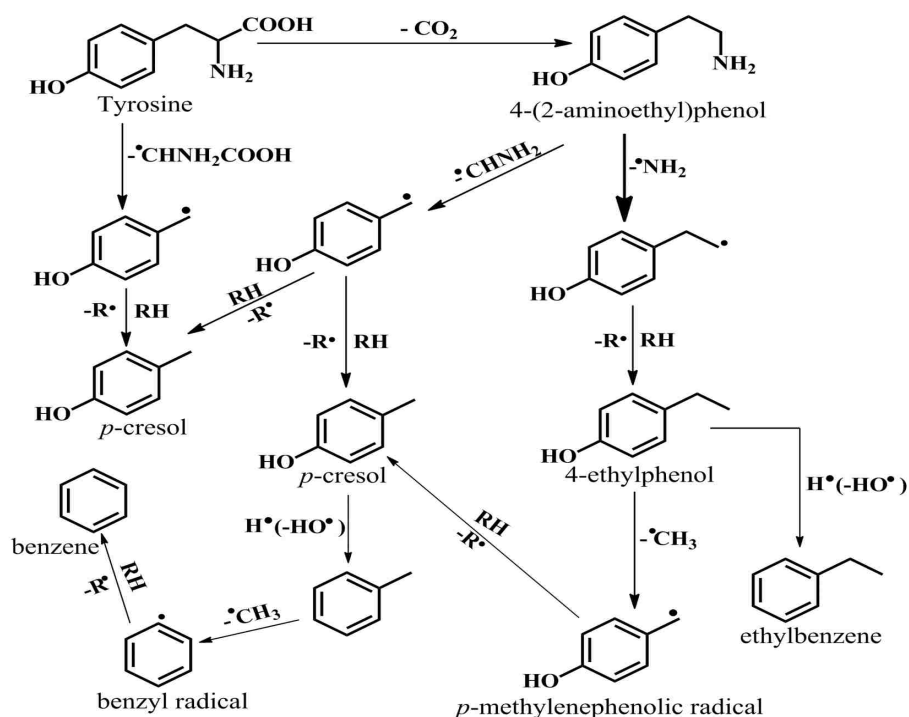
Scheme 4.4. Proposed mechanism for the formation of major phenolic and hydrocarbon products from the thermal decomposition of tyrosine

decomposition of ethyl benzene and toluene to precursor methyl and ethyl radicals (major route). Ethyl radicals can react with a methyl radical to form propane, or propene (by release of H_2). It is clear from the low concentrations of hydrocarbons (propene, propane, and 1-butene) that ring opening of benzene is not a major route. It is therefore likely that formation of aromatic

hydrocarbons via a molecular growth process of small hydrocarbons (molecular condensation) is negligible. [12]

4.2.3. New class of compounds not reported in literature

Oxidative pyrolysis of tyrosine yielded other important compounds of biological interest: hydroquinone, *p*-benzoquinone, benzofuran, dibenzofuran, and dibenzo-*p*-dioxin. The main precursor for formation of hydroquinone and ultimately *p*-benzoquinone is *p*-cresol (cf. Scheme 4.5). An OH radical displaces the methyl in *p*-cresol, yielding hydroquinone. Subsequently, *p*-benzoquinone formation is initiated via endothermic dissociation of a phenoxyl-hydrogen (ΔH_{rxn} = 81.3 kcal/mol) or H$^•$ abstraction by $^•$OH to form *p*-semiquinone radical [40, 50]. Subsequent loss of phenoxyl-hydrogen by unimolecular decomposition (ΔH_{rxn} = 87 kcal mol^{-1}) [41] or
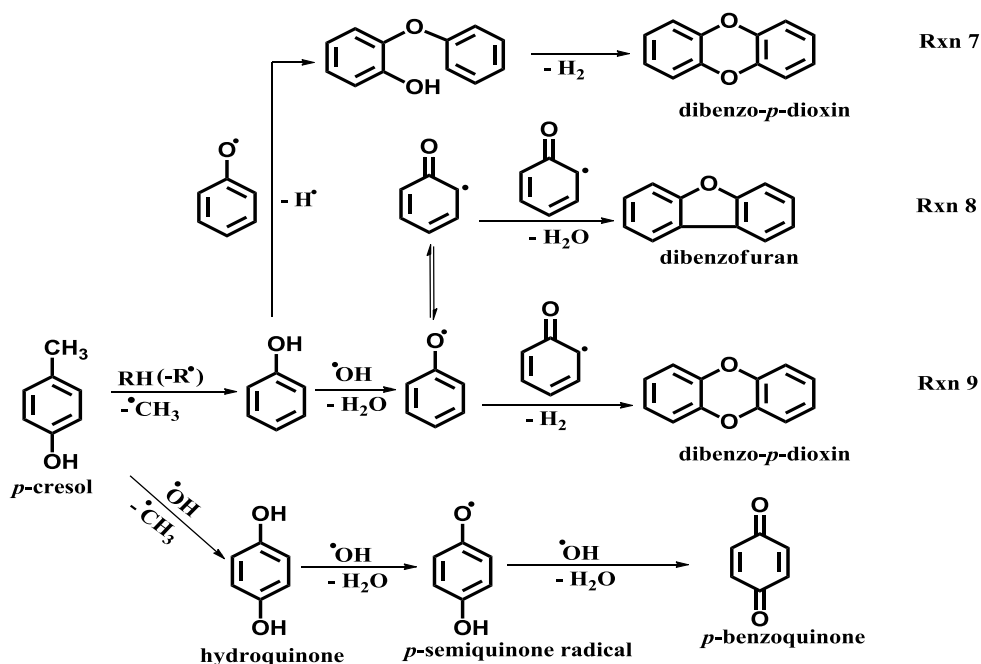
Scheme 4.5. Formation of hydroquinone, *p*-benzoquinone, dibenzofuran, and dibenzo-*p*-dioxin

---

abstraction (ΔH_{rxn} = 40 kcal mol^{-1}) [51] by OH radical results in the formation of *p*-benzoquinone.

The formation of dibenzo-*p*-dioxin and dibenzofuran from oxidative pyrolysis of tyrosine has captured our attention because of the health impacts of the chlorinated analogues of these compounds [52, 53]. Although these compounds are reported extensively in literature, never before have they been documented during the combustion of amino acids. Hydroxyl radical is believed to play a critical role during oxidative pyrolysis of tyrosine and influences the reaction products observed. The precursor for these compounds is phenol.

When subjected to heat, phenol forms both dibenzofuran [51] and dibenzo-*p*-dioxin [47, 54-57]. The formation pathway for dibenzo-*p*-dioxin/dibenzofuran proceeds via free radical mechanisms either through radical-molecule or radical-radical pathways [47, 54-59]. In the radical-molecule pathway the enol form of the phenoxy radical displaces a ring hydrogen of the phenol molecule to form a hydroxyl biphenyl ether intermediate, rxn 7 followed by ring closure and ultimately the formation of dibenzo-*p*-dioxin [40, 47, 51, 54-59] (cf. Scheme 4.5). In the radical-radical pathway two keto mesomers (resonance structures) can react with each other (cf. Scheme 4.5, rxn 8) to form dibenzofuran, while keto- and enol- mesomers react to form dibenzo-*p*-dioxin, rxn 9.

4.3. The mechanistic pathways for pyrolysis of glutamic acid[13]

The major reactions for glutamic acid are dehydration, decarboxylation, and deamination [60]. Glutamic acid contains two acidic (— CO_2H) groups and one basic (— NH_2) group which can react to form large molecules at high temperatures [33, 61]. Therefore, different functional

---

[13] Reproduced in part with permission from Kibet J. K.; Lavrent K., and Dellinger, B. *Molecular Products from the Pyrolysis and Oxidative Pyrolysis of Glutamic Acid in a Flow Reactor*, Energy & Fuels, 2013. Copyright American Chemical Society, 2013. (In progress).

groups are expected to have different pyrolysis characteristics as well as give different pyrolysis products [62]. For example, at low temperatures ($\sim 300°C$) low molecular weight heterocyclic compounds are formed, whereas at high temperatures ($> 500°C$), polycyclic aromatic hydrocarbons are expected to form [49].

4.3.1. Primary decomposition reactions of glutamic acid

The major primary reaction reported in literature for the thermal degradation of glutamic acid is condensation [37, 63, 64]. Reactions 1-3 were speculated to occur during the initial decomposition of glutamic acid [63, 64]. The three reactions are accompanied by a direct loss of
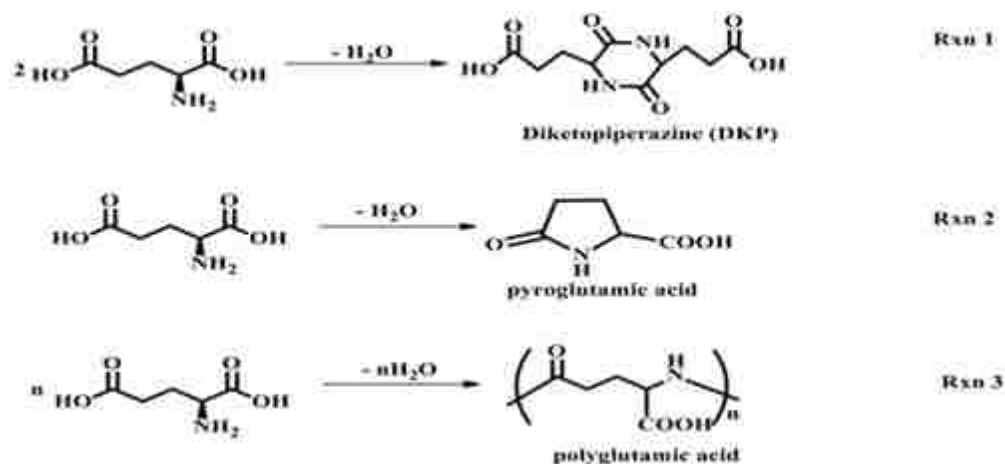
a water molecule per formula unit of glutamic acid [63]. Reaction 1 shows the dimerization of glutamic acid to yield a diketo piperazine (DKP) while reaction 2 shows the internal cyclization of glutamic acid to produce pyroglutamic acid [63-65]. Reaction 3 shows the formation of polyglutamic acid from polymerization of glutamic acid [63]. We believe Rnxs 1-3 are competing reactions during the thermal decomposition of glutamic acid to yield intermediate products which further react to form observed reaction products. However, it is not easy to infer with certainty which reaction dominates over the other without the use of elaborate analytical techniques. Nevertheless, with the identification of pyroglutamic acid in our system (cf. Figure

3.17, *vide supra*), we propose reaction 2 is dominant. Reaction 1 is also widely reported in literature although it is believed the concentration of diketo piperazine (dipeptide) is very low in the gas-phase of thermal systems [49]. In principle, dipeptides will be non-detectable intermediates in amino acid pyrolysis because of their high thermal reactivity and low volatility which keeps them in the thermal zone until they react further [49]. Reaction 3 is speculated to occur but is very unlikely that polyglutamic acid owing to its high molecular weight and high absorptivity is transported to the gas-phase during pyrolysis, and therefore cannot be considered a dominant product in the gas-phase. Accordingly, this study concludes reaction 2 is the principal condensation process during the decomposition of glutamic acid as confirmed by mass-spectrum peak at Retention Time 17.5 minutes (cf. Figure 3.17, *vide supra*). This finding is consistent with the work of Nunes and Cavalheiro [64] where a TG-FTIR and ^{1}H NMR studies suggested pyroglutamic acid was a major product of the thermal decomposition of glutamic acid. It would appear pyroglutamic acid is formed in low concentrations under pyrolysis, (cf. Figure 3.19, *vide supra*). This is because under an oxidative atmosphere, the rate of reaction 2 is increased rapidly in presence of OH radical as compared to an H radical under a pyrolytic regime. The formation of cyclic amides would also release water in a primary decomposition step, and have been suggested as intermediates in several reactions [37]. However, secondary decomposition reactions such as dehydration of amides must also be considered as a source of water [37].

4.3.2. Decomposition pathways for glutamic acid

The mechanistic considerations for pyrolysis experiments of amino acids have been extensively studied [20, 21, 33-37]. Previously, the decarboxylation of amino acids has been conducted using density functional theory (DFT) in the gas phase, and found that the decarboxylation channel for most amino acids including glutamic acid proceeds from the higher-

energy anti carboxylic hydrogen conformer and involves the direct heterolytic loss of CO_2 accompanied by direct proton transfer [38] (cf. Scheme 4.2, *vide supra*). The energy barriers towards decarboxylation for most amino acids in the gas phase are about 72 kcal mol^{-1} [38].

The use of ^{14}C-labelled amino acids provide excellent evidence that decarboxylation is the predominant decomposition pathway for amino acids [66]. Decarboxylation reactions of amino acids yield an amine as the major product [66] and clearly the major decomposition pathway as evidenced from the yield of CO_2 [37].

Maleimide (2,5-pyrroledione) may be formed from glutamic acid via dehydrative cyclization and loss of water [37]. It would seem succinimide can be formed from reduction of maleimide but experiments performed by Sharma et al. showed that independent pyrolysis of maleimide did not yield succinimide [49]. This observation is attributed to the fact that maleimide is very stable and can transfer from the thermal zone prior to degradation yielding itself (maleimide) and no other components [49, 67]. However, pyrolysis of succinimide yielded maleimide as one of the reaction products [67]. Ultimately, succinimide was proposed to be formed from disproportionation reactions resulting from thermal decomposition of cyclic amides [49]. Early studies postulated pyrolysis of succinimide yielded mainly CO, H_2O and acetonitrile [68]. This may suggest a secondary route for the formation of acetonitrile. Choudhar et al. proposed an activation energy of 52 kcal mol^{-1} for the ring opening of succinimide [68].

4.3.3. Mechanistic pathways for formation of succinimide and maleimide

The major product during fractional pyrolysis as well fractional oxidative pyrolysis was succinimide surprisingly non-dedected in previous studies [49]. Our studies, however; have since shown that pyrolysis of glutamic acid in N_2 and 4% O_2 in N_2 would in fact yield succinimide and maleimide. Maleimide was formed in much less amounts than succinimide. The yields of

110

maleimide did not change significantly when the pyrolysis environment was changed from N_2 to 4% O_2 in N_2. Succinimide for instance was exclusively the major product under oxidative pyrolysis contributing about 40% of the products analyzed while under pyrolysis it contributed over 20% of the products analyzed. Whereas previously succinimide has been detected from the thermal degradation of aspartic acid, asparagine, and glutamine, no succinimide has been detected from the thermal degradation of glutamic acid [49]. The mechanistic channel for succinimide and maleimide formation from aspartic and asparagine is known, however; succinimide and maleimide formation from glutamine and glutamic acid is not yet understood [49].

Succinimide and maleimide nevertheless, are structures that are characteristic of amino acids containing additional carboxylic or amino functional groups [33]. Accordingly, we propose the formation of succinimide proceeds via an intermediate, a tricyclic diketo piperazine (DKP), which would eventually, decompose to succinimide and 2-pyridone (cf. Scheme 4.6, *vide infra*). From this pathway, maleimide appears to be formed from the dehydrogenation of succinimide, and may explain why succinimide was formed in higher concentrations than maleimide. It was previously proven experimentally by Sharma *et al*. that direct degradation of succinmide yielded maleimide [49].

The formation of diketo piperazine, DKP requires two molecules of pyroglutamic acid [49]. This product forms in trace and significant amounts in pyrolysis and oxidative pyrolysis respectively, *vide supra* Figure 3.17. Peptide forming reactions occur readily because they involve simple dehydration reactions [49]. In principle, peptides will be non-detectable intermediates in amino acid pyrolysis because of their high thermal reactivity and low volatility which keeps them in the thermal zone until they react further [49]. Consequently, we speculate

111

DKP thermally degrades to succinimide and 2-pyridone (cf. Scheme 4.6). 2-pyridone was one of
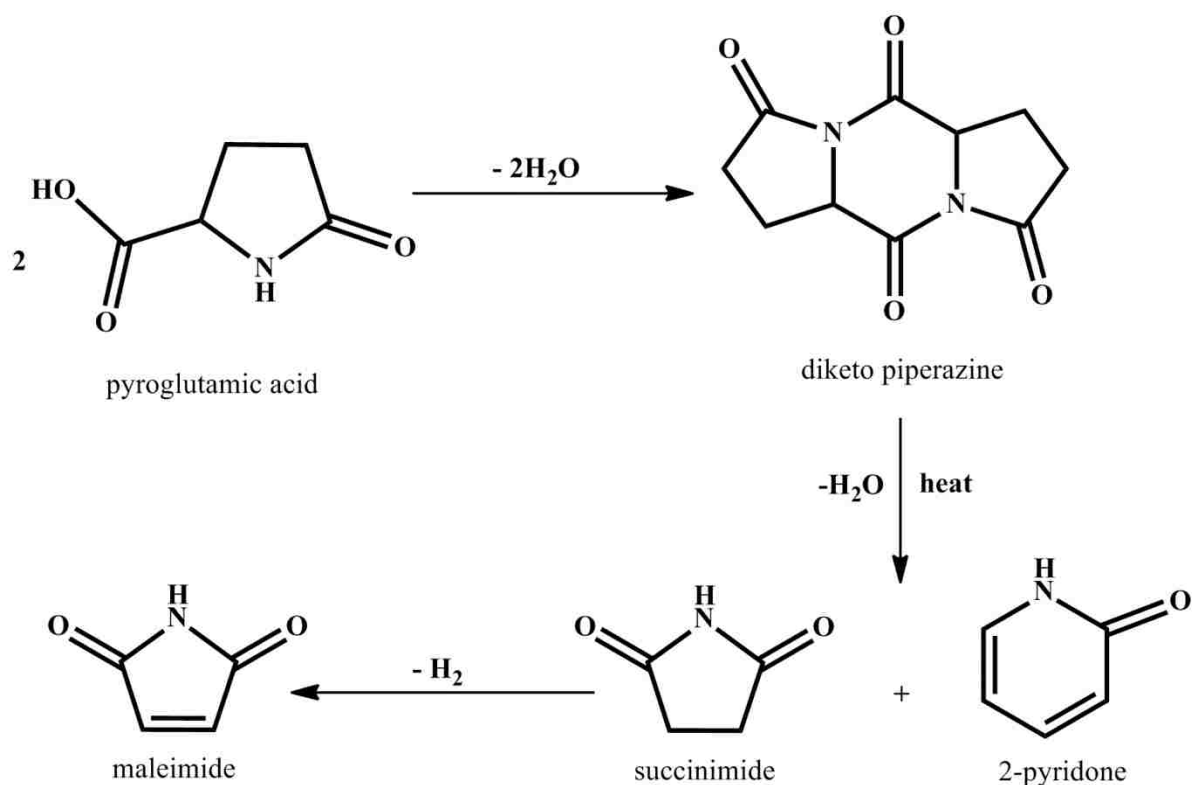
Scheme 4.6. Formation of diketo piperazine from pyroglutamic acid, and succinimide and maleimde from diketo piperazine.

the major products from the thermal degradation of glutamic acid under pyrolysis but a minor product under oxidative pyrolysis. This is because, although an oxidizing environment accelerates the formation of pyrolysis products, it may also oxidize certain reaction products into water, CO, or CO_2 and subsequently decrease their yields.

Scheme 4.6 predicts equal amounts of succinimide and 2-pyridone. Experimentally it was found the yields of succinimide prevailed over the yields of 2-pyridone by a factor of 2. This may be possible because 2-pyridone is susceptible to hydrogenation in presence of abundant pool of hydrogen atoms in pyrolysis and char (as a catalyst). Also the high polarisability of 2-

pyridone [69] in comparison with succinimide (symmetric structure) [70], enhances its absorptivity on the GC column and consequently minimizing its detection. The marked difference in yields between succinimide and 2-pyridone are evident in oxidative pyrolysis. 2-pyridone may be easily oxidized by oxygen or most importantly by abundant hydroxyl radicals (characteristic of oxidative processes) into water, CO, or CO_2 and subsequently decrease its yield, making it a minor product.

The key finding during oxidation is that the yield of succinimide grows up suddenly predominating over all other products' yields significantly. Pyroglutamic acid, an important

Gas-Phase Transition State

R= CH_2CH_2COOH
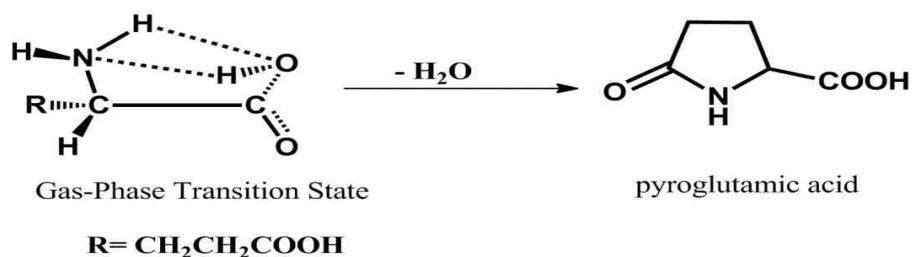
pyroglutamic acid

Scheme 4.7. Proposed transition state for dehydration of glutamic acid in the gas-phase

precursor for formation of succinimide (cf. Scheme 4.7) was observed experimentally in detectable amounts in oxidative conditions, Figure 3.19 *vide supra* (blue chromatogram at RT ~ 17.3 minutes) but in trace amounts under pyrolytic conditions. As an important intermediate product, pyroglutamic acid may form from internal cyclization of glutamic acid via dehydration processes [63-65]. Dehydration is a very common reaction for amino acids and usually occurs in the gas-phase through a four-centered concerted mechanism (cf. Scheme 4.7, *vide supra*). As expected, hydroxyl radicals during oxidative pyrolysis will facilitate this concerted mechanism towards formation of pyroglutamic acid (by increasing the polarizability of hydroxyl O-H bond in carboxylic group).

4.3.4. Mechanistic channels for the formation of pyrroles

The thermal degradation of glutamic acid appears to be a major process not only in the pyrosynthesis of succinimide but also pyrroles (pyrrole, 2-methylpyrrole, 2,4-dimethylpyrrole, and 2,5-dimethylpyrrole). The production of pyrrole from glutamic acid clearly indicates one
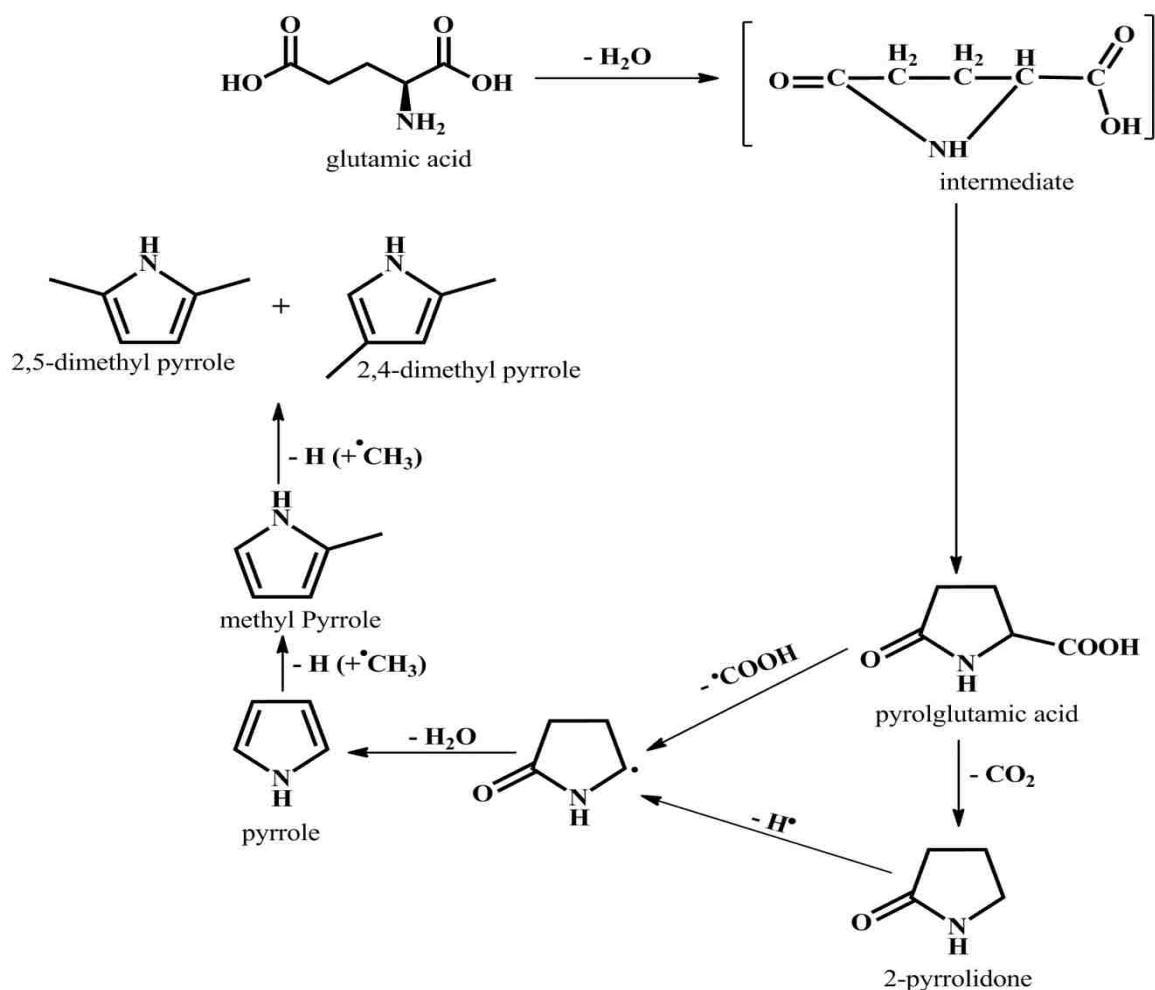
Scheme 4.8. Proposed mechanism for the formation of pyroglutamic acid, 2-pyrrolidone, pyrrole, and methylated pyrroles

carboxyl group is lost as carbon dioxide (cf. Scheme 4.8) whereas the second carboxyl group is incorporated into 2-pyrrrolidone ring before converting to pyrrole [71, 72]. In this study, we propose the precursor for the formation of pyrrole is pyroglutamic acid. Two parallel pathways

are suggested: (1) the loss of COOH radical from pyroglutamic acid to form 2-pyrrolidonyl radical and (2) formation of 2-pyrrolidone via decarboxylation followed by dehydrogenation of 2-pyrrolidone to yield 2-pyrrolidnonyl radical. 2-pyrrolidonyl radical is postulated to undergo dehydration to form pyrrole. Methylation of pyrrole leads to 2-methyl pyrrole and ultimately 2,4-dimethy pyrrole and 2,5-dimethyl pyrrole.

It has been postulated previously that pyrrole decomposes to yield predominantly HCN in addition to hydrocarbon products [73]. This implies pyrrole yield peaks at a lower temperatures while that of HCN and hydrocarbons (propane, propene, etc.) is expected to peak at high temperatures.

4.4. Toxicological considerations of pyrolysis compounds

Decomposition of lignin and tyrosine yielded compounds of biological importance. In this chapter, a detailed discussion on the formation and toxicological implications of these compounds is presented. Phenolic compounds (phenol, catechol, *o*-cresol, and *m*-cresol) were common products from the thermal degradation of lignin and tyrosine. Of the simple phenolic compounds, phenol was the most abundant. Phenolic compounds are known products of tobacco burning which undergo H abstraction to form phenoxy radicals and semiquinone radicals, leading to increased lifetimes, and ultimately causing extensive cellular damage [74]. Additionally, phenoxy radicals are precursors for formation of dibenzo-*p*-dioxin/dibenzofuran, which are easily chlorinated in the presence of a redox-active transition metal such as copper or iron to form polychlorinated dibenzo-*p*-dioxin/dibenzofuran (PCDD/F) [75]. Other phenolic compounds found in cigarette smoke which are considered toxic are those which are proposed to originate from thermal degradation of lignin; a major component of tobacco [74]. These include compounds such as guaiacol, 4-vinylguaiacol, syringol, and vanillin, which bear electron-

donating substituents and would therefore be expected to be more toxic because they are more

stable and have longer lifetimes [74, 76]. Such radicals with longer lifetimes are considered
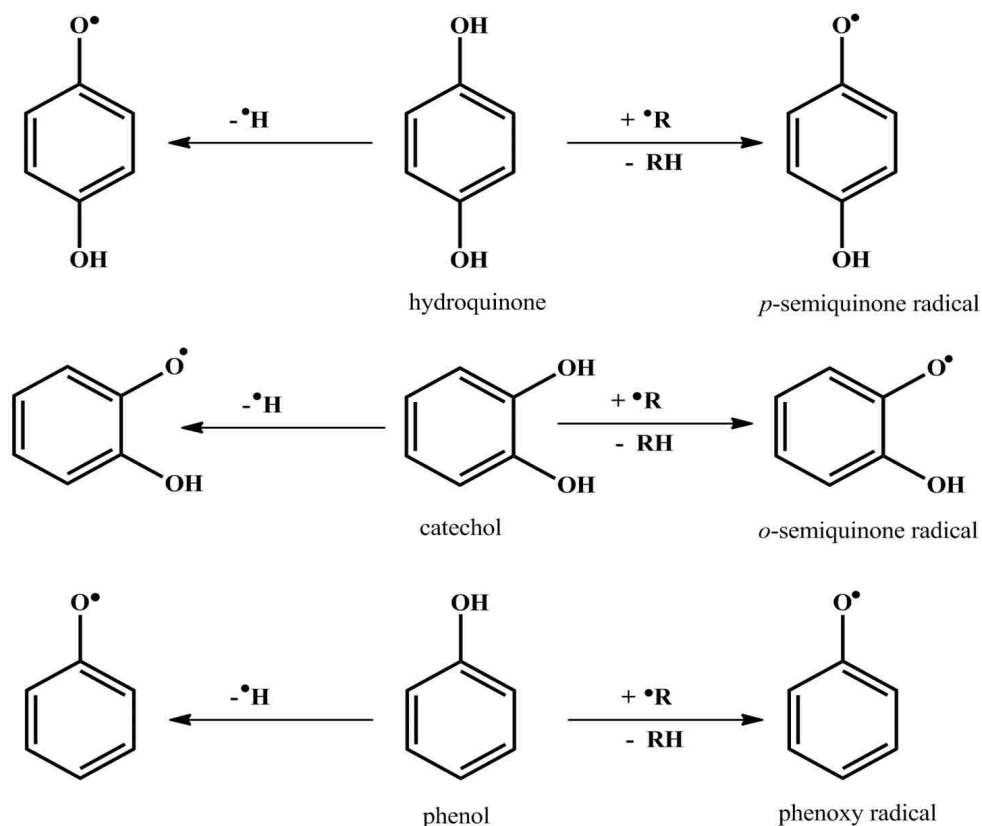
Scheme 4.9. General formation of semiquinone and phenoxy radical in the gas-phase [75].

environmentally persistent free radicals (EPFRs) and are thus biologically very toxic.

Scheme 4.9 shows the formation of phenoxy and semiquinone radicals from phenolic

compounds. Phenolic compounds are reported to be toxic and have the ability to cause cancer

[77]. Radical reactions in chemistry and chemical-biological systems have led to the finding that

phenols exhibit toxicity [76, 75]. Phenolic compounds have been known to rapidly divide cells to

produce more reactive oxygen species (ROS) which help convert phenols to toxic phenoxy

radicals [76]. Oxidations of phenols by various enzymes also yield reactive phenoxy radicals [76,

77]. It is observed that following H radical abstraction from the phenol hydroxyl group, the

resultant phenoxy radical exhibit some electron-deficient character, Scheme 4.8 [75] which would be stabilized by electron-donating substituents such as amino, methoxy, and methyl groups and consequently may possess longer life times to facilitate biological damage[74]. [14]

4.5. The kinetic model for lignin pyrolysis

The pseudo 1st order reaction kinetic model is depicted below, Scheme 4.10 according the CHEMKIN format. All reactions discussed in previous sections chapter 3, i.e The first 6 reactions (rxns.1-6) are the formation reactions of syringol, B(S); phenol, B(ph); furfural, B(furf); toluene, B(tol); benzene, B and 4-vinylguaiacol, B(V) in parallel decomposition reactions of lignin, B(L). Reactions 10-15 represent the decomposition (destruction) reactions of these products, i.e. product B(Ps) is from syringol, B(S); product B(Pph) from phenol, B(ph); product B (Pfurf) from furfural, B(furf); product B (Ptol) from toluene, B(tol); product B(P) from

Reactions	A	n	Ea
1. B(L)=>B(S)	3.47E+02	0.0	6000.0
2. B(L)=>B(ph)	3.55E+03	0.0	10000.0
3. B(L)=>B(furf)	5.75E+01	0.0	3600.0
4. B(L)=>B(tol)	8.32E+05	0.0	17000.0
5. B(L)=>B	6.31E+06	0.0	22400.0
6. B(L)=>B(V)	4.90E+01	0.0	3200.0
7. B(L)=>B(G1)	9.97E-05	0.0	0.0
Landau-Teller Parameters: B= 0.17254E+05, C=-0.90612E+07			
8. B(L)=>B(C1)	1.07E-03	0.0	0.0
Landau-Teller Parameters: B= 0.10224E+05, C=-0.61231E+07			
9. B(C1)=>B(C2)	8.26E+05	0.0	20000.0
10. B(S)=>B(Ps)	1.98E+05	0.0	19000.0
11. B(ph)=>B(Pph)	4.00E+02	0.0	6300.0
12. B(furf)=>B(Pfurf)	5.60E+03	0.0	9000.0
13. B(tol)=>B(Ptol)	7.20E+02	0.0	7500.0
14. B=>B(P)	4.10E+02	0.0	7000.0
15. B(V)=>B(Pv)	2.10E+02	0.0	5000.0

Scheme 4.10. The reactions model considered for lignin pyrolysis. The units for the preceding reactions are: $A, (s^{-1}), Ea, cal\,mol^{-1}$. The reaction rate constant expression is given by

$$k = A\,x\,T^n \exp\left(-\frac{Ea}{RT}\right).$$

benzene, B and B (Pv) from 4-vinylguaiacol, B(V). All kinetic parameters were calculated as discussed in chapter 3. Reactions 7, 8 and 9 were adapted from literature, equation 3.28 *vide supra*.

	Reaction	A (s^{-1})	n	Ea (cal/mol)		Reaction	A (s^{-1})	n	Ea (cal/mol)
1.	$L \rightarrow syringol$	3.47E+02	0.0	6000.0	8.	$phenol \rightarrow products$	4.00E+02	0.0	6300.0
2.	$L \rightarrow phenol$	3.55E+03	0.0	10000.0	9.	$furfural \rightarrow products$	5.60E+03	0.0	9000.0
3.	$L \rightarrow furfural$	5.75E+01	0.0	5600.0	10.	$toluene \rightarrow products$	7.20E+02	0.0	7500.0
4.	$L \rightarrow toluene$	8.32E+05	0.0	17000.0	11.	$benzene \rightarrow products$	4.10E+02	0.0	7000.0
5.	$L \rightarrow benzene$	6.31E+06	0.0	22400.0	12.	$4vguaiacol \rightarrow products$	2.10E+02	0.0	5000.0
6.	$L \rightarrow 4-vinyl\lg uaiacol$	4.90E+01	0.0	4200.0	13.	$L \rightarrow Gases$	1.10E+02	0.0	4600.0
7.	$syringol \rightarrow products$	1.98E+05	0.0	19000.0					

Scheme 4.11. Reduced reactions model considered for lignin pyrolysis. The units for the preceding reactions are: $A,(s^{-1})$, $Ea, cal\,mol^{-1}$. The reaction rate constant expression is given by

$$k = A\,x\,T^{n} \exp\left(-\frac{Ea}{RT}\right).$$

The rate constants for the reactions 1-6 and 10-15 are pseudo rate constants and therefore may not be used to compare with the values of real, elementary reaction rate constants. Nevertheless, they can be used for the kinetic calculations for the system from which they were extracted. The rate constants for the reactions 7-9 were calculated from theoretical modeling of lignin pyrolysis [78]. To maintain the uniqueness of the calculated rate constants, the rate constants for these reactions were removed from Scheme 4.11. Instead, the reaction # 13 was added (cf. Scheme 4.11) which represents decomposition of lignin into volatiles and light gases such as CO, CO_2, CH_4 (abbreviated as G1) etc. The rate constant for reaction 13 was calculated

in similar manner as for reactions 7-12 in Scheme 4.10, *vide supra*. These data are summarized in Table 3.14 and Figure 3.24, *vide supra*.

From the parametric results shown in Figure 4.3, it is clear that simulation curves are similar to the experimental curves to a very high degree of accuracy. This implies that we have
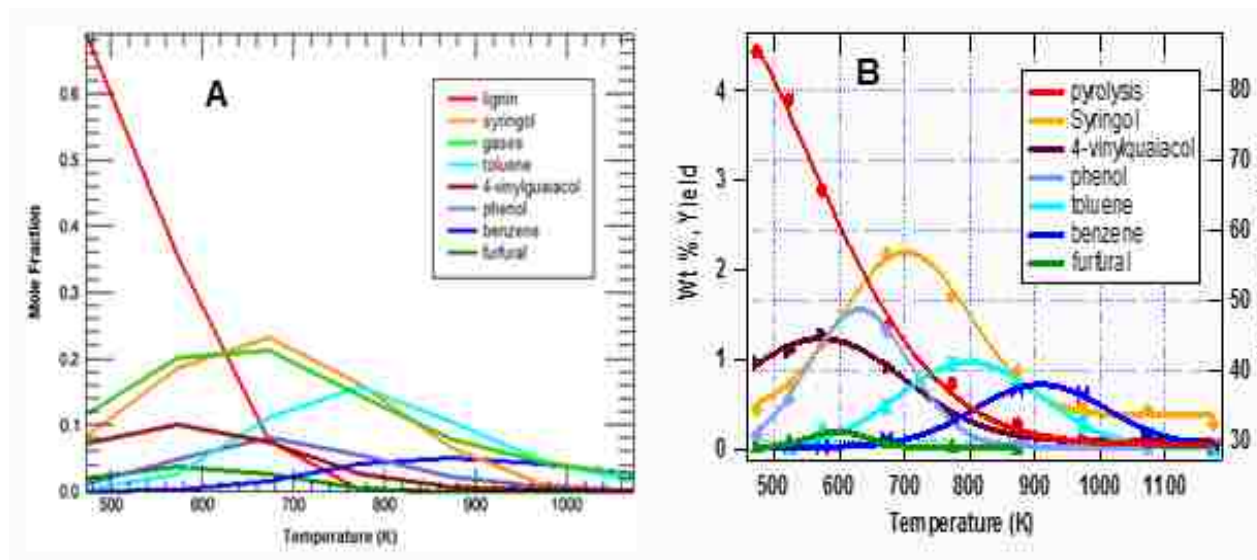
Figure 4.3. Comparison between simulation results (**A**) and experimental results (**B**) from the pyrolysis of lignin in N_2 at 1 atm.

successfully developed a model for lignin pyrolysis that can be used to investigate the pyrolysis of lignin under various reaction conditions of temperature, pressure, oxygen concentration, and heating rates. The model also predicts the curve for gas yield, a phenomenon not investigated experimentally. This follows that modeling is a powerful technique which can be used to study events under conditions not accessible experimentally and can be used to postulate phenomena with reasonable accuracy.

The major compounds in terms of yield follow the same order as those found from experiments. Nevertheless, the model predicts high yields of toluene at high temperature which

is still reasonable considering the fact that aromatic compounds form at high temperature during the pyrolysis of biomass materials. In order to further develop the model to ensure the yields of toluene do not blow out unnecessarily in this model, more CHEMKIN runs and sensitivity analysis will be conducted in future.

The Lignin curve (red line, Figure 4.3 *vide supra*) represents the degradation of pure lignin. Consequently, the lignin curve should not be used to mean char yield. There is therefore no direct comparison between this curve and the degradation profile of lignin obtained from experimental data. In future investigations, the char component will be simulated to match the experimental findings. Future CHEMKIN runs will also include data for the other reaction products such as the methoxybenzenes (1,2,4-trimethoxybenzene and 3,5-dimethoxybenzene) which were not included in this study.

4.6. CHEMKIN calculations

The Scheme 4.11 was subjected to CHEMKIN analysis. The CHEMKIN input, CHEMKIN Gas Phase, CHEMKIN Output files, as an example, is represented in Appendix 3. The CHEMKIN 4 Pro has an advantage to perform a parametric analysis which varies the reaction temperature from 450 to 1100 $^{\rm o}$C (in increments of 100 $^{\rm o}$C) simultaneously in the process of one run at constant pressure 1 atm. and residence time 0.2 s. The results of parametric analysis are presented in Figure 4.3, *vide supra*. Future work will aim at examining the robustness of the kinetic model by conducting sensitivity analysis tests. This will be achieved by changing the experimental parameters such as pressure, heating rate, and residence time. Also, pyrolysis temperature will be varied in steps of 50 ˚C instead of 100 ˚C.

The kinetic model developed for lignin pyrolysis in this study was entirely based on pseudo-1$^{\rm st}$ order rate law. To take into consideration the complexity of lignin pyrolysis, 2$^{\rm nd}$ order

rate law will be considered in future work, for the formation and destruction of intermediates. Half order reactions may also be explored.

4.7. The product sequence in CHEMKIN model

CHEMKIN Pro 4 provides the sequence of the reaction path of formation of each intermediate. For instance, product assigned by thickness of arrow in Figure 4.4 at three different temperatures (573 K, 773 K and 1073 K) indicate the relative yields of the product intermediate. Accordingly, the yields of products increase from left to right as shown by the thickness of the arrow.

573 K

gases   syringol   4-vinylguaiacol   phenol   furfural   toluene   benzene

1073 K

toluene   benzene   phenol   syringol   gases   4-vinylguaiacol   furfural
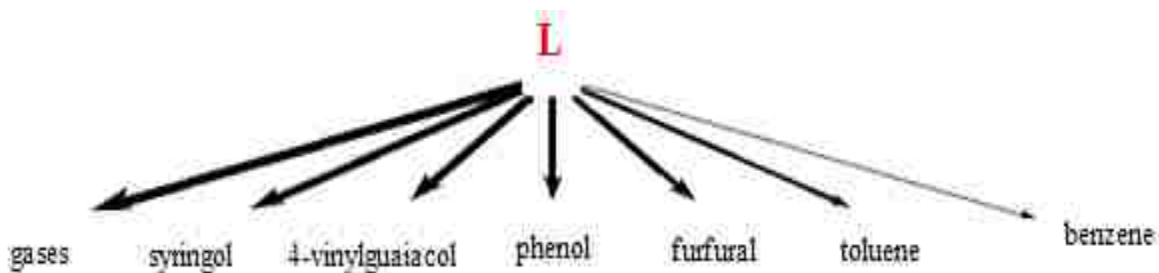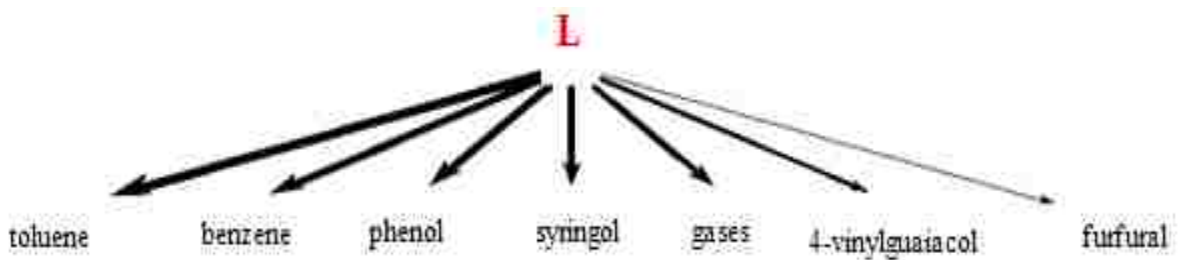
Figure 4.4. The Efficiency of the CHEMKIN model showing the order of product yields from left to right, where L represents lignin.

4.8. References

1.   Zhou, S., et al., *Pyrolysis behavior of pectin under the conditions that simulate cigarette smoking.* Journal of Analytical and Applied Pyrolysis, 2011. **91** (1): p. 232-240.

2.   Dorrestijn, E., et al., *The occurrence and reactivity of phenoxyl linkages in lignin and low rank coal.* Journal of Analytical and Applied Pyrolysis, 2000. **54** (1-2): p. 153-192.

3.   Jiang, Z.H. and D.S. Argyropoulos, *Coupling P-31 NMR with the Mannich reaction for the quantitative analysis of lignin.* Canadian Journal of Chemistry-Revue Canadienne De Chimie, 1998. **76** (5): p. 612-622.

4.   Xia, Z.C., L.G. Akim, and D.S. Argyropoulos, *Quantitative C-13 NMR analysis of lignins with internal standards.* Journal of Agricultural and Food Chemistry, 2001. **49** (8): p. 3573-3578.

5.   Milne, T.A., et al., *Standardized analytical methods.* Biomass & Bioenergy, 1992. **2** (1-6): p. 341-366.

6.   Jakab, E., O. Faix, and F. Till, *Thermal decomposition of milled wood lignins studied by thermogravimetry mass spectrometry.* Journal of Analytical and Applied Pyrolysis, 1997. **40-1**: p. 171-186.

7.   Brezny, R., V. Mihalov, and V. Kovacik, *Low-temperature thermolysis of lignins .1. Reactions of beta-O-4 model compounds.* Holzforschung, 1983. **37** (4): p. 199-204.

8.   Ramiah, M.V., *Thermogravimetric and differential thermal analysis of cellulose, hemicellulose, and lignin.* Journal of Applied Polymer Science, 1970. **14** (5): p. 1323-&.

9.   Kawamoto, H., M. Ryoritani, and S. Saka, *Different pyrolytic cleavage mechanisms of beta-ether bond depending on the side-chain structure of lignin dimers.* Journal of Analytical and Applied Pyrolysis, 2008. **81** (1): p. 88-94.

10.   Nakamura, T., H. Kawamoto, and S. Saka, *Pyrolysis behavior of Japanese cedar wood lignin studied with various model dimers.* Journal of Analytical and Applied Pyrolysis, 2008. **81** (2): p. 173-182.

11.   Ben, H.X. and A.J. Ragauskas, *NMR characterization of pyrolysis oils from kraft lignin.* Energy & Fuels, 2011. **25** (5): p. 2322-2332.

12.   Shafizadeh, F., *Introduction to Pyrolysis of Biomass.* Journal of Analytical and Applied Pyrolysis, 1982. **3** (4): p. 283-305.

13.   Evans, R.J., T.A. Milne, and M.N. Soltys, *Direct Mass-Spectrometric Studies of The Pyrolysis of Carbonaceous Fuels .3. Primary Pyrolysis of Lignin.* Journal of Analytical and Applied Pyrolysis, 1986. **9** (3): p. 207-236.

14.   Cai, X.M. and C. Dass, *Conformational analysis of proteins and peptides.* Current Organic Chemistry, 2003. **7** (18): p. 1841-1854.

15.   Britt, P.F., et al., *Pyrolysis mechanisms of lignin - Surface-immobilized model-compound investigation of acid-catalyzed and free-radical reaction pathways.* Journal of Analytical and Applied Pyrolysis, 1995. **33**: p. 1-19.

16.   Leary, G., *Chemistry of reactive lignin intermediates .1. Transients in coniferyl alcohol photolysis.* Journal of the Chemical Society-Perkin Transactions 2, 1972 (5): p. 640-&.

17.   Jezierski, A., et al., *Quantitative EPR study on free radicals in the natural polyphenols interacting with metal ions and other environmental pollutants.* Spectrochimica Acta Part A-Molecular and Biomolecular Spectroscopy, 2002. **58** (6): p. 1293-1300.

18.   Czechowski, F., I. Golonka, and A. Jezierski, *Organic matter transformation in the environment investigated by quantitative electron paramagnetic resonance (EPR) spectroscopy: studies on lignins.* Spectrochimica Acta Part A-Molecular and Biomolecular Spectroscopy, 2004. **60** (6): p. 1387-1394.

19.   Freudenb.K, *Lignin - Its constitution and formation from p-hydroxycinnamyl alcohols.* Science, 1965. **148** (3670): p. 595-&.

20.   Li, J., et al., *The investigation of thermal decomposition pathways of phenylalanine and tyrosine by TG-FTIR.* Thermochimica Acta, 2008. **467** (1-2): p. 20-29.

21.   Basiuk, V.A., *Pyrolysis of valine and leucine at 500 degrees C: Identification of less-volatile products using gas chromatography Fourier transform infrared spectroscopy mass spectrometry.* Journal of Analytical and Applied Pyrolysis, 1998. **47** (2): p. 127-143.

22.   Brai, M., et al., *Electronic paramagnetic resonance power saturation of wooden samples.* Journal of Applied Physics, 2009. **105** (9).

23.   Kuzina, S.I., et al., *Free radicals in the photolysis and radiolysis of polymers: IV. Radicals in gamma- and UV-irradiated wood and lignin.* High Energy Chemistry, 2004. **38** (5): p. 298-305.

24.   Graf, F., Loth, K., and Gunthard, H-H., *Chlorine hyperfine splittings and spin density distribution of peroxy radicals. An ESR and Quantum chemical study.* Helvetica Chimica Acta., 1977. **60** (76): p. 710-721.

25.   Stone, T.J., Waters, W.A., *Aryloxy-radicals. Part1. ESR spectra of radicals from some substituted monohydric phenols.* J.Chem.Soc., 1964. **213**: p. 213-218.

26.   Hansch, C., A. Leo, and R.W. Taft, *A survey of Hammett substituent constants and resonance and field parameters.* Chemical Reviews, 1991. **91** (2): p. 165-195.

27.   Khachatryan, L., J. Adounkpe, and B. Dellinger, *Radicals from the gas-phase pyrolysis of hydroquinone: 2. Identification of alkyl peroxy radicals.* Energy & Fuels, 2008. **22** (6): p. 3810-3813.

28.   Bussandri, A., and Willigen, H. van, *FT-EPR study of the wavelength dependence of the photochemistry of phenols.* J.Chem.Phys, 2002. **106**: p. 1524-1532.

29.   Jeevarajan, A.S., and Fessenden, R.W., *Unusual chemically induced dynamic electron polarization of electrons by photoionization.* J.Chem.Phys, 1992. **96**: p. 1520-1523.

30.   Calvert, J.G., and Pitts, J.N. Jr, *Photochemistry.* 1966. **John Wiley & Sons, Inc.**: p. 499.

31.   Dellinger, B., et al., *Formation and stabilization of persistent free radicals* Proceedings of the Combustion Institute, 2007. **31**: p. 521-528.

32.   Adounkpe, J., L. Khachatryan, and B. and Dellinger, *Radicals from the gas-phase pyrolysis of hydroquinone 1. Temperature dependence of the total yields of radicals.* Energy & Fuels, 2008. **22**: p. 2986-2990

33.   Chiavari, G. and G.C. Galletti, *Pyrolysis-gas chromatography mass-spectrometry of amino-acids.* Journal of Analytical and Applied Pyrolysis, 1992. **24** (2): p. 123-137.

34.   Basiuk, V.A. and J. Douda, *Pyrolysis of simple amino acids and nucleobases: survivability limits and implications for extra-terrestrial delivery.* Planetary and Space Science, 1999. **47** (3-4): p. 577-584.

35.   Basiuk, V.A. and J. Douda, *Pyrolysis of poly-glycine and poly-L-alanine: Analysis of less-volatile products by gas chromatography/fourier transform infrared spectroscopy/mass spectrometry.* Journal of Analytical and Applied Pyrolysis, 2000. **55** (2): p. 235-246.

36.   Ratcliff, M.A., E.E. Medley, and P.G. Simmonds, *Pyrolysis of amino-acids - Mechanistic considerations.* Journal of Organic Chemistry, 1974. **39** (11): p. 1481-1490.

37.   Simmonds, P.G., et al., *Thermal-Decomposition of aliphatic monoamino-monocarboxylic acids.* Analytical Chemistry, 1972. **44** (12): p. 2060-&.

38.   Li, J. and T.B. Brill, *Decarboxylation mechanism of amino acids by density functional theory.* Journal of Physical Chemistry A, 2003. **107** (31): p. 5993-5997.

39.   Alexandrova, A.N. and W.L. Jorgensen, *On the mechanism and rate of spontaneous decomposition of amino acids.* Journal of Physical Chemistry B, 2011. **115** (46): p. 13624-13632.

40.   Lucarini, M., V. Mugnaini, and G.F. Pedulli, *Bond dissociation enthalpies of polyphenols: The importance of cooperative effects.* Journal of Organic Chemistry, 2002. **67**(3): p. 928-931.

41.   Mulder, P., et al., *Critical re-evaluation of the O-H bond dissociation enthalpy in phenol.* Journal of Physical Chemistry A, 2005. **109** (11): p. 2647-2655.

42.   Gomes, J.R.B., M. da Silva, and M. da Silva, *Solvent and structural effects in the N-H bond homolytic dissociation energy.* Journal of Physical Chemistry A, 2004. **108** (11): p. 2119-2130.

43.   Davico, G.E., et al., *The C-H bond-energy of benzene.* Journal of the American Chemical Society, 1995. **117** (9): p. 2590-2599.

44.   Blanksby, S.J. and G.B. Ellison, *Bond dissociation energies of organic molecules.* Accounts of Chemical Research, 2003. **36** (4): p. 255-263.

45.   Wu, Y.D., et al., *Substituent effects on the C-H bond dissociation energy of toluene. A density functional study.* Journal of Organic Chemistry, 1996. **61** (2): p. 746-750.

46.   Tumanov, V.E. and E.T. Denisov, *A bond energy database for hydrocarbons and related compounds.* Petroleum Chemistry, 2003. **43** (1): p. 62-64.

47.   Khachatryan, L., R. Asatryan, and B. Dellinger, *Development of expanded and core kinetic models for the gas phase formation of dioxins from chlorinated phenols.* Chemosphere, 2003. **52** (4): p. 695-708.

48.   Maskos, Z., L. Khachatryan, and B. Dellinger, *Formation of the persistent primary radicals from the pyrolysis of tobacco.* Energy & Fuels, 2008. **22** (2): p. 1027-1033.

49.   Sharma, R.K., et al., *On the role of peptides in the pyrolysis of amino acids.* Journal of Analytical and Applied Pyrolysis, 2004. **72** (1): p. 153-163.

50.   McFerrin, C.A., R.W. Hall, and B. Dellinger, *Ab initio study of the formation and degradation reactions of chlorinated phenols.* Journal of Molecular Structure-Theochem, 2009. **902** (1-3): p. 5-14.

51.   Wiater, I., J.G.P. Born, and R. Louw, *Products, rates, and mechanism of the gas-phase condensation of phenoxy radicals between 500-840 K.* European Journal of Organic Chemistry, 2000 (6): p. 921-928.

52.   Dellinger, B., et al., *Combustion byproducts and their health effects: Summary of the 10 (th) International Congress.* Environmental Engineering Science, 2008. **25** (8): p. 1107-1114.

53.   Zheng, G.J., et al., *Polychlorinated dibenzo-p-dioxins and dibenzofurans pollution in China: Sources, environmental levels and potential human health impacts.* Environment International, 2008. **34** (7): p. 1050-1061.

54.   Evans, C.S. and B. Dellinger, *Mechanisms of dioxin formation from the high-temperature pyrolysis of 2-bromophenol.* Environmental Science & Technology, 2003. **37** (24): p. 5574-5580.

55.   Evans, C.S. and B. Dellinger, *Mechanisms of dioxin formation from the high-temperature pyrolysis of 2-chlorophenol.* Environmental Science & Technology, 2003. **37** (7): p. 1325-1330.

56.   Evans, C.S. and B. Dellinger, *Mechanisms of dioxin formation from the high-temperature oxidation of 2-bromophenol.* Environmental Science & Technology, 2005. **39** (7): p. 2128-2134.

57.   Evans, C.S. and B. Dellinger, *Mechanisms of dioxin formation from the high-temperature oxidation of 2-chlorophenol.* Environmental Science & Technology, 2005. **39** (1): p. 122-127.

58.   Asatryan, R., et al., *Molecular modeling studies of the reactions of phenoxy radical dimers: Pathways to dibenzofurans.* Journal of Physical Chemistry A, 2005. **109** (49): p. 11198-11205.

59.   Louw, R. and S.I. Ahonkhai, *Radical/radical vs radical/molecule reactions in the formation of PCDD/Fs from (chloro)phenols in incinerators.* Chemosphere, 2002. **46** (9-10): p. 1273-1278.

60.   Sharma, R.K., W.G. Chan, and M.R. Hajaligol, *Product compositions from pyrolysis of some aliphatic alpha-amino acids.* Journal of Analytical and Applied Pyrolysis, 2006. **75** (2): p. 69-81.

61.   Choi, S.S. and J.E. Ko, *Analysis of cyclic pyrolysis products formed from amino acid monomer.* Journal of Chromatography A, 2011. **1218** (46): p. 8443-8455.

62.   Hansson, K.M., et al., *The temperature's influence on the selectivity between HNCO and HCN from pyrolysis of 2,5-diketopiperazine and 2-pyridone.* Fuel, 2003. **82** (18): p. 2163-2172.

63.   Wu, H., et al., *Phase transformations of glutamic acid and its decomposition products.* Crystal Growth & Design, 2010. **10** (2): p. 988-994.

64.   Nunes, R.S. and E.T.G. Cavalheiro, *Thermal behavior of glutamic acid and its sodium, lithium and ammonium salts.* Journal of Thermal Analysis and Calorimetry, 2007. **87** (3): p. 627-630.

65.   Vlase, T., et al., *Specificity of decomposition of solids in non-isothermal conditions.* Journal of Thermal Analysis and Calorimetry, 2003. **72** (2): p. 597-604.

66.   Vollmin, J., et al., *Structural elucidation with a thermal fragmentation-gas chromatography-mass spectrometry combination.* Microchemical Journal, 1966. **11** (1): p. 73-&.

67.   Sharma, R.K., et al., *Formation of low molecular weight heterocycles and polycyclic aromatic compounds (PACs) in the pyrolysis of alpha-amino acids.* Journal of Analytical and Applied Pyrolysis, 2003. **66** (1-2): p. 97-121.

68.   Choudhar.G, A.M. Cameron, and R.A. Back, *Photolysis and pyrolysis of succinimide vapor.* Journal of Physical Chemistry, 1968. **72** (7): p. 2289-&.

69.   Hammes, G.G. and P.J. Lillford, *Kinetic and equilibrium study of the hydrogen bond dimerization of 2-pyridone in hydrogen bonding solvents.* Journal of the American Chemical Society, 1970. **92** (26): p. 7578-7585.

70.   Cowley, E.G. and J.R. Partington, *Studies in dielectric polarisation. Part XV. The dipole moments of five-membered nitrogen ring compounds: Indole, skatole, carbazole, isatin, phthalimide, and succinimide.* Journal of the Chemical Society, 1936: p. 47-50.

71.   Haidar, N.F., et al., *Effects of structure on pyrolysis gases from amino-acids.* Journal of Agricultural and Food Chemistry, 1981. **29** (1): p. 163-165.

72.   Patterso.Jm, et al., *Pyrolysis of phenylalanine, 3,6-dibenzyl-2,5-piperazinedione, and phenethylamine.* Journal of Organic Chemistry, 1973. **38** (4): p. 663-666.

73.   Blank, D.A., S.W. North, and Y.T. Lee, *The ultraviolet photodissociation dynamics of pyrrole.* Chemical Physics, 1994. **187** (1-2): p. 35-47.

74.   Smith, C.J. and C. Hansch, *The relative toxicity of compounds in mainstream cigarette smoke condensate.* Food and Chemical Toxicology, 2000. **38** (7): p. 637-646.

75.   Dellinger, B., et al., *Formation and stabilization of persistent free radicals.* Proceedings of the Combustion Institute, 2007. **31**: p. 521-528.

76.   Lynch, B.S., E.S. Delzell, and D.H. Bechtel, *Toxicology review and risk assessment of resorcinol: Thyroid effects.* Regulatory Toxicology and Pharmacology, 2002. **36** (2): p. 198-210.

77.   D. Selassie, C., et al., *On the toxicity of phenols to fast growing cells. A QSAR model for a radical-based toxicity.* Journal of the Chemical Society, Perkin Transactions 2, 1999 (12): p. 2729-2733.

78.   Koufopanos, C.A., G. Maschio, and A. Lucchesi, *Kinetic modeling of the pyrolysis of biomass and biomass components.* Canadian Journal of Chemical Engineering, 1989. **67**(1): p. 75-84.

CHAPTER 5: SUMMARY

In this study the thermal decomposition characteristics of lignin, tyrosine, and glutamic acid were investigated in detail using a Pyr-GC-MS analytical technique. It is clear from this work temperature, residence time and oxygen concentration has a significant influence on the concentration and type of products released during thermolysis of biomass components. While some products such as hydrocarbons were favored under a nitrogen atmosphere, oxygenates (furan, acetone etc.) were generally favored by an oxidative regime.

Several compounds overlapped during thermolysis of biomass materials. For example, phenol, *p*-cresol, *o*-cresol were common products from thermal decomposition of lignin, and tyrosine. Hydrogen cyanide, acetonitrile, propionitrile, and pyrrole were characteristic products from thermal degradation of tyrosine, and glutamic acid. Generally, lignin and tyrosine were large generators of phenolic compounds. Compounds of biological interest, hydroquinone, *p*-benzoquinone, dibenzofuran, and dibenzo-*p*-dioxin, were formed when tyrosine was pyrolyzed under and oxidative atmosphere.

The maximum evolution of products from thermal degradation of biomass material occurred between 200 and 450 ˚C. Above 400 ˚C, hydrocarbon products were generally formed mainly from pyrolysis. Hydrocarbon products from oxidative pyrolysis experiments were suppressed because their precursors were oxidized to carbon dioxide and carbon monoxide. The thermal decomposition profiles for most biomass materials were therefore markedly varied. Pyrolysis is of great importance in the use of biomass materials in tobacco, food, and flavor industries [2]. Despite these benefits, the chemistry of pyrolysis products is not only poorly understood but their pathways and formation remain debatable [2].

5.1. The unique yields of catechol from the fractional pyrolysis of lignin[15]

To explain the surprisingly low yields of catechol from the thermal degradation of lignin we consider its formation from guaiacol. The homolytic pathway for 2-methoxy phenol (Rxn 5.1) starts with the cleavage of the weak phenoxy-methyl bond ($O-CH_3$), 243-245 kJ mol^{-1} [3, 4]. The methyl and the 2-hydroxyphenoxyl radicals abstract a hydrogen atom from a donor compound RH, to yield methane and catechol [3].

guaiacol   2-hydroxyphenoxy radical   catechol
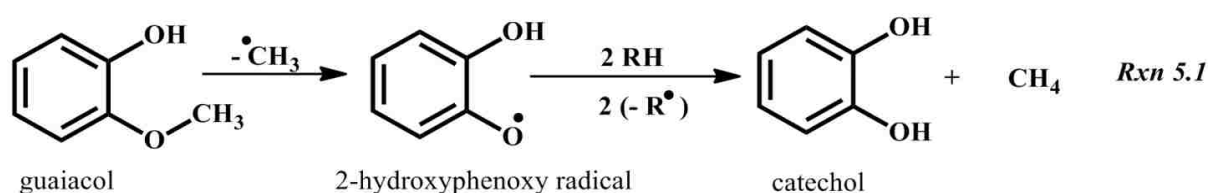
For this reason, the main source of catechol in the pyrolysis of lignin is guaiacol. This implies the yields of catechol would be expected to be lower than that of guaiacol. It is well established in general, catechol is a product formed from further secondary reactions of guaiacol [4, 5]. As a result, catechol yields mimic the yields of guaiacol although in much lower yields (Figures 3.4 and 3.6. A significant difference between guaiacol and catechol has been observed under oxidative partial pyrolysis *vide supra* Figure 3.4 A. From this observation, it would appear catechol oxidizes much faster under oxidative partial pyrolysis in comparison to phenol (a similar product as catechol). Interestingly, a highly oxidative environment has been observed in char formation process during partial oxidative pyrolysis Figure 3.7, *vide supra*. This may imply that at each pyrolysis temperature, some highly active intermediate species (for instance hydroperoxides) may adsorb on char surfaces during cool-down processes and initiate the

---

process of lignin pyrolysis at the next pyrolysis temperature. Based on polarization data which shows the dipole moment of catechol is significantly higher (2.21D) than that of phenol (1.54 D), catechol being highly polar is better adsorbed on char surfaces than phenol [6, 7]. This means the amounts of catechol adsorbed on the surface is much higher than that of phenol. Therefore, less amounts of catechol are released into the gas phase due to decomposition of catechol by adsorbed intermediates.

5.2. Thermal degradation of lignin

The product distribution from thermolysis of lignin in N_2 and 4% O_2 in N_2 indicated that the principal products were phenol, syringol, and guaiacol (2-methoxyphenol). Methoxy phenols have often been used as model compounds for lignin, *e.g.* in investigations of the effect of solvent, substituents, and processing conditions [3].
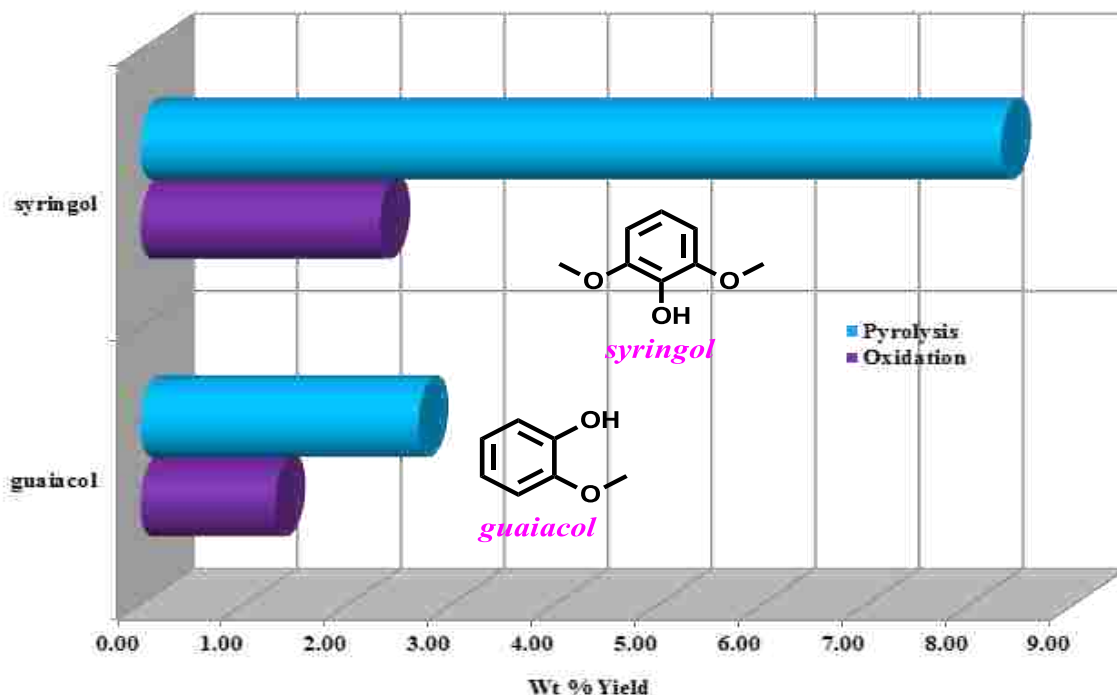
Figure 5.1. Yields of syringol and guaiacol from pyrolysis of lignin in N_2 and 4% O_2 in N_2 at 1 atm.

Figures 5.1 and 5.2 *vide infra* give the cumulative yields of the major products (syringol, guaiacol, and phenol) over the entire thermolysis temperature range. Accordingly, pyrolysis gives high yields of syringol, phenol, guaiacol in comparison to oxidative pyrolysis. This because an oxidizing environment converts some the products to H_2O, CO_2, and H_2O therefore decreasing their yields. Nevertheless, an oxidizing environment can enhance the yields of certain reaction products by speeding up the rate of the reaction. This is attributed to the relative reaction rates between OH and H radicals. The ratio of reactivities between OH and H radicals in this study was calculated to be about 1.0×10^5 at 673 K. This implies OH radical is considerably very reactive and has an overall impact on the type and yield of products observed. Consider a hypothetical reaction of the form:

$$A \xrightarrow{k_1} B \qquad\qquad\qquad Equation~5.2$$

$$A + O_2 \xrightarrow{k_2} B \qquad\qquad\qquad Equation~5.3$$

Where k_1 and k_2 are respectively the rate constants for pyrolysis and oxidation respectively such

that $$k_1 = 3.2x10^{15} \exp\left(\frac{-86500\,cal\,mol^{-1}}{RT}\right) s^{-1} \qquad\text{and}$$

$$k_2 = 10^{12}(10^{14}) \exp\left(\frac{-41500\,cal\,mol^{-1}}{RT}\right) cm^3\ mol^{-1}\ s^{-1}[8].$$ Consequently, $\dfrac{k_2}{k_1} = 0.91x10^5$,

where the concentration of 4% oxygen has the equivalent of 4.50×10^{17} molecules/cm^3 (4% O_2 in N_2). From the expressions for k_1 and k_2, the ratio $\dfrac{k_1}{k_2}$ is temperature dependent. A temperature of 673 K was chosen because it corresponds with the peak concentration of many reaction products. Reaction 5.2 is unimolecular while reaction 5.3 is bimolecular.

A comparison between yields of phenol from the thermal degradation of lignin, and tyrosine is presented in Figure 5.2, *vide supra*. Clearly, the thermolysis of tyrosine gives rise to high yields of phenol. The yield Phenol from tyrosine is 8.6 times higher than the yields of phenol from pyrolysis of lignin. On the other hand, the yields of phenol from oxidative pyrolysis of tyrosine were 12 times higher than the yields of phenol from oxidative pyrolysis of lignin.
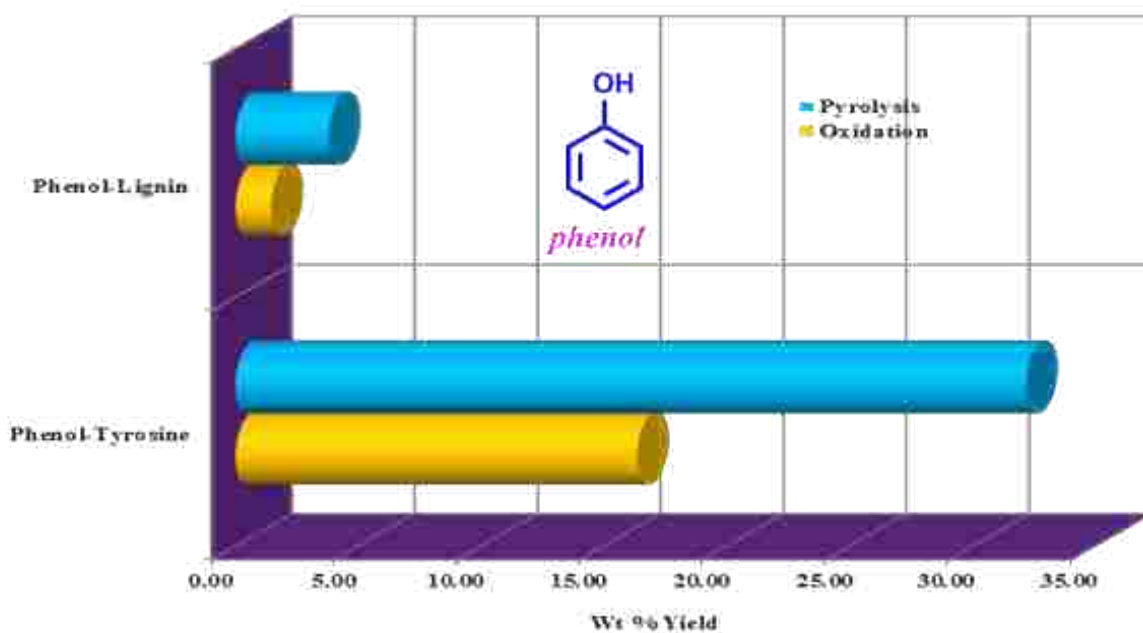
Figure 5.2. Wt % yields of phenol from pyrolysis of lignin and tyrosine in N_2 and 4% O_2 in N_2 respectively at 1 atm.

5.3. Yields of aromatic hydrocarbon products from thermolysis of lignin, tyrosine and glutamic acid

Thermal degradation of lignin, tyrosine, and glutamic acid produced aromatic products which are important in toxicology (cf. Figure 5.3, *vide infra*). This included mainly, benzene, toluene, *p*-xylene, and ethyl benzene. Small hydrocarbon products were also detected and included propane, propene, and 1-butene. Glutamic acid produced the lowest amount of aromatic hydrocarbons (only benzene and toluene) probably be because it contains a few carbon atoms in

its structure in addition to the fact that decarboxylation is the major route for decomposition, and this shortens the chain further inhibiting formation of aromatic compounds. Tyrosine was expected to be the highest generator of aromatic products because it contains an aromatic ring in its structure. Tyrosine may produce precursors such as methylene phenolic radical that can form
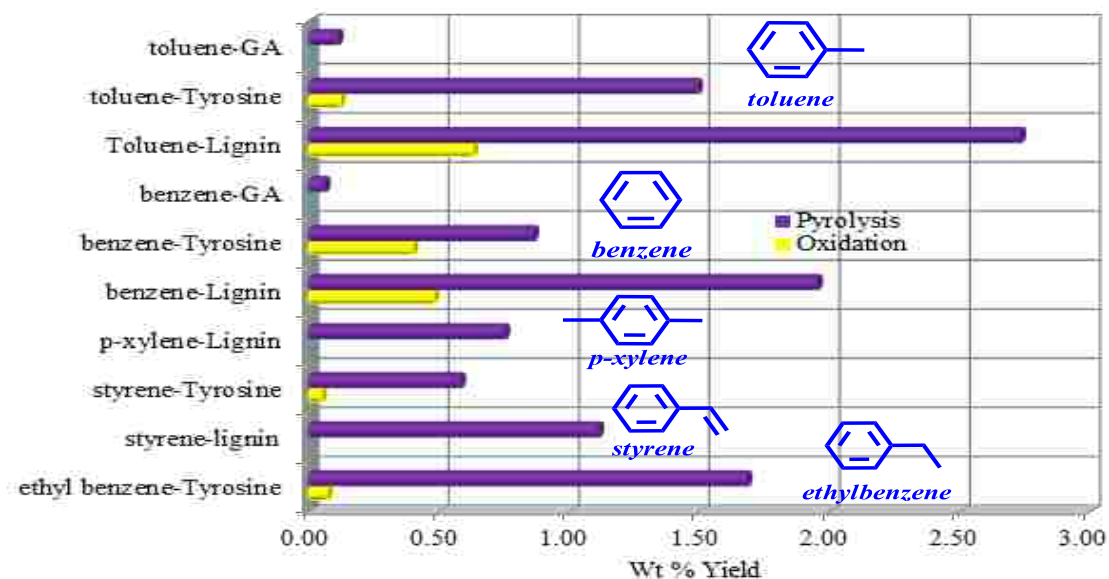
Figure 5.3. Wt % yields of aromatic hydrocarbons from pyrolysis of lignin, tyrosine, and glutamic acid in N_2 and 4% O_2 in N_2 respectively. The suffix after each compound indicates the origin of the compound, eg. Toluene-GA shows the compound originates from glutamic acid, etc.

aromatic hydrocarbons. However, this does not happen because the methylene phenolic radical is converted to *p*-cresol by addition of hydrogen from a donor compound, RH. On the other hand, despite its complex structure, lignin gave the highest yields of benzene, toluene, and styrene.

Benzene is known to be both hematotoxic and leukemogenic in humans, causing a variety of hematological disorders, including aplastic anemia, myelodysplastic syndrome, and acute myelogenous leukemia [9-11]. Benzene must be metabolized to mediate its toxic effects and a

133

number of polyphenolic and open-ringed metabolites have been studied for their hematotoxic potential [11, 12].

5.4. Compounds of biological interest from oxidative pyrolysis of tyrosine

Pyrolysis of tyrosine in 4% O_2 in N_2, yielded compounds considered biologically important because of the health impacts they cause. These compounds included hydroquinone, *p*-benzoquinone, benzofuran, dibenzofuran, and dibenzo-*p*-dioxin (cf. Figure 5.4). Quinones are a class of toxicological intermediates which are believed to create a variety of hazardous effects in vivo, including acute cytotoxicity, immunotoxicity, and carcinogenesis [13-15]. Quinones are
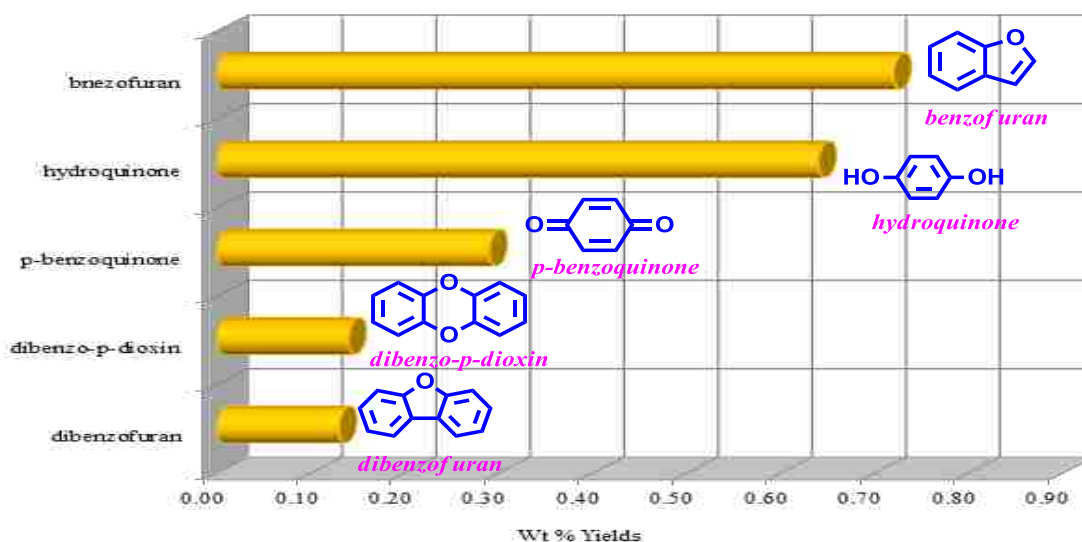
Figure 5.4. Yields of hydroquinone, benzofuran, *p*-benzoquinone, dibenzo-*p*-dioxin, and dibenzofuran from pyrolysis of tyrosine in N_2 and 4% O_2 in N_2.

Michael acceptors (undergo nucleophilic addition), and cellular damage may occur through alkylation of cellular proteins and/or DNA [13]. Quinones are highly redox active compounds which redox cycle with their respective semiquinone radicals, resulting in the formation of reactive oxygen species (ROS), including superoxide ($O_2^{\bullet-}$), hydrogen peroxide (H_2O_2), and ultimately the hydroxyl radical (${}^\bullet OH$) [13, 14]. Production of ROS may cause severe oxidative

stress within cells through oxidation of cellular macromolecules, including lipids, proteins, and DNA [13-15].

Whereas dioxins are formed of two benzene rings bonded together via two oxygen bridges, dibenzofurans are formed of two benzene rings bonded together by one carbon bond and one oxygen bridge [16]. Dioxins are classified as well-known human carcinogens, although they also cause noncancerous effects such as atherosclerosis, hypertension, and diabetes [16]. Long-term exposures to dioxins interfere with the nervous system, reproductive health, and endocrine, and immune systems [16, 18]. Temporal exposure to high concentrations impairs the liver function; and causes chloracne [16, 18]. The most sensitive population to dioxin exposure are the unborn and infants [16]. Dioxins are among the most toxic chemicals known to man [16, 18].

From Figure 5.4, it was observed hydroquinone was formed in high yields from the oxidative pyrolysis of tyrosine. The other major compounds in order of decreasing importance were benzofuran, *p*-benzoquinone, dibenzo-*p*-dioxin, and dibenzofuran.

5.5. Principal products from thermal degradation of glutamic acid

5.5.1. Cyclic imides

One of the remarkable results of this study was glutamic acid formed large yields of succinimide (pyrrolidine-2,5-dione) under pyrolysis and oxidative pyrolysis (cf. Figure 5.5, *vide infra*). This finding has never been observed before. Maleimide (2,5-pyrroledione) also has never been observed before during the pyrolysis of glutamic acid. These new and interesting results advance new knowledge to the thermal decomposition of glutamic acid. To ensure that the component (succinimide) was actually formed, a thorough analysis of the mass spectrum (m/z = 28, 56 and 99 amu) was performed, and the mass hits were excellent.

It is important to note that succinimide formed from oxidative pyrolysis of glutamic acid was 4 times higher than that formed under pyrolysis. This is because a reactive atmosphere (oxidizing atmosphere) speeds up the rate of reaction leading to the formation of high yields of
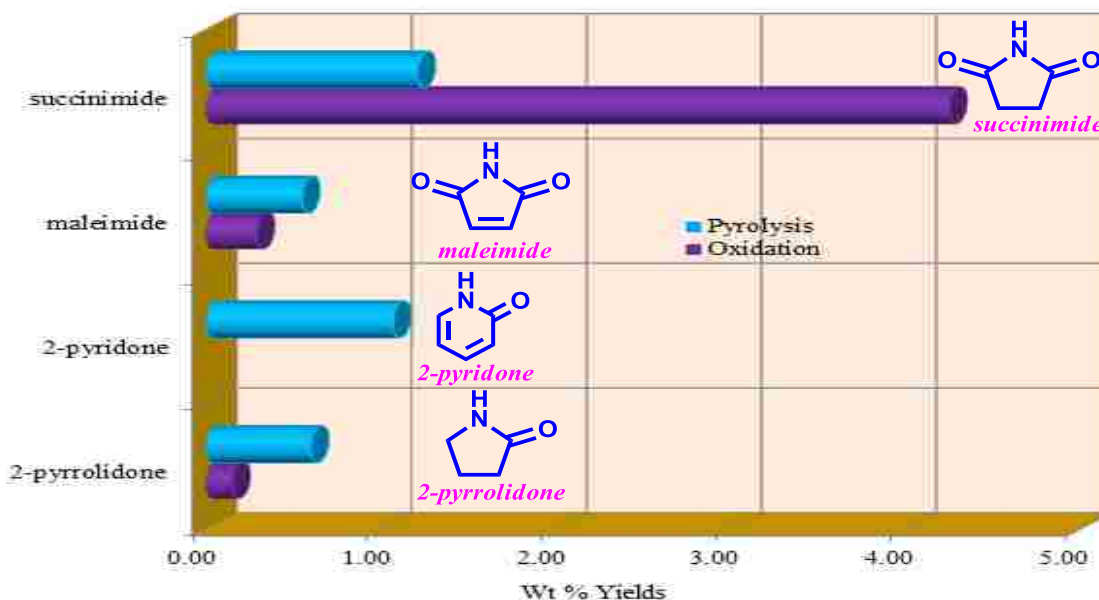
Figure 5.5. Yields of phenol from pyrolysis of glutamic acid in N_2 and 4% O_2 in N_2.

certain reaction products. However, an oxidizing atmosphere may also oxidize a reaction product to other small compounds such as H_2O, CO_2, and CO and thus decrease the concentration of the pyrolysis product. In some cases, an oxidizing environment may completely inhibit the formation of some reaction products. A good example is the absence of 2-pyridone under an oxidative regime during the thermal degradation of glutamic acid. Nonetheless, other reaction products such as ethanol and α-propiolactone were favored under an oxidative environment.

To explain the formation of reduced reaction products such as maleimide and succinimide, disproportionation reactions were considered by Sharma *et al*. [17] but this study postulates the major product succinimide from pyrolysis and oxidative pyrolysis of glutamic acid may actually be formed from the thermal degradation of the intermediate peptide, a tricyclic

diketo piperazine (DPK). We conclude pyroglutamic acid is an important intermediate product from the thermal degradation of glutamic acid which polymerizes to diketo piperazine before ultimately decomposing to high yields of succinimide especially during oxidative pyrolysis. Maleimide which was also detected for the first time in this work is most probably a minor product resulting from dehydrogenation of succinimide as predicted in literature.

5.5.2. Low molecular weight N-compounds

A comparison was made between the yields of small N-compounds generated from the thermal degradation of glutamic acid and tyrosine, Figure 5.6. It is obvious from Figure 5.6 that hydrogen cyanide was the major product from the pyrolysis of tyrosine while pyrrole was the
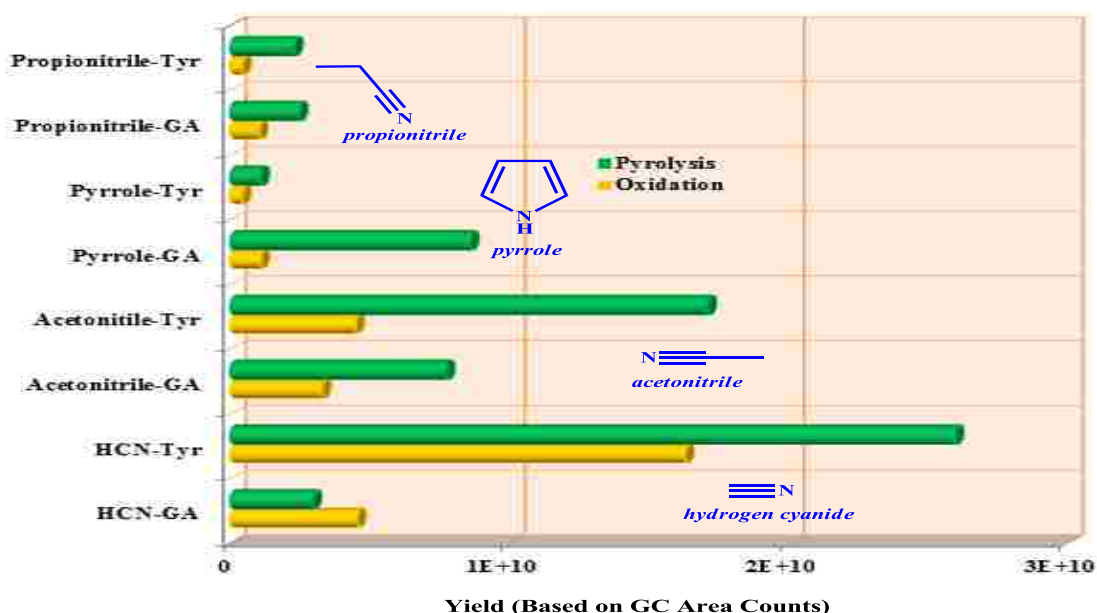
Figure 5.6. Yields of low molecular weight nitrogen containing compounds from pyrolysis of glutamic acid and tyrosine in N_2 and 4% O_2 in N_2 respectively. The suffix after the Compound shows the origin of the compound, e.g. HCN-Tyr indicates that hydrogen cyanide comes from tyrosine while HCN-GA indicates that hydrogen cyanide comes from glutamic acid.

major product from the pyrolysis of glutamic acid. In order of decreasing importance, glutamic

137

acid yielded acetonitrile, pyrrole, HCN, and propionitrile. On the other hand, tyrosine yielded HCN > acetonitrile > propionitrile > pyrrole, according to (cf. Figure, 5.6, *vide infra*). The high level of HCN produced from the thermolysis of tyrosine is interesting to note. HCN is a very poisonous substance that attacks the nervous system and may lead to death if the patient is not treated on time [19]. Tyrosine is therefore a large generator of HCN in addition to phenolic compounds.

5.6. Recapitulation

Tables 5.1-5.3 represent comparative analysis of the different classes of compounds determined during the thermal degradation of lignin, tyrosine, and glutamic acid. Table 5.1 shows that under oxidative pyrolysis of lignin, major phenolic compounds were depressed by 51-74% relative to the yields of phenolic compounds from pyrolysis of lignin. This would imply oxidative pyrolysis can be used to reduce the concentration of phenolic compounds during the thermal degradation of biomass materials such as lignin.

Table 5.1. Relative yields of the major phenolic compounds from the thermal degradation of lignin, and tyrosine in N_2 and 4% O_2 in N_2 at 1 atm.

Biomass Component	Experimental Conditions	Concentration of Pyrolysis Products Relative to Lignin Pyrolysis					
		phenol	*p*-cresol	catechol	syringol	guaiacol	4-vinylguaiacol
Lignin	Pyrolysis	1.00	1.00	1.00	1.00	1.00	1.00
	Oxidative Pyrolysis	0.39	0.31	0.26	0.37	0.49	0.33
Tyrosine	Pyrolysis	8.59	11.90	-	-	-	-
	Oxidative Pyrolysis	4.41	39.39	-	-	-	-

Whereas the yields of catechol, syringol, and 4-vinylguaiacol were suppressed for both pyrolysis and oxidative pyrolysis experiments for lignin-tyrosine mixture, the yields of guaiacol were augmented by about 2 times. This observation implies strong interaction between lignin and tyrosine during pyrolysis. The yields of phenol and *p*-cresol from pyrolysis and oxidative

pyrolysis of tyrosine were about 9 and 12 times higher than the yields of phenol and *p*-cresol from the thermal degradation of lignin.

Table 5.2; *vide infra* gives the relative concentration between low molecular weight oxygenates from the thermal degradation of lignin and tyrosine. It was determined oxidative pyrolysis of lignin lead to decreased yields of methanol, acetic acid, furan and 2-methyl furan by 64, 60, 31, and 39% respectively. However, the yields of furfural, and furfuryl alcohol increased about 1.3 and 6 times respectively in pyrolysis.

Table 5.2. Relative yields of low molecular weight oxygenated products from the thermal degradation of lignin, and tyrosine in N_2 and 4% O_2 in N_2 at 1 atm.

Biomass	Experimental Conditions	Concentration of Pyrolysis Products Relative to Lignin Pyrolysis					
		methanol	acetic acid	furan	2-methylfuran	furfural	furfuryl alcohol
Lignin	Pyrolysis	1.00	1.00	1.00	1.00	1.00	1.00
	Oxidative Pyrolysis	0.36	0.40	0.69	0.61	1.32	5.72

From Table 5.3 below, it was shown that of all biomass components investigated in this work, lignin produced the highest yields of hydrocarbons products while glutamic acid was the least generator of hydrocarbon products. Generally, oxidative pyrolysis depressed the yields of hydrocarbon products by 65-77%. Interestingly, pyrolysis of tyrosine gave similar yields of propene as pyrolysis of glutamic acid. No hydrocarbon products were detected from the oxidative pyrolysis of glutamic acid. This may be attributed to the fact, glutamic acid is highly oxygenated and consequently, the precursors for hydrocarbon formation in presence of an oxidative environment are easily converted to CO and CO_2. Glutamic acid also is believed to pyrolyze to a polymeric material which preferentially degrades to heterocyclic compounds.

Table 5.3. Relative yields of the major hydrocarbon products from the thermal degradation of lignin, and tyrosine in N_2 and 4% O_2 in N_2 at 1 atm.

Biomass	Experimental Conditions	Concentration of Pyrolysis Product Relative to Lignin Pyrolysis					
		propane	propene	benzene	toluene	p-xylene	styrene
Lignin	Pyrolysis	1.00	1.00	1.00	1.00	1.00	1.00
	Oxidative Pyrolysis	0.32	0.35	0.24	0.23	-	-
Tyrosine	Pyrolysis	0.18	0.26	0.44	0.55	-	0.78
	Oxidative Pyrolysis	-	-	0.20	0.05	-	0.05
Glutamic acid	Pyrolysis	0.39	0.29	0.06	0.04	-	-
	Oxidative Pyrolysis	-	-	-	-	-	-

5.7. The kinetics of lignin pyrolysis

The modeling of biomass pyrolysis is a complex process which involves simplifying a large body of equations. Large number of chemical reactions and the species involved increases the complexity of the thermal degradation of biomass. It is therefore necessary that the input parameters and physical properties chosen by researchers are simplified in order to provoke the greatest possible influence on the overall kinetic parameters. Consequently, there is need for a detailed kinetic scheme of biomass pyrolysis that considers the distribution of molecular weight and the solution of a high-dimensional system of differential equations. Fortunately, mathematical modeling, and the present state of knowledge in computation allows individual yield predictions of biomass pyrolysis products possible.

In this study, a model for the thermal degradation of lignin has been presented. A 15 reaction model was developed to determine the kinetic as well as the thermodynamic parameters of reaction products with reasonable accuracy. By use of pseudo first order rate law, the rate constants for various products were calculated. Arrhenius equation, *vide supra* equation 3.26 was

used to compute the pre-exponential factor *A*, as well as the activation energy *Ea* for numerous reaction products such as phenol, guaiacol, syringol, 4-vinylguaiacol, toluene, and benzene.

The results obtained from the model showed that the experimental data matched the computation data. The model of lignin pyrolysis developed in this study used CHEMKIN combustion code to fit calculated and experimental data for selected 6 representative products of lignin pyrolysis (Group [Syr + Gua], Group [Phenolic], Group [Furf + Meth], Group [Tol + Styr], and Group [4-Vinylgua], Group [Benz + Eth]). The efficiency of the model was tested using CHEMKIN and found to be remarkably close to experimental data.
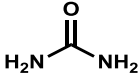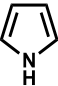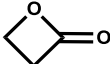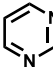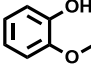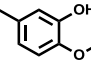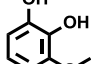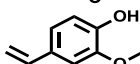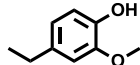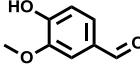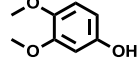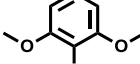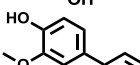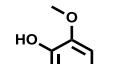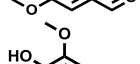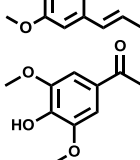
5.8. References

1. Shen, C., et al., *Pyrolysis of D-Glucose to Acrolein.* Chinese Journal of Chemical Physics, 2011. **24** (3): p. 249-252.

2. Paine, J.B., III, Y.B. Pithawalla, and J.D. Naworal, *Carbohydrate pyrolysis mechanisms from isotopic labeling. Part 3. The Pyrolysis of D-glucose: Formation of C-3 and C-4 carbonyl compounds and a cyclopentenedione isomer by electrocyclic fragmentation mechanisms.* Journal of Analytical and Applied Pyrolysis, 2008. **82** (1): p. 42-69.

3. Dorrestijn, E. and P. Mulder, *The radical-induced decomposition of 2-methoxyphenol.* Journal of the Chemical Society-Perkin Transactions 2, 1999(4): p. 777-780.

4. Vuori, A., *Thermal and catalytic reactions of the C-O bond in lignin and coal related aromatic methyl ethers.* Acta Polytechnica Scandinavica-Chemical Technology Series, 1986(176): p. 1-131.

5. Asmadi, M., H. Kawamoto, and S. Saka, *Thermal reactions of guaiacol and syringol as lignin model aromatic nuclei.* Journal of Analytical and Applied Pyrolysis, 2011. **92** (1): p. 88-98.

6. Lander, J.J. and W.J. Svirbely, *The dipole moments of catechol, resorcinol and hydroquinone.* Journal of the American Chemical Society, 1945. **67** (2): p. 322-324.

7. Goode, E.V. and D.A. Ibbitson, *Dipole moments of a series of substituted phenols in benzene.* Journal of the Chemical Society, 1960 (NOV): p. 4265-4270.

8. Khachatryan, L., R. Asatryan, and B. Dellinger, *Development of expanded and core kinetic models for the gas phase formation of dioxins from chlorinated phenols.* Chemosphere, 2003. **52** (4): p. 695-708.

9.   Yin, S.N., et al., *Leukemia in benzene workers - A retrospective cohort study.* British Journal of Industrial Medicine, 1987. **44** (2): p. 124-128.

10.   Yin, S.N., et al., *A retrospective cohort study of leukemia and other cancers in benzene workers.* Environmental Health Perspectives, 1989. **82**: p. 207-213.

11.   Snyder, R., et al., *Studies on the mechanism of benzene toxicity.* Environmental Health Perspectives, 1989. **82**: p. 31-35.

12.   Eastmond, D.A., M.T. Smith, and R.D. Irons, *An interaction of benzene metabolites reproduces the myelotoxicity observed with benzene exposure.* Toxicology and Applied Pharmacology, 1987. **91**(1): p. 85-95.

13.   Bolton, J.L., et al., *Role of quinones in toxicology.* Chemical Research in Toxicology, 2000. **13**(3): p. 135-160.

14.   DeCaprio, A.P., *The toxicology of hydroquinone - Relevance to occupational and environmental exposure.* Critical Reviews in Toxicology, 1999. **29** (3): p. 283-330.

15.   Hirakawa, K., et al., *Catechol and hydroquinone have different redox properties responsible for their differential DNA-damaging ability.* Chemical Research in Toxicology, 2002. **15** (1): p. 76-82.

16.   Marinkovic, N., et al., *Dioxins and human toxicity.* Arhiv Za Higijenu Rada I Toksikologiju, 2010. **61**(4): p. 445-453.

17.   Samara, F., et al., *Toxicity comparison of chlorinated and brominated dibenzo-p-dioxins and dibenzofurans in industrial source samples by HRGC/HRMS and enzyme immunoassay.* Environment International, 2010. **36** (3): p. 247-253.

18.   Chen, H.L., et al., *Interactive effects between CYP1A1 genotypes and environmental polychlorinated dibenzo-p-dioxins and dibenzofurans exposures on liver function profile.* Journal of Toxicology and Environmental Health-Part a-Current Issues, 2006. **69** (4): p. 269-281.

19.   Siegien, I. and R. Bogatek, *Cyanide action in plants - from toxic to regulatory.* Acta Physiologiae Plantarum, 2006. **28** (5): p. 483-497.

APPENDIX 1. STRUCTURAL FORMULAS OF SELECTED REACTION PRODUCTS

A1.1. Structural formulas of some major products from the thermal degradation of biomass materials.

No.	Common Name	IUPAC Name	Structure	Mw (g/mol)
1.	Urea	carbonyl diamide		60
2.	pyrrole	1H-pyrrole		67
3	propiolactone	3-hydroxypropanoic acid lactone		72
4.	Pyrimidine	1,3-diazine		80
5.	guaiacol	2-methoxy phenol		124
6.	5-methyl guaiacol	2-methoxy-5-methylphenol		138
7.	3-methoxy catechol	3-methoxy-1,2-benzenediol		140
8.	4-vinyl guaiacol	4-hydroxy-3-methoxystyrene		150
9.	4-ethyl guaiacol	2-methoxy-4-ethylphenol		152
10.	vanillin	4-hydroxy-3-methoxybenzaldehyde		152
11.	3,4-dimethoxyphenol	3,4-dimethoxyphenol		154
12.	syringol	2,6-dimethoxy phenol		154
13.	eugenol	2-methoxy-4-(2-propenyl)phenol		164
14.	syringaldehyde	4-hydroxy-3,5-dimethoxybenzaldehyde		182
15.	4-propenyl syringol	2,6-dimethoxy-4-propenylphenol		194
16.	acetosyringone	4'-hydroxy-3',5'-dimethoxyacetophenone		196

APPENDIX 2. TYPICAL TOTAL ION CHROMATOGRAMS (TIC)
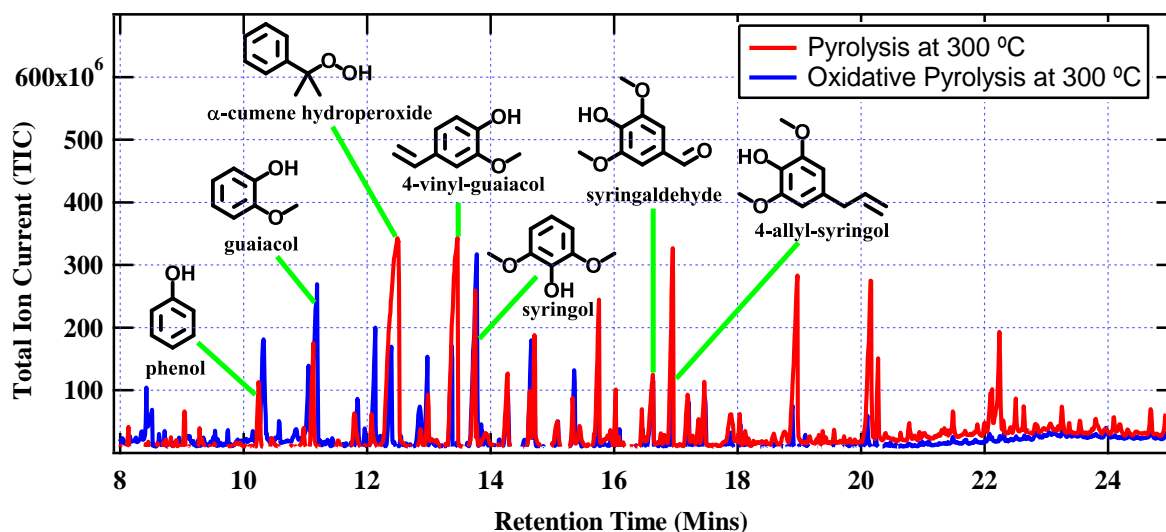
A2.1. Typical GC-MS chromatograms from pyrolysis (red line) and oxidative pyrolysis (blue line) of lignin at 300 ˚C obtained using a DB5-MS column.
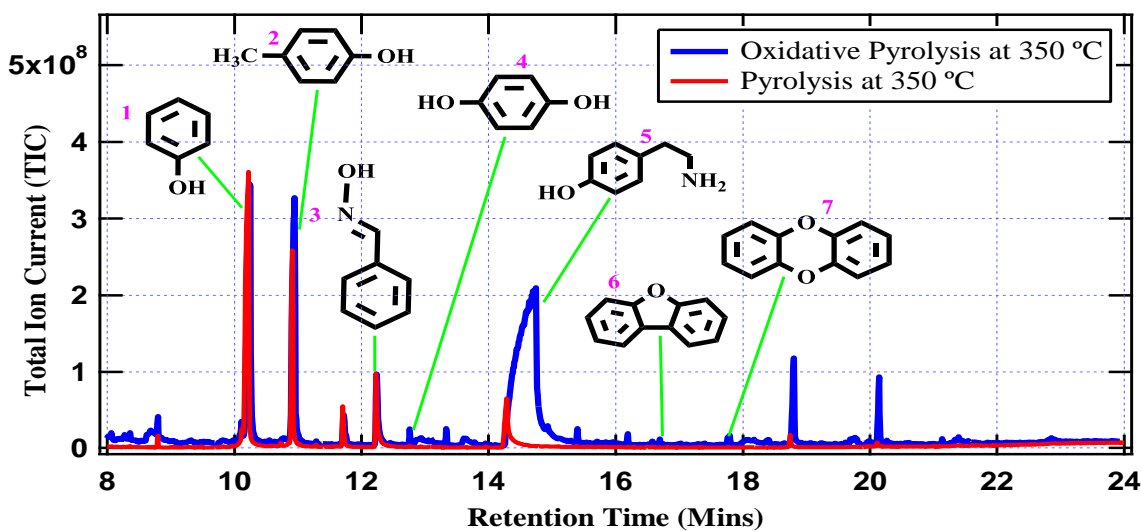
A2.2. Typical GC-MS spectrum from the pyrolysis (redd line) and oxidative pyrolysis (blue line) of tyrosine at 350 ˚C. Compounds 1-7 are: phenol, *p*-cresol, benzaldoxime, hydroquinone, *p*-tyramine, dibenzofuran, and dibenzo-*p*-dioxin respectively obtained using a DB5-MS column.

APPENDIX 3. CHEMKIN CALCULATIONS

```
!
! problem type definition
!
MOMEN ON    ! Turn on Momentum Equation
PLUG    ! Plug Flow Reactor
RTIME ON    ! Turn on Residence Time Calculation
TGIV    ! Fix Gas Temperature
!
! physical property
!
!Surface_Temperature    ! Surface Temperature Same as Gas Temperature
PRES 1.0    ! Pressure (atm)
SCCM 132.0    ! Volumetric Flow Rate in SCCM (standard-cm3/min@298.15K)
TEMP 973.0    ! Temperature (K)
VIS 0.0    ! Mixture Viscosity (g/cm-sec)
!
! reactor dimension definition
!
DIAM 0.35    ! Diameter (cm)
XEND 12.5    ! Ending Axial Position (cm)
XSTR 0.0    ! Starting Axial Position (cm)
!
! species property
!
REAC B(L) 1.0    ! Reactant Fraction (mole fraction)
!
! solver control
!
ADAP    ! Save Additional Adaptive Points
ASTEPS 10    ! Use Solver Integration Steps
DX 1.75    ! Distance Interval for Printing Data (cm)
NNEG    ! Force Non-negative Solution
!
! output control and other misc. property
!
GFAC 1.0    ! Gas Reaction Rate Multiplier
END
```

```
*****************************************************************
*                 CHEMKIN-PRO Release 15101                    *
*                     CHEM Application                         *
*                GAS-PHASE MECHANISM INTERPRETER               *
* Copyright(c) 1997-2010 Reaction Design.  All Rights Reserved. *
*****************************************************************
```

Initializing CHEMKIN Gas-phase Interpreter a component of CHEMKIN-PRO Release 15101, Build date: Sep 13, 2010
This and All Other CHEMKIN(R) Libraries are Copyright (c) 1997-2010 Reaction Design. All rights reserved.

LICENSE INFORMATION:

```
              WORKING SPACE REQUIREMENTS
                 PROVIDED        REQUIRED
LOGICAL             17              17
INTEGER           1212            1212
REAL              2699            2699
CHARACTER          166             166
```

This problem requires   0.021MB of memory for the REAL array.

```
                    ---------------------
                    ELEMENTS    ATOMIC
                    CONSIDERED  WEIGHT
                    ---------------------
                    1. B        10.8110
                    ---------------------
```

    Warning...unrecognized REACTION units string ignored...CONSIDERED
    WARNING...extra thermo parameters found for B
    WARNING...extra thermo parameters found for B(S)
    WARNING...extra thermo parameters found for B(L)

```
----------------------------------------------------------------------------
                      C
                   P  H
                   H  A
                   A  R
SPECIES            S  G  MOLECULAR  TEMPERATURE  ELEMENT COUNT
CONSIDERED         E  E  WEIGHT     LOW    HIGH       B
----------------------------------------------------------------------------
```

```
   -----------------------------------------------------------------------------
    1.  B(L)              L    0 1.0811E+01      200     5000              1
    2.  B(furf)           G    0 1.0811E+01      300     5000              1
    3.  B                 G    0 1.0811E+01      200     6000              1
    4.  B(S)              S    0 1.0811E+01      300     5000              1
    5.  B(ph)             G    0 1.0811E+01      300     5000              1
    6.  B(tol)            G    0 1.0811E+01      300     5000              1
    7.  B(V)              G    0 1.0811E+01      300     5000              1
    8.  B(G1)             G    0 1.0811E+01      300     5000              1
    9.  B(C1)             G    0 1.0811E+01      300     5000              1
   10.  B(G2)             G    0 1.0811E+01      300     5000              1
   11.  B(C2)             G    0 1.0811E+01      300     5000              1
   12.  B(Ps)             G    0 1.0811E+01      300     5000              1
   13.  B(Pph)            G    0 1.0811E+01      300     5000              1
   14.  B(Pfurf)          G    0 1.0811E+01      300     5000              1
   15.  B(Ptol)           G    0 1.0811E+01      300     5000              1
   16.  B(P)              G    0 1.0811E+01      300     5000              1
   17.  B(Pv)             G    0 1.0811E+01      300     5000              1
   -----------------------------------------------------------------------------
```

```
                                                 (k = A T**b exp(-E/RT))
          REACTIONS CONSIDERED                    A          b         E

    1.  B(L)=>B(S)                               3.47E+02    0.0     6000.0
    2.  B(L)=>B(ph)                              3.55E+03    0.0    10000.0
    3.  B(L)=>B(furf)                            5.75E+01    0.0     5600.0
    4.  B(L)=>B(tol)                             8.32E+05    0.0    17000.0
    5.  B(L)=>B                                  6.31E+06    0.0    22400.0
    6.  B(L)=>B(V)                               4.90E+01    0.0     4200.0
    7.  B(S)=>B(Ps)                              1.98E+05    0.0    19000.0
    8.  B(ph)=>B(Pph)                            4.00E+02    0.0     6300.0
    9.  B(furf)=>B(Pfurf)                        5.60E+03    0.0     9000.0
   10.  B(tol)=>B(Ptol)                          7.20E+02    0.0     7500.0
   11.  B=>B(P)                                  4.10E+02    0.0     7000.0
   12.  B(V)=>B(Pv)                              2.10E+02    0.0     5000.0
   13.  B(L)=>B(G1)                              1.10E+02    0.0     4600.0
```

UNITS for the preceding reactions (unless otherwise noted):
    A units mole-cm-sec-K, E units cal/mole

NO ERRORS FOUND ON INPUT:
ASCII Vers. 4.5.0 CHEMKIN linkfile chem.asc written.

      NOTE (for information purposes only),
      the following species do not participate in any reaction:
      B(C1)   B(G2)   B(C2)

GAS PHASE WORKING SPACE REQUIREMENTS ARE
    INTEGER: 708
    REAL: 587
    CHARACTER: 18

NOTE: There are WARNING messages in the printout above

Total CPUtime: 3 (seconds)

```
************************************************************
*                CHEMKIN-PRO Release 15101                 *
*                   AURORA Application                      *
*         PERFECTLY STIRRED OR PLUG FLOW REACTOR MODEL      *
*    Copyright(c) 1997-2010 Reaction Design.  All Rights Reserved. *
************************************************************


Running CHEMKIN-PRO
Running Multi-threaded mode

              WORKING SPACE REQUIREMENTS
                 PROVIDED         REQUIRED
  LOGICAL            73               73
  INTEGER          2274             2274
  REAL             4546             4546
  CHARACTER          42               42

This problem requires    0.035MB of memory for the REAL array.

Initializing CHEMKIN Gas-phase Library a component of CHEMKIN-PRO Release 15101, Build date: Sep 13, 2010
This and all other CHEMKIN(R) Libraries are Copyright (c) 1997-2010 Reaction Design.  All rights reserved.


LICENSE INFORMATION:
|

LicNum: 2661
 Licensed to Louisiana State University
 Contact: Lavrent Khachatryan
 Expiring: 26-jul-2012
 Platform: win64

     KEYWORD INPUT

     !
     ! problem type definition
     !
     MOMEN ON    ! Turn on Momentum Equation
     PLUG    ! Plug Flow Reactor
     RTIME ON    ! Turn on Residence Time Calculation
     TGIV    ! Fix Gas Temperature
     !
     ! physical property
     !
     !Surface_Temperature    ! Surface Temperature Same as Gas Temperature
     PRES 1.0    ! Pressure (atm)
     SCCM 132.0    ! Volumetric Flow Rate in SCCM (standard-cm3/min@298.15K)
     TEMP 973.0    ! Temperature (K)
     VIS 0.0    ! Mixture Viscosity (g/cm-sec)
     !
     ! reactor dimension definition
     !
     DIAM 0.35    ! Diameter (cm)
     XEND 12.5    ! Ending Axial Position (cm)
     XSTR 0.0    ! Starting Axial Position (cm)
     !
     ! species property
     !
     REAC B(L) 1.0    ! Reactant Fraction (mole fraction)
     !
     ! solver control
     !
```

```
ADAP   ! Save Additional Adaptive Points
ASTEPS 10   ! Use Solver Integration Steps
DX 1.75   ! Distance Interval for Printing Data (cm)
NNEG   ! Force Non-negative Solution
!
! output control and other misc. property
!
GFAC 1.0   ! Gas Reaction Rate Multiplier
END
```

===

KINETICS MECHANISM:
   Total number of gas phase species   = 17
   Total number of gas phase reactions   = 13
   Total number of surface materials =   1

   Material: MATERIAL1
      Total number of surface phase species =   0
      Total number of surface phases =   0
      Total number of bulk phase species =   0
      Total number of bulk phases =   0
      Total number of surface phase reactions =   0

===

===

REACTOR #   1 CONDITIONS FOR INLET NAMED: INLET1
      Inlet mass flow rate =   9.722E-04 gm/sec
            (which, based on an estimated reactor density =   1.354E-04 gm/cm^3
                     and on a residence time =   0.00   sec
                  produces an estimated reactor volume) =   1.20   cm^3

      Inlet temperature = 973.00   Kelvin
      Inlet pressure (assumed equal to reactor pressure) =   1.00   atm
      Inlet density = 1.35405E-04 gm/cm^3
      Inlet mean molecular weight = 10.811   gm/mole
      Inlet molar flow rate   = 8.99228E-05 moles/sec
      Inlet volumetric flow rate = 7.1796   cm^3/sec
            (based on reactor pressure and inlet temperature)
                              = 132.00   SCCM
                              = 0.13200   SLPM

149
```

INLET CONDITIONS FOR GAS PHASE MOLECULAR SPECIES IN INLET1

| Species | mole_frac | moles/sec | gm/sec | cm^3/sec | SCCM | SLPM |
|---|---|---|---|---|---|---|
| B(L) | 1.0000 | 8.99228E-005 | 9.72155E-004 | 7.1796 | 132.00 | 0.13200 |
| B(furf) | 0.0000 | 0.0000 | 0.0000 | 0.0000 | 0.0000 | 0.0000 |
| B | 0.0000 | 0.0000 | 0.0000 | 0.0000 | 0.0000 | 0.0000 |
| B(S) | 0.0000 | 0.0000 | 0.0000 | 0.0000 | 0.0000 | 0.0000 |
| B(ph) | 0.0000 | 0.0000 | 0.0000 | 0.0000 | 0.0000 | 0.0000 |
| B(tol) | 0.0000 | 0.0000 | 0.0000 | 0.0000 | 0.0000 | 0.0000 |
| B(V) | 0.0000 | 0.0000 | 0.0000 | 0.0000 | 0.0000 | 0.0000 |
| B(G1) | 0.0000 | 0.0000 | 0.0000 | 0.0000 | 0.0000 | 0.0000 |
| B(C1) | 0.0000 | 0.0000 | 0.0000 | 0.0000 | 0.0000 | 0.0000 |
| B(G2) | 0.0000 | 0.0000 | 0.0000 | 0.0000 | 0.0000 | 0.0000 |
| B(C2) | 0.0000 | 0.0000 | 0.0000 | 0.0000 | 0.0000 | 0.0000 |
| B(Ps) | 0.0000 | 0.0000 | 0.0000 | 0.0000 | 0.0000 | 0.0000 |
| B(Pph) | 0.0000 | 0.0000 | 0.0000 | 0.0000 | 0.0000 | 0.0000 |
| B(Pfurf) | 0.0000 | 0.0000 | 0.0000 | 0.0000 | 0.0000 | 0.0000 |
| B(Ptol) | 0.0000 | 0.0000 | 0.0000 | 0.0000 | 0.0000 | 0.0000 |
| B(P) | 0.0000 | 0.0000 | 0.0000 | 0.0000 | 0.0000 | 0.0000 |
| B(Pv) | 0.0000 | 0.0000 | 0.0000 | 0.0000 | 0.0000 | 0.0000 |

==================================================================================

==================================================================================
PSPRNT: Printing of current solution from DDASPK:
==================================================================================

DDASPK Plug-flow Solution at Distance =  0.0000E+00 cm

```
                RESIDENCE TIME                0.0000E+00  SEC
                MASS FLOW RATE                9.7216E-04  GM/SEC
                PRESSURE                      1.000       ATM
                MASS DENSITY                  1.3541E-04  GM/CM^3
                VELOCITY                      74.62       CM/S
                CROSS-FLOW AREA               9.6211E-02  CM^2
                LOCAL DADX                    0.000       CM
                INT. SURFACE AREA PER LENGTH  1.100       CM
                EXT. SURFACE AREA PER LENGTH  1.100       CM
                GAS CHEM HEAT PRODUCTION     -5.8930E+01  CAL/S/CM^3
                TEMPERATURE (FIXED)           973.0000    K
                SURF TEMP, MATERIAL1          973.0000    K  (same as gas temp)
```

REACTOR GAS PHASE MOLE FRACTIONS

B(L)	=	1.000	B(furf)	=	0.000	B	=	0.000
B(S)	=	0.000	B(ph)	=	0.000	B(tol)	=	0.000
B(V)	=	0.000	B(G1)	=	0.000	B(C1)	=	0.000
B(G2)	=	0.000	B(C2)	=	0.000	B(Ps)	=	0.000
B(Pph)	=	0.000	B(Pfurf)	=	0.000	B(Ptol)	=	0.000
B(P)	=	0.000	B(Pv)	=	0.000			

==

```
========================================================================================
                    PSPRNT: Printing of current solution from DDASPK:
========================================================================================


    DDASPK Plug-flow Solution at Distance =   1.4126E+00 cm

                    RESIDENCE TIME              1.8930E-02  SEC
                    MASS FLOW RATE             9.7216E-04  GM/SEC
                    PRESSURE                    1.000      ATM
                    MASS DENSITY               1.3541E-04  GM/CM^3
                    VELOCITY                   74.62       CM/S
                    CROSS-FLOW AREA            9.6211E-02  CM^2
                    LOCAL DADX                  0.000      CM
                    INT. SURFACE AREA PER LENGTH   1.100   CM
                    EXT. SURFACE AREA PER LENGTH   1.100   CM
                    GAS CHEM HEAT PRODUCTION    3.2739E+00  CAL/S/CM^3
                    TEMPERATURE (FIXED)         973.0000   K
                    SURF TEMP, MATERIAL1        973.0000   K  (same as gas temp)


    REACTOR GAS PHASE MOLE FRACTIONS

    B(L)      = 1.0679E-02    B(furf)   = 6.0268E-03    B        = 0.2057
    B(S)      = 5.4828E-02    B(ph)     = 6.6124E-02    B(tol)   = 0.4180
    B(V)      = 1.8208E-02    B(G1)     = 4.2041E-02    B(C1)    = 3.3896E-21
    B(G2)     =  0.000        B(C2)     =  0.000        B(Ps)    = 9.4635E-03
    B(Pph)    = 1.6979E-02    B(Pfurf)  = 7.0752E-03    B(Ptol)  = 0.1035
    B(P)      = 3.6529E-02    B(PV)     = 4.8231E-03


========================================================================================

========================================================================================
                    PSPRNT: Printing of current solution from DDASPK:
========================================================================================


    DDASPK Plug-flow Solution at Distance =   3.1626E+00 cm

                    RESIDENCE TIME              4.2381E-02  SEC
                    MASS FLOW RATE             9.7217E-04  GM/SEC
                    PRESSURE                    1.000      ATM
                    MASS DENSITY               1.3541E-04  GM/CM^3
                    VELOCITY                   74.62       CM/S
                    CROSS-FLOW AREA            9.6211E-02  CM^2
                    LOCAL DADX                  0.000      CM
                    INT. SURFACE AREA PER LENGTH   1.100   CM
                    EXT. SURFACE AREA PER LENGTH   1.100   CM
                    GAS CHEM HEAT PRODUCTION    3.0551E+00  CAL/S/CM^3
                    TEMPERATURE (FIXED)         973.0000   K
                    SURF TEMP, MATERIAL1        973.0000   K  (same as gas temp)


    REACTOR GAS PHASE MOLE FRACTIONS

    B(L)      = 3.8564E-05    B(furf)   = 1.7783E-03    B        = 0.1611
    B(S)      = 4.3230E-02    B(ph)     = 4.6764E-02    B(tol)   = 0.2990
    B(V)      = 1.2747E-02    B(G1)     = 4.2493E-02    B(C1)    = 3.3709E-21
    B(G2)     =  0.000        B(C2)     =  0.000        B(Ps)    = 2.1753E-02
    B(Pph)    = 3.7233E-02    B(Pfurf)  = 1.1465E-02    B(Ptol)  = 0.2281
    B(P)      = 8.3721E-02    B(PV)     = 1.0531E-02
```

151

DDASPK Plug-flow Solution at Distance =   4.9126E+00 cm

                RESIDENCE TIME   6.5832E-02 SEC
                MASS FLOW RATE   9.7216E-04 GM/SEC
                PRESSURE   1.000   ATM
                MASS DENSITY   1.3541E-04 GM/CM^3
                VELOCITY   74.62   CM/S
                CROSS-FLOW AREA   9.6211E-02 CM^2
                LOCAL DADX   0.000   CM
                INT. SURFACE AREA PER LENGTH   1.100   CM
                EXT. SURFACE AREA PER LENGTH   1.100   CM
                GAS CHEM HEAT PRODUCTION   2.3637E+00 CAL/S/CM^3
                TEMPERATURE (FIXED)   973.0000   K
                SURF TEMP, MATERIAL1   973.0000   K (same as gas temp)

REACTOR GAS PHASE MOLE FRACTIONS

B(L)   = 1.3823E-07   B(furf) = 5.0973E-04   B   = 0.1246
B(S)   = 3.3644E-02   B(ph)   = 3.2605E-02   B(tol)   = 0.2109
B(V)   = 8.7972E-03   B(G1)   = 4.2494E-02   B(C1)   = 3.3731E-21
B(G2)   = 0.000   B(C2)   = 0.000   B(Ps)   = 3.1341E-02
B(Pph)   = 5.1396E-02   B(Pfurf) = 1.2734E-02   B(Ptol) = 0.3162
B(P)   = 0.1203   B(Pv)   = 1.4483E-02

===

===
PSPRNT: Printing of current solution from DDASPK:
===

```
================================================================
              PSPRNT: Printing of current solution from DDASPK:
================================================================


    DDASPK Plug-flow Solution at Distance =   6.6626E+00 cm

                RESIDENCE TIME              8.9283E-02  SEC
                MASS FLOW RATE             9.7216E-04  GM/SEC
                PRESSURE                    1.000      ATM
                MASS DENSITY                1.3541E-04  GM/CM^3
                VELOCITY                    74.62      CM/S
                CROSS-FLOW AREA             9.6211E-02  CM^2
                LOCAL DADX                  0.000      CM
                INT. SURFACE AREA PER LENGTH 1.100     CM
                EXT. SURFACE AREA PER LENGTH 1.100     CM
                GAS CHEM HEAT PRODUCTION    1.8272E+00  CAL/S/CM^3
                TEMPERATURE (FIXED)         973.0000   K
                SURF TEMP, MATERIAL1        973.0000   K  (same as gas temp)


    REACTOR GAS PHASE MOLE FRACTIONS

    B(L)      = 4.4229E-10    B(furf)   = 1.4605E-04    B         = 9.6297E-02
    B(S)      = 2.6182E-02    B(ph)     = 2.2731E-02    B(tol)    = 0.1488
    B(V)      = 6.0707E-03    B(G1)     = 4.2494E-02    B(C1)     = 3.3731E-21
    B(G2)     =   0.000       B(C2)     =   0.000       B(Ps)     = 3.8804E-02
    B(Pph)    = 6.1269E-02    B(Pfurf)  = 1.3097E-02    B(Ptol)   = 0.3783
    B(P)      = 0.1486        B(Pv)     = 1.7209E-02


================================================================
              PSPRNT: Printing of current solution from DDASPK:
================================================================


    DDASPK Plug-flow Solution at Distance =   8.4126E+00 cm

                RESIDENCE TIME              1.1273E-01  SEC
                MASS FLOW RATE             9.7216E-04  GM/SEC
                PRESSURE                    1.000      ATM
                MASS DENSITY                1.3541E-04  GM/CM^3
                VELOCITY                    74.62      CM/S
                CROSS-FLOW AREA             9.6211E-02  CM^2
                LOCAL DADX                  0.000      CM
                INT. SURFACE AREA PER LENGTH 1.100     CM
                EXT. SURFACE AREA PER LENGTH 1.100     CM
                GAS CHEM HEAT PRODUCTION    1.4126E+00  CAL/S/CM^3
                TEMPERATURE (FIXED)         973.0000   K
                SURF TEMP, MATERIAL1        973.0000   K  (same as gas temp)


    REACTOR GAS PHASE MOLE FRACTIONS

    B(L)      = 4.2039E-12    B(furf)   = 4.1848E-05    B         = 7.4440E-02
    B(S)      = 2.0375E-02    B(ph)     = 1.5847E-02    B(tol)    = 0.1049
    B(V)      = 4.1891E-03    B(G1)     = 4.2494E-02    B(C1)     = 3.3731E-21
    B(G2)     =   0.000       B(C2)     =   0.000       B(Ps)     = 4.4611E-02
    B(Pph)    = 6.8153E-02    B(Pfurf)  = 1.3202E-02    B(Ptol)   = 0.4222
    B(P)      = 0.1704        B(Pv)     = 1.9091E-02

================================================================
```

153

```
================================================================================
                PSPRNT: Printing of current solution from DDASPK:
================================================================================


  DDASPK Plug-flow Solution at Distance =   1.0163E+01 cm

              RESIDENCE TIME            1.3619E-01  SEC
              MASS FLOW RATE            9.7216E-04  GM/SEC
              PRESSURE                  1.000       ATM
              MASS DENSITY              1.3541E-04  GM/CM^3
              VELOCITY                  74.62       CM/S
              CROSS-FLOW AREA           9.6211E-02  CM^2
              LOCAL DADX                0.000       CM
              INT. SURFACE AREA PER LENGTH  1.100   CM
              EXT. SURFACE AREA PER LENGTH  1.100   CM
              GAS CHEM HEAT PRODUCTION  1.0920E+00  CAL/S/CM^3
              TEMPERATURE (FIXED)       973.0000    K
              SURF TEMP, MATERIAL1      973.0000    K  (same as gas temp)


  REACTOR GAS PHASE MOLE FRACTIONS

  B(L)     =  4.0796E-14   B(furf)  =  1.1993E-05   B        =  5.7544E-02
  B(S)     =  1.5856E-02   B(ph)    =  1.1048E-02   B(tol)   =  7.4019E-02
  B(V)     =  2.8908E-03   B(G1)    =  4.2494E-02   B(C1)    =  3.3734E-21
  B(G2)    =  0.000        B(C2)    =  0.000        B(Ps)    =  4.9130E-02
  B(Pph)   =  7.2952E-02   B(Pfurf) =  1.3231E-02   B(Ptol)  =  0.4531
  B(P)     =  0.1873       B(Pv)    =  2.0389E-02


================================================================================


================================================================================
                PSPRNT: Printing of current solution from DDASPK:
================================================================================


  DDASPK Plug-flow Solution at Distance =   1.1913E+01 cm

              RESIDENCE TIME            1.5964E-01  SEC
              MASS FLOW RATE            9.7216E-04  GM/SEC
              PRESSURE                  1.000       ATM
              MASS DENSITY              1.3541E-04  GM/CM^3
              VELOCITY                  74.62       CM/S
              CROSS-FLOW AREA           9.6211E-02  CM^2
              LOCAL DADX                0.000       CM
              INT. SURFACE AREA PER LENGTH  1.100   CM
              EXT. SURFACE AREA PER LENGTH  1.100   CM
              GAS CHEM HEAT PRODUCTION  8.4417E-01  CAL/S/CM^3
              TEMPERATURE (FIXED)       973.0000    K
              SURF TEMP, MATERIAL1      973.0000    K  (same as gas temp)
```

154

REACTOR GAS PHASE MOLE FRACTIONS

```
B(L)     = 1.9607E-14    B(furf)  = 3.4385E-06    B        = 4.4483E-02
B(S)     = 1.2339E-02    B(ph)    = 7.7023E-03    B(tol)   = 5.2208E-02
B(V)     = 1.9948E-03    B(G1)    = 4.2494E-02    B(C1)    = 3.3647E-21
B(G2)    =   0.000       B(C2)    =   0.000       B(Ps)    = 5.2646E-02
B(Pph)   = 7.6298E-02    B(Pfurf) = 1.3240E-02    B(Ptol)  = 0.4749
B(P)     = 0.2004        B(Pv)    = 2.1285E-02
```

===

===
                 PSPRNT: Printing of current solution from DDASPK:
===

DDASPK Plug-flow Solution at Distance = 1.2500E+01 cm

```
            RESIDENCE TIME                1.6751E-01  SEC
            MASS FLOW RATE                9.7216E-04  GM/SEC
            PRESSURE                      1.000       ATM
            MASS DENSITY                  1.3541E-04  GM/CM^3
            VELOCITY                      74.62       CM/S
            CROSS-FLOW AREA               9.6211E-02  CM^2
            LOCAL DADX                    0.000       CM
            INT. SURFACE AREA PER LENGTH  1.100       CM
            EXT. SURFACE AREA PER LENGTH  1.100       CM
            GAS CHEM HEAT PRODUCTION      7.7430E-01  CAL/S/CM^3
            TEMPERATURE (FIXED)           973.0000    K
            SURF TEMP, MATERIAL1          973.0000    K  (same as gas temp)
```

REACTOR GAS PHASE MOLE FRACTIONS

```
B(L)     = 2.2035E-13    B(furf)  = 2.2606E-06    B        = 4.0800E-02
B(S)     = 1.1343E-02    B(ph)    = 6.8239E-03    B(tol)   = 4.6435E-02
B(V)     = 1.7613E-03    B(G1)    = 4.2494E-02    B(C1)    = 3.3592E-21
B(G2)    =   0.000       B(C2)    =   0.000       B(Ps)    = 5.3642E-02
B(Pph)   = 7.7176E-02    B(Pfurf) = 1.3241E-02    B(Ptol)  = 0.4807
B(P)     = 0.2041        B(Pv)    = 2.1519E-02
```

===

           THE SPECIFIED END DISTANCE HAS BEEN REACHED

===
  PEAK TEMPERATURE AND PRESSURE INFORMATION:
      Peak gas temperature =   973.0   K
      Peak gas pressure   = 1.0132E+06 dyne/cm^2
===

Total CPUtime: 3 (seconds)

APPENDIX 4. COPYRIGHT PERMISSIONS

4.1. ACS publications

4.2. Permission from Elsevier

RE: Permission to use Excerpts of the article [CHEM_13574]

Narasimhan, Karunamurthy (ELS-CHN)
to me ▾

Dear Dr. Kibet,

If proper reference is made to the article, this can indeed be freely used for thesis.

Kind regards,

Karuna

Karunamurthy Narasimhan

Journal Manager - Editorial Production Journals

Elsevier India
(A division of Reed Elsevier India Pvt. Ltd.)

International Tech Park | Crest – 12th Floor | Taramani Road | Taramani | Chennai 600 113 | India|Tel: +91 44 4299 4643 | Fax: +91 44 4299 4568 | E-mail: k.narasimhan@elsevier.com | url:www.elsevier.com
My Team Manager's e-mail: V.Neralla@elsevier.com

4.3. ACS publications division guidelines for theses and dissertations

ATTENTION: STUDENTS, STUDENT ADVISORS, AND TEACHERS

Permission is automatically granted to include your paper(s) or portions of your paper(s) in your thesis; please pay special attention to the implications paragraph below. The Copyright Subcommittee of the Joint Board/Council Committees on Publications approved the following:

<u>Copyright permission for published and submitted material from theses and dissertations</u>
ACS extends blanket permission to students to include in their theses and dissertations their own articles, or portions thereof, that have been published in ACS journals or submitted to ACS journals for publication, provided that the ACS copyright credit line is noted on the appropriate page(s).

<u>Publishing implications of electronic publication of theses and dissertation material</u>
Students and their mentors should be aware that posting of theses and dissertation material on the Web prior to submission of material from that thesis or dissertation to an ACS journal may affect publication in that journal. Whether Web posting is considered prior publication may be evaluated on a case-by-case basis by the journal's editor. If an ACS journal editor considers Web posting to be "prior publication", the paper will not be accepted for publication in that journal. If you intend to submit your unpublished paper to ACS for publication, check with the appropriate editor prior to posting your manuscript electronically.

<u>If your paper has **not** yet been published by ACS</u>, we have no objection to your including the text or portions of the text in your thesis/dissertation in **print and microfilm formats**; please note, however, that electronic distribution or Web posting of the unpublished paper as part of your thesis in electronic formats might jeopardize publication of your paper by ACS. Please print the following credit line on the first page of your article: "Reproduced (or 'Reproduced in part') with permission from [JOURNAL NAME], in press (or 'submitted for publication'). Unpublished work copyright [CURRENT YEAR] American Chemical Society."

SUMMARY: The inclusion of your ACS unpublished or published manuscript is permitted in your thesis in print and microfilm formats. If ACS has published your paper you may include the manuscript in your thesis on an intranet that is not publicly available. Your ACS article cannot be posted electronically on a publicly available medium, such as but not limited to, electronic archives, Internet, intranet, library server, etc. The only material from your paper that can be posted on a public electronic medium is the article abstract, figures, and tables and you may link to the article's DOI.

Questions? Please contact the ACS Publications Division Copyright Office at copyright@acs.org or at 202-872-4368.

August 1998, March 2003, October 2003

VITA

Joshua K. Kibet was born in 1974, in Eldoret, Kenya. He earned a Bachelor of Education Science degree in Chemistry and Physics from Egerton University, Kenya in 2004. In 2007, He earned a Master of Philosophy degree in Analytical Chemistry from Moi University, Kenya. He is a teacher by profession and taught for 10 years prior to joining Louisiana State University (LSU) for his Doctor of Philosophy degree in Chemistry. During his Ph.D. studies at Louisiana State University, he attended the Chapel at the Campus for his spiritual needs, and was a great football fun. His research was under the supervision of Prof. Barry Dellinger, Patrick F. Taylor Chair, Department of Chemistry. He will receive his Doctor of Philosophy degree in May, 2013.